INFRARED SPECTROELECTROCHEMICAL STUDIES OF COORDINATION COMPOUNDS

by

Slava Alexandra Ciniawsky

A thesis presented in partial fulfilment of the requirements for the Doctor of Philosophy Degree of the University of London

Department of Chemistry

University College London

1992

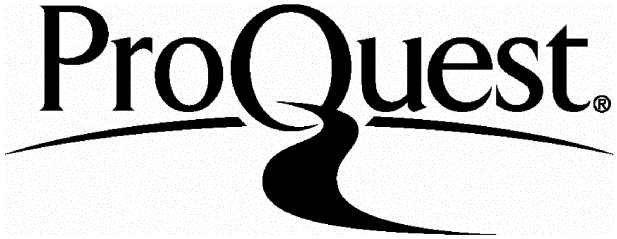

To my Parents

Учітеся, брати мої!
Думайте, читайте,
І чужому научайтесь,-
Свого не цурайтесь:

Тарас Шевченко
"Посланіє"

Abstract

The discovery of metal-containing constituents in many biological systems has stimulated research into the redox activity of transition metal complexes with non-innocent ligands. Interest has centred upon synthesising model compounds, which have similar spectroscopic or structural characteristics to the metal site of metalloproteins. In this way, a better understanding is gained of the behaviour of metalloenzymes such as the molybdenum-containing co-factors of nitrogenase, the oxotransferases, and the iron-containing ferredoxin electron-transfer agents.

The work carried out involved the electrochemical study of inorganic species, supplemented by infrared and ultra-violet/visible spectroelectrochemical experiments. By these means, it was possible to obtain a more precise evaluation of the changes occurring on oxidation or reduction, this being related to the frontier molecular orbitals of the complex.

The extremely reactive and short-lived nature of many electrogenerated products required the development of controlled, strictly anaerobic sample-handling procedures for spectroelectrochemical experiments. This was achieved by modifying the design of the spectroelectrochemical cell. The limitations of standard spectroelectrochemical techniques for the study of reactive short-lived species in solution prompted the development of the "Modulation Technique". This involved computer control and synchronisation of spectral data acquisition with the change of potential applied to the electrode. By the reversible generation, for a maximum of 2-3s, of the reactive species reliable spectroscopic results could be obtained. Modification of the working electrode enabled these experiments to be performed on a reduced timescale and at reduced temperatures to those previously possible.

Using this technique, spectra were recorded of a large range of previously unobserved and unstable species, such as the tetra-anionic tris maleonitriledithiolate complexes of vanadium, chromium, molybdenum and rhenium. The complicated series of chemical and electrochemical transformations initiated by oxidation of the

oxomolybdenum compound $MoOmnt_2^{2-}$ was also investigated and the intermediates identified. Significant insights were gained into the behaviour upon reduction of the carbonyl- and nitrosyl-containing compound $cpMo(CO)_2(NO)$. Spectral data were obtained for $Fe_4S_4(NO)_4$, a model compound for the iron-sulphur electron transfer proteins, in four different oxidation states, the evidence suggesting that the molecule retains its stable, cubane-like structure throughout all the redox steps.

Contents

List of Tables

List of Figures

Acknowledgements

The work carried out for this thesis would never have been possible without the contribution of a large number of people. Primary amongst these is my supervisor, Dr. S. P. Best, to whom I would like to express my sincerest thanks for for his guidance, patience, support and understanding throughout the three years of my PhD, and without whom this work would not have been possible. I would also like to extend my appreciation to the Chemistry Department of University College London for their award to me of a Departmental Research Studentship.

I would like to thank the numerous members of the technical support facilities within the Department for their unfailing and cheerful help in the vital tasks of the development of new apparatus and the maintenance of existing equipment. Special thanks are due to Mr John Hill for his valiant efforts to keep the temperamental Bruker FTIR spectrometer in working order; Mr. Gordon Carter and the gentlemen of the workshop for the construction of the IRRAS cell and the numerous spectrometer accessories required for my research; Mr. Mike Williams and his colleagues of the glassblowing workshop for the repeated production of all platinum-wire glass electrodes; Mr. Dave Bowman's team of electronics experts for building the electronic equipment, without which the "Modulation Technique" could not have been realised; Mr. Dave Knapp and Mr. Pete Pettit for their immeasurable patience when confronted with a seemingly endless series of loose connections, faulty pumps and leaking seals throughout the years of my PhD.

I would also like to thank Phil, Rob, Dan O., Dan G., Navjot, Pete, Dave, Chris, Hiro, Elliot and Mr. Wasyl Tertiuk for their companionship, both in and out of the laboratory. Thanks are also due to Ostap Kurlak for the loan of a personal computer for the writing of this thesis and Dr. Derek Tocher and my sister, Olha, for proof-reading the final product. Last, but not least, I would like to express my gratitude to my parents for their unfailing encouragement, assistance and support, both moral and financial, throughout my student years.

Abbreviations

ATP	*adenosine triphosphate*
cp	*cyclopentadienyl*
cys	*cysteine*
Cyt	*cytochrome*
dtc	*diethyldithiocarbamate*
EMIRS	*electrochemically modulated infrared spectroscopy*
$\mathbf{E_{½}}$	*half-wave redox potential*
$\mathbf{E_{Pa}}$	*anodic potential*
$\mathbf{E_{Pc}}$	*cathodic potential*
$\mathbf{i_{Pa}}$	*anodic current*
$\mathbf{i_{Pc}}$	*cathodic current*
Fe-Mo-co	*iron molybdenum co-factor*
[4Fe-4S]	$Fe_4(\mu_3\text{-}S^*)_4$ *cubane-like cluster*
FTIR	*Fourier transform infrared*
IRRAS	*infrared reflection-absorption spectroscopy*
MCT	*mercury-cadmium-telluride detector*
mnt	*maleonitriledithiolate*
Mo-co	*molybdenum co-factor*
OTTLE	*Optically transparent thin-layer electrode*
SCE	*saturated calomel electrode*
sh	*shoulder*
SNIFTERS	*subtractively normalised interfacial Fourier transform infrared spectroscopy*
$\mathbf{V_f}$	*final potential*
$\mathbf{V_i}$	*initial potential*

Introduction

For many decades, the study of transition metals and their compounds has been at the forefront of inorganic chemical research. Investigations revealed that transition metals formed a larger variety of compounds and exhibited a much richer and more varied electrochemistry than main group metals. This stimulated an interest in the redox chemistry of transition metal complexes and its possible modification by the alteration of the ligands coordinated to the metal centre. Significant attention was focussed upon the redox activity of transition metal complexes with non-innocent ligands. The electronic structure and stereochemistry of such molecules are significantly more complex and the possibility arises of metal- or ligand-based redox chemistry.

A natural progression is the investigation of the electrochemistry of complexes of transition metals with extensive ligands systems. Many examples of this type of complex occur as constituent parts of biological systems. Electrochemical techniques have proved to be especially useful in the study of metalloenzymes, which primarily involve such metals as magnesium, iron and copper.

One of the lesser known biologically-active transition metals is molybdenum. Although elemental molybdenum is moderately toxic and teratogenic[1], once it is incorporated into enzymes as their active sites, it becomes the only transition metal below the first series to be essential to living organisms. The availability of molybdenum arises from the high solubility of MoO_4^{2-} and polymolybdate ions, such as $Mo_7O_{24}^{6-}$, in water. As a result, despite its relatively low overall natural abundance (1.2 p.p.m in the Earth's crust[2]; 1.5 p.p.m. in the lithosphere[3]), molybdenum is the most abundant transition metal in seawater, at a concentration of 10 $\mu g l^{-1}$.[3]

Molybdenum has long been noted for the diversity of its compounds and its ability to exist in a wide range of oxidation states (from Mo^{-II} to Mo^{VI}). This extremely varied behaviour is reflected in the broad range of biological processes catalysed by enzymes which contain molybdenum as an essential component. These

include nitrogen "fixation", nitrate reduction and aldehyde oxidation. Examples of some of the more common and widely-studied molybdenum enzymes are given in **Table 1.**

Table 1 * Molybdenum enzymes

ENZYME	SOURCE	R.M.M.	TYPICAL CONTENTS	FUNCTION
Nitrogenase molybdo-ferredoxin	*Azobacter vinelandii*	220 000	2Mo 24-32Fe 24-32S	$N_2 \rightarrow NH_3$
Xanthine oxidase	Bovine milk	283 000	2Mo 8Fe 8S 2Flavin	Xanthine→ uric acid
Xanthine dehydrogenase	Chicken liver	300 000	2Mo 8Fe 8S 2Flavin	"
Aldehyde oxidase	Rabbit liver	346 000	2Mo 8Fe 8S 2Flavin	$RCHO \rightarrow RCO_2H$
Sulphite oxidase	Rat liver	120 000	2Mo 2Cyt-b_5	$SO_3^{2-} \rightarrow SO_4^{2-}$
Nitrate reductase	*Neurospora crassa*	230 000	1Mo 2Cyt-b_{557}	$NO_3^- \rightarrow NO_2^-$

* Table compiled using data from references ***1, 2*** and ***3***

It is generally found to be convenient to classify molybdoenzymes into two categories - *oxo-transferases* and *nitrogenases.* Although both types of enzymes have reasonably large molecular masses, the active sites have been traced to relatively small prosthetic groups containing molybdenum. These prosthetic groups, or *cofactors*, can

dissociate reversibly from the main body of the protein and are vital to the catalytic activity of the molybdoenzyme.

Initial theories postulating a common, interchangeable molybdenum cofactor for all molybdoenzymes was soon disproved by the work of Shah and Brill[4,5]. They were able to isolate a cofactor unique to *nitrogenases*, in the form of an N-methylformamide extract - this was termed the iron-molybdenum cofactor or **FeMo-co**. Subsequent studies indicated the existence of a common cofactor for all *oxo-transferases* - designated **Mo-co**.

Molybdenum oxo-transferases

Oxo-transferases catalyse the transfer of oxygen atoms to or from substrates according to the general reaction:-

$$X + H_2O \rightleftharpoons XO + 2H^+ + 2e^- \qquad X=\text{substrate}$$

Certain members of this group of enzymes catalyse the transfer of an oxo group to the substrate, e.g. *aldehyde oxidase*:-

$$RCHO + \tfrac{1}{2}O_2 \rightarrow RCO_2H$$

Other *oxo-transferases* catalyse the removal of an oxo group from the substrate e.g. *nitrate reductase*:-

$$NO_3^- + 2e^- \rightarrow NO_2^- + O^{2-}$$

Evidence from EXAFS experiments[6-9], performed on cofactor **Mo-co**, and information from other spectroscopic techniques, indicate the presence of a mononuclear molybdenum site linked to sulphur-donor ligands and terminal oxo groups.

The isolation of an oxidised, inactive form of Mo-co and the similarity of its fluorescence properties to that of a pterin enabled Johnson and Rajagopalan[10] to propose a "molybdopterin" structure for **Mo-co (Fig.1).**

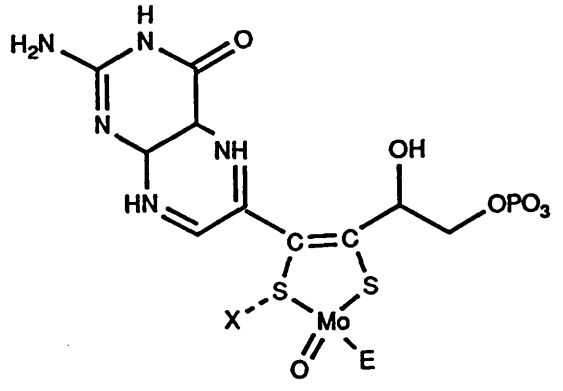

Fig. 1 Molybdopterin

The molybdenum atom is believed to be coordinated to the pterin system through dithiolene sulphur atoms. This is consistent with bond-length data for molybdenum dithiolene complexes, which yield values of 2.3-2.4Å for Mo-S bonds.[3] Distances of 2.4-2.5Å are obtained for the analogous bonds in **Mo-co** from K-edge EXAFS studies.[7,8,9] The fact that dithiolene complexes of transition metals undergo facile, reversible one-electron redox processes, is consistent with this theory.

Nitrogenases

Nitrogenases catalyse the 6-electron reduction of dinitrogen to ammonia (a process commonly known as nitrogen fixation):-

$$N_2 + 6H^+ + 6e^- \rightarrow 2NH_3$$

Blue-green algae and a large number of bacteria, including facultative aerobes such as *Klebsiella pneumoniae* and anaerobic species such as *Clostridium pasteurianum*,[1] contain *nitrogenase*. In a strictly anaerobic environment, *nitrogenase* will reduce dinitrogen in the presence of ATP, protons, a divalent cation (usually

Mg^{2+}) and a reductant (ferredoxin or flavodoxin in vivo; sodium dithionite in vitro). The enzyme consists of an iron-molybdenum (*molybdoferredoxin*) protein, containing the active site, and an iron protein (*azoferredoxin*) acting as a storage unit for electrons.[3,11] For substrate reduction electrons flow from the reduced iron protein to a reduced form of the iron-molybdenum protein, causing the former to become oxidised and the latter super-reduced.

The iron protein consists of two identical subunits of one [4Fe-4S] cluster, with similar electrochemical properties to the bacterial ferredoxins. The iron-molybdenum protein takes the form of an $\alpha_2\beta_2$ tetramer and is further subdivided into two M-type, one S-type and four P-type clusters. Each P-type cluster has a tetranuclear unit of four iron atoms of comparable structure to the [4Fe-4S] proteins. The dimeric iron units making up the diamagnetic S-clusters remain unchanged on oxidation. Undoubtedly, the most important part of the iron-molybdenum protein is the M-cluster, which corresponds to the above mentioned **FeMo-co** - the site of substrate reduction. This extremely oxygen-sensitive component is unstable in water and cycles between three redox-active forms during enzyme turnover - super-reduced, reduced and oxidised. The UW45 mutant strain of the iron-molybdenum protein[12] from *Azobacter vinelandii* is the best characterised so far and has been shown to possess molybdenum, iron and sulphur in the ratio 1:8:6 in each M-cluster.

Model systems

A significant amount of work has been directed towards the synthesis of compounds which model the molybdenum sites both in **Mo-co** and **FeMo-co** in an attempt to better understand their oxo-transfer and redox properties. Specific emphasis has been laid on compounds of molybdenum involving oxidation states IV, V and VI, the redox states involved in the normal catalytic cycle of these enzymatic systems. Particular interest has been shown in compounds with sulphur-donor ligands, since most experiments seem to indicate that both co-factors are linked directly to thiolate entities.

The investigation of oxo species is also essential to any study of molybdenum in oxidation states IV, V and VI, since they predominate in the chemistry of the higher oxidation states of molybdenum. Oxomolybdenum, or molybdenyl, compounds generally undergo comparatively facile redox reactions which may, however, be complicated by changes of coordination number, stereochemistry and monomer/dimer equilibria. An indication of the structural complexity and diversity of molybdenyl species can be obtained by consulting **Fig. 2.**

The Mo=O stretching frequency in all molybdenyl compounds is determined largely by the molybdenum-oxygen bond strength and is, therefore, indicative of the electron distribution within the complex. The number of bands appearing in spectra and their wavenumbers are diagnostic of the nature of the bonding in the complexes as well as the number of oxo groups. Study of ν(Mo=O), and the changes in this vibrational frequency, for $MoOmnt_2^{2-}$ and all the molybdenyl compounds with diethyldithiocarbamate, has allowed some clarification of the nature of the structural changes occuring on reduction/oxidation.

Numerous studies have been conducted which attempt to model the oxo-transfer properties of many metalloenzymes.[13-16] Special attention has been given to elucidating the mechanism of *oxotransferase* molybdoenzymes by synthesising a great variety of molybdenyl compounds.[3] The problem encountered during the earlier studies of complexes using less bulky ligands, such as N,N-diethyldithiocarbamate[17-19] (dtc), was the formation of a μ-oxo dimer of Mo^V. The appearance of this dimer is particularly undesirable, especially in the form $Mo_2O_3^{4+}$, since it inhibits all enzymic activity as a result of its kinetic inertness. There have been some kinetic and mechanistic studies into the autocatalytic behaviour of MoO_2dtc_2 in non-aqueous media with triphenylphosphine[17,18]:-

$$MoO_2dtc_2 + PPh_3 \rightharpoonup MoOdtc_2 + POPh_3$$

Recent attention, however, has centred upon preparing compounds with larger ligands,[20-24] which hinder the approach of the two metal atoms and prevent dimerisation.

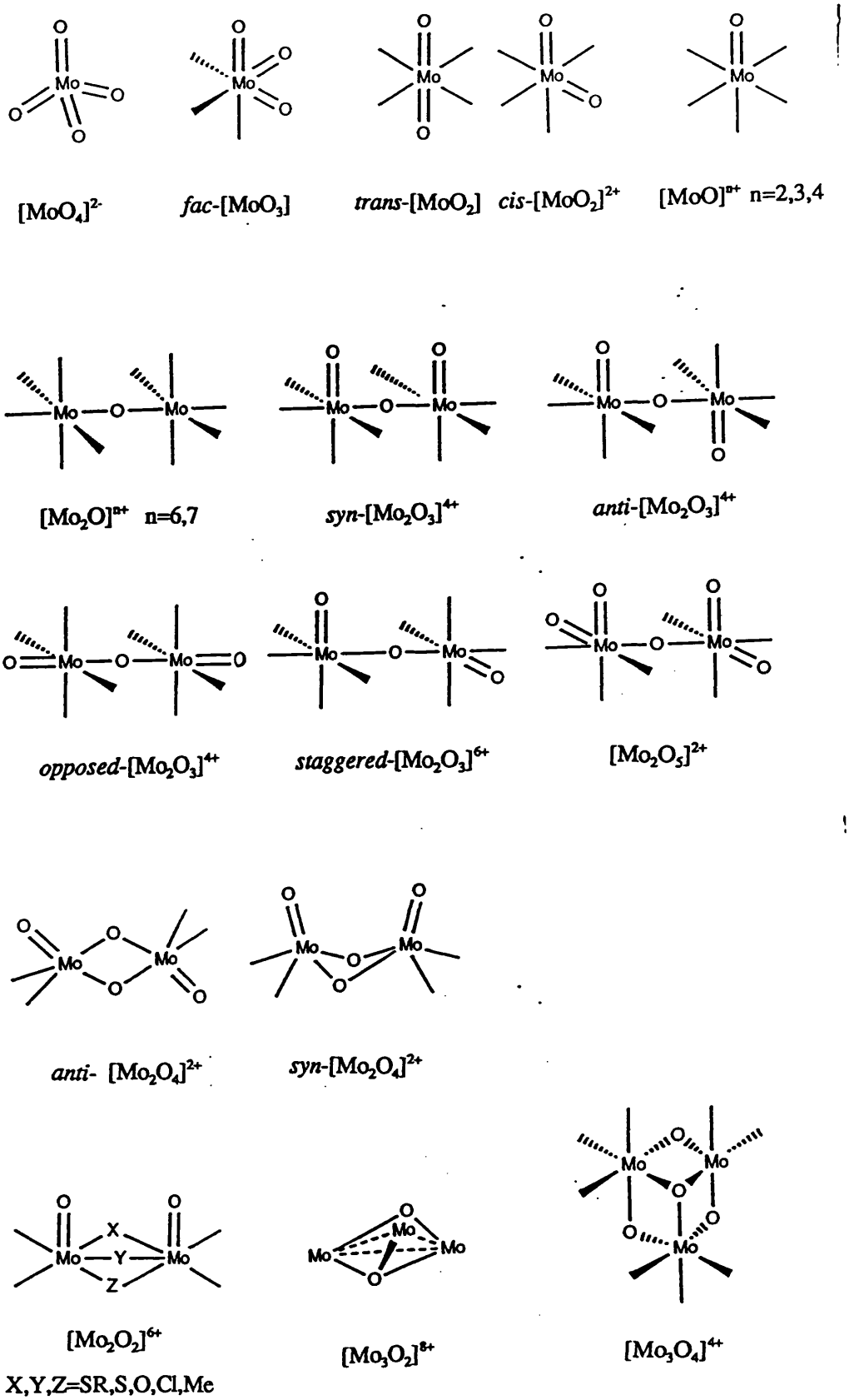

Fig. 2 Structurally characterised oxomolybdenum centres

Our investigations in this area of research have concentrated on the study of transition metal complexes with the ligand maleonitriledithiolate (cis-1,2-dicyano-1,2-ethylene-dithiolate), which structurally resembles the dithiolate chelate ring of the molybdopterin system (**Fig. 3**). The delocalisation of charge throughout the molecules means that, although a formal oxidation state cannot be assigned to the metals concerned, they are characterised by a very rich electrochemistry and are, therefore, convenient and relatively simple model systems for **FeMo-co** and **Mo-co.**

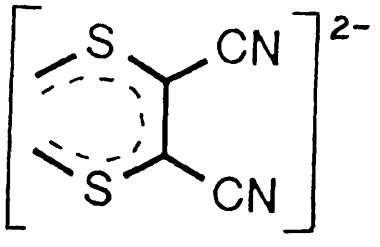

Fig. 3 Maleonitriledithiolate ligand

Virtually all transition metals react with the maleonitriledithiolate ligand (or mnt) to form complexes of the type $M(mnt)_2^{n-}$ or $M(mnt)_3^{n-}$. Molybdenum also reacts with mnt to form the oxo species $MoO(mnt)_2^{2-}$. Unlike the tris-mnt complexes, this molybdenyl compound has only one facile redox step, but has been widely used as a model for the molybdopterin unit of **Mo-co.**

The most valuable insights into the behaviour of molybdenum species on electron transfer were obtained from spectroelectrochemical studies in the infrared and ultra-violet/visible regions. Each compound investigated had at least one easily observed vibrational mode, giving rise to a very intense band in the infrared region, and one electronic transition, occurring in the visible region. Only those bands which occured in regions of the spectrum unobscured by solvent or electrolyte bands and were, therefore, easily monitored were selected for investigation. For $MoOmnt_2^{2-}$, as well as monitoring ν(Mo=O), the cyanide stretching vibrational mode ν(C=N) of the mnt ligand was also examined. This has been shown to be sensitive to metal-ligand π-bonding in tris-mnt compounds.

Iron-sulphur proteins

Although **Mo-co** and **Fe-Mo-co** form the active site of molybdoenzymes, they cannot function in the absence of efficient electron storage and transfer agents.[11] These

usually take the form of iron clusters with the general formula $Fe_nS_n(SR)_n$ (n=2, 3, 4; R=Me, Et, Ph) and, depending on the biological system, can either exist independently of the active site or as a constituent part of the metalloenzyme. The most widely studied members of this group are the tetranuclear $Fe_4S_4R_4$ cubane-type molecules, the best-known examples of which are the ferredoxins, the iron protein (*azoferredoxin*) and the P-cluster of the iron-molybdenum protein (*molybdoferredoxin*) of nitrogenase. All exhibit extensive and varied electrochemistry.

Of particular interest for spectroelectrochemistry is the tetranuclear iron species $Fe_4S_4(NO)_4$. This compound combines the important Fe_4S_4 unit with nitrosyl ligands, which can be monitored spectroscopically with ease as the complex undergoes three reversible redox steps.

In order to better define the spectroscopic changes attendant on a change in the mode of coordination of the nitrosyl ligand, studies were performed upon (η^5-C_5H_5)$Mo(CO)_2(NO)$ and its radical cation. This study revealed a set of complex reactions following the initial electron transfer and the resulting change in the mode of coordination of the ligand.

Experimental techniques for the study of metalloenzymes

A complete study of a metalloenzyme requires the determination of the structure of the super-molecule (or, at least, its active site) in all the stages of its catalytic cycle. The most important techniques used to probe the molecular structure include electron paramagnetic resonance, extended X-ray absorption fine structure, nuclear magnetic resonance and Mössbauer spectroscopy. Electrochemical techniques have proved invaluable in explaining the reaction of the enzyme with the substrate and the mechanism of electron transfer. Owing to difficulties in working with metalloenzymes, model compounds, which offer the advantages of simpler molecular and electronic structures, are investigated.

The electrochemical properties of many of these species are of particular interest. From the study of the redox properties of the model compounds and the spectroscopic changes observed on electron transfer, the redistribution of charge within

the molecule could be assessed. Comparison of the results with existing molecular orbital schemes/calculations enabled the frontier molecular orbitals of these systems to be defined and possible intra- or intermolecular rearrangements or structural changes detected. Cyclic voltammetry was of particular use, because the potential and reversibilty, or otherwise, of the redox reactions could be determined.

Spectroelectrochemical analysis of model compounds

Spectroelectrochemical techniques were found to be particularly applicable for the study of model compounds of metalloenzymes. To this end, several techniques were devised to monitor the in situ electrogeneration of the oxidised or reduced species in solution at the electrode surface. They enabled reactive complexes to be studied under the conditions of electrochemistry, without requiring them to be chemically isolated. Many of these techniques, however, were originally designed for the study of gases or films on surfaces whilst others required the use of transmission spectroscopic methods. Their usefulness in detecting transient electrogenerated species in solution was limited and an important aspect of this work, therefore, has been the development of improved techniques for the investigation of the complexes described above.

The developments and modifications were based around the infrared reflection-absorption spectroscopy (IRRAS) cell, which was adapted to enable work to be carried out under completely anaerobic conditions on small volumes of solution. The study of species present in situ in a thin film of solution (of approximately 10-20 μm thickness) meant that the IRRAS cell was ideal for use both in infrared and ultra-violet/visible spectroelectrochemical experiments. The experimental conditions in the cell could be reliably reproduced for all experiments in both spectral regions.

The more stable electrochemically-generated species were studied under conditions of bulk electrolysis over long timescales, the lifetime of shorter-lived species being extended by utilising an intrinsic feature of the cell - its ability to be cooled for work to be carried out at low temperatures. However, these conditions precluded standard spectroelectrochemistry from being a feasible option when the

oxidised/reduced product of the electrochemical reaction had a lifetime of the order of a few seconds or when the electron transfer process initiated a series of chemical and stuctural changes.

In order to be able to obtain infrared spectra of short-lived species, a new and more flexible technique was developed - the "Modulation Technique". This involved the repeated cycling of the potential between two predetermined values - a reference potential and an active potential, at which electron transfer is observed. Spectra were collected at the end of each cycle, prior to the switching of potential, using a Fourier Transform infrared spectrometer with rapid data acquisition facilities. In this way, the oxidised/reduced species were generated in solution for minimal periods of time, preventing extensive decomposition. The timescale of the experiment and the number of spectra collected could be regulated to suit the requirements of the species under investigation.

Working under rigorously anaerobic conditions, using a combination of the modulation spectroelectrochemical technique and reduced temperatures, spectra were recorded of several transient and short-lived - "hot" - species. The techniques used to handle these compounds and analyse the data produced were initially perfected using well-characterised compounds. The experience gained was subsequently put to use in the study of less well-characterised complexes exhibiting complicated electrochemical behaviour or series of chemical and electrochemical transformations.

References

1. J. E. Huheey, "Inorganic Chemistry", 3rd ed. Harper & Row, New York (1983)

2. N. N. Greenwood, A. Earnshaw, "Chemistry of the Elements", Pergamon Press, New York (1984)

3. "Molybdenum Enzymes", ed. T. G. Spiro, Wiley-Interscience, New York (1985) and references therein

4. V. K. Shah, W. J. Brill, *Proc. Natl. Acad. Sci. USA*, (1977), **74**, 3249

5. P. T. Pienkos, V. K. Shah, W. J. Brill, *Proc. Natl. Acad. Sci. USA*, (1977), **74**, 5468

6. S. P. Cramer, H. B. Gray, K. V. Rajagopalan, *J. Am. Chem. Soc.*, (1979), **101**, 2772

7. S. P. Cramer, R. Wahl, K. V. Rajagopalan, *J. Am. Chem. Soc.*, (1981), **103**, 7721

8. J. Bordas, R. C. Bray, C. D. Garner, S. Gutteridge, S. S. Hasnain, *Biochem. J.*, (1980), **191**, 499

9. S. P. Cramer, "Advances in Inorganic and Bioinorganic Mechanisms", Vol.2, A. G. Sykes, ed., Academic, London, (1983)

10. J. L. Johnson, K. V. Rajagopalan, *Proc. Natl. Acad. Sci. USA*, (1982), **79**, 6856

11. "Iron-Sulphur Proteins", ed. T. G. Spiro, Wiley-Interscience, New York, (1982) and references therein

12. H. H. Nagatani, W. J. Brill, *Biochim. Biophis. Acta*, (1974), **362**, 160; H. H. Nagatani, V. K. Shah, W. J. Brill, *J. Bacteriol.*, (1974), **120**, 697; P. T. Pienkos, S. Klevickis, W. J. Brill, *J. Bacteriol.*, (1981), **145**, 248

13. Y. Zhang, R. H. Holm, *Inorg. Chem*, (1990), **29**, 911

14. D. W. Pipes, M. Bakir, S. E. Vitols, D. J. Hodgson, T. J. Meyer, *J. Am. Chem. Soc.*, (1990),**112**, 5507

15. G. J-J. Chen, J. W. McDonald, W. E. Newton, *Inorg. Chim. Acta*, (1976), **19**, L67

16. R. H. Holm, *Chem. Rev.*, (1987), **87**, 1401

17. R. Barral, C. Bocard, J. S. de Roch, L. Sajus, *Tet. Lett.*, (1972), **17**, 1693

18. M. S. Reynolds, J. M. Berg, R. H. Holm, *Inorg. Chem.*, (1984), **23**, 3057

19. K. G. Moloy, *Inorg. Chem.*, (1988), **27**, 677

20. J. M. Berg, R. H. Holm, *J. Am. Chem. Soc.*, (1985), **107**, 925

21. E. W. Harlan, J. M. Berg, R. H. Holm, *J. Am. Chem. Soc.*, (1986), **108**, 6992

22. J. Topich, J. T. Lyon, *Inorg. Chem.*, (1984), **23**, 3202

23. N. Ueyama, N. Yoshinaga, A. Nakamura, *J. Chem. Soc., Dalton Trans.*, (1990), 387

24. J. A. Craig, E. W. Harlan, B. S. Snyder, M. A. Whitener, R. H. Holm, *Inorg. Chem.*, (1989), **28**, 2082

Chapter 1

Experimental

Spectroelectrochemistry is the probing of electrogenerated oxidised or reduced species using spectroscopic methods. It is, therefore, the simultaneous combination of two techniques - electrochemistry and spectroscopy - and requires the use of specialised apparatus and procedures. All spectroelectrochemical experiments are necessarily preceded by preliminary electrochemical analysis of the compound in question using cyclic voltammetry.

The subsequent spectroelectrochemical experiments were carried out in a cell specially-designed for use with a Fourier Transform infrared interferometer and a ultra-violet/visible spectrometer with a multi-channel detection system. All the procedures used in sample preparation, design of equipment, maintenance of apparatus, data analysis, as well as experimental techniques, are detailed below.

As normally practised, spectroelectrochemical techniques involve the in situ bulk electrosynthesis of the oxidised/reduced species in a spectroelectrochemical cell. Since this technique relies on the quantitative electrogeneration of the species under study, there are problems associated with the examination of highly-reactive products. In order to circumvent this difficulty, modulation techniques were developed which involved the generation of reactive species in lower concentration and on a shorter timescale. This required accurate synchronisation to be maintained between the timebase for the data acquisition cycles of the interferometer and the changes of potential at the working electrode.

The correct experimental conditions could easily be accomplished by programming a microcomputer to recognise signals from the interferometer and, acting on them, to control the behaviour of the potentiostat supplying the potential to the spectroelectrochemical cell. The process is explained in detail below.

1.1 Cyclic Voltammetry

1.1.1 Background

Cyclic voltammetry is the study of the current as a function of the potential applied to a small stationary working electrode.[1-7] The rate of sweep of the potential range is linear and variable. As the potential approaches that at which the compound being studied undergoes an electrochemical reaction, a flow of current is observed. For a general electrochemical reaction:-

$$Ox + ne^- \rightleftharpoons Red$$

Ox=oxidised species
Red=reduced species
n=number of electrons transferred

Electron transfer to or from the electrode occurs as the potential applied to the electrode is altered. The resulting changes in the relative concentrations of the oxidised and reduced species in the solution directly in contact with the electrode surface, but not in the bulk solution, conform to the Nernst Equation:-

$$E = E^{\ominus} + \frac{RT}{nF}\ln(a_{Ox}/a_{Red})$$

E=applied potential
$E^{\ominus}$=standard electrode potential
R=gas constant
T=temperature
n=number of electrons involved in the electrode reaction
F=Faraday constant
a=activity

In most cases, the activities of the species are approximated by their concentrations, giving:-

$$E = E^{\ominus} + \frac{RT}{nF}.\ln([Ox]/[Red])$$

The result is displayed in the form of a current versus potential graph or voltammogram (**Fig. 1.1**). The positive, or cathodic peak, E_{Pc}, corresponds to the formation of a reduced species; the negative, anodic peak, E_{Pa}, represents the generation of an oxidised species. In solution, these two peaks will not coincide. The midpoint of E_{Pa} and E_{Pc} (the anodic peak minimum and the cathodic peak maximum respectively) is termed $E_{½}$ - the half-wave redox potential. The magnitudes of the cathodic and anodic peak currents are known as i_{Pc} and i_{Pa} respectively.

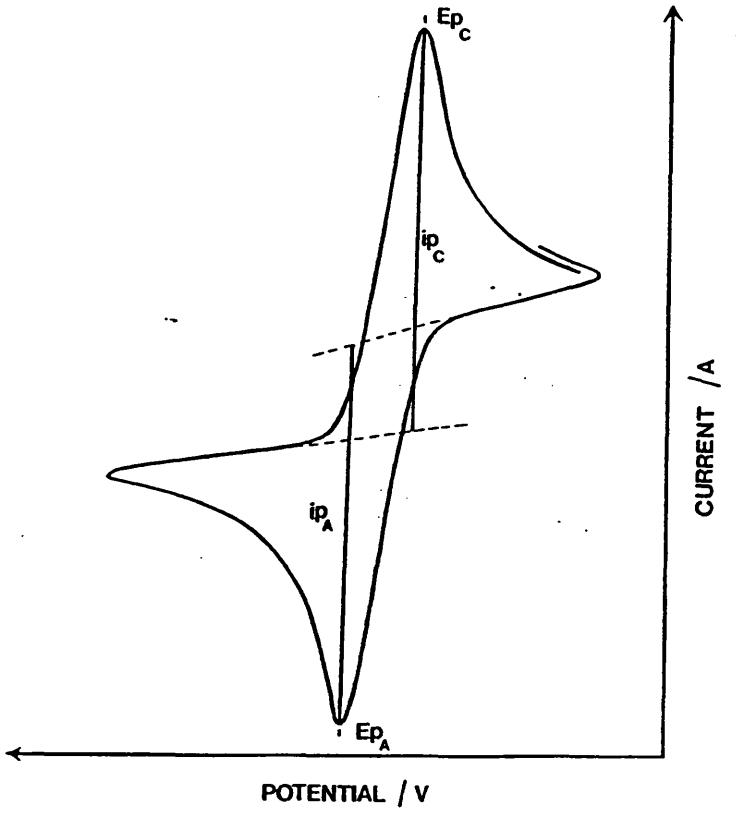

Fig. 1.1 Example of a cyclic voltammogram

When the electron transfer to the compound is rapid and any accompanying structural change is minimal and fast, with respect to the timescale of the experiment, then the electrochemical reaction is said to be electrochemically "reversible". The flow of current is a function of mass transport processes (e.g. diffusion, convection) alone and may be determined from the Nernst equation. Similarly, if a chemical reaction follows the charge transfer and both are rapid, with respect to the scan rate, then the process is also considered to be Nernstian, although it may no longer be chemically reversible.

When a molecule undergoes extensive chemical or structural rearrangement as a consequence of the electron transfer, the energy barrier to electron transfer is expected to increase. The flow of current ceases to be a function of mass transport alone and is dependent, to a large degree, on the kinetics of the electron transfer. In these cases, the Nernst equation no longer applies. When the rate of electron transfer is not fast enough to establish a Nernstian equilibrium at the electrode surface, the energy barrier to electron transfer is of moderate magnitude. The resulting electrochemical process is termed "quasi-reversible".

Processes classified as being electrochemically "irreversible", have very high energy barriers to electron transfer and, consequently, slow charge transfer rates. The rate of the backward electron transfer process is vanishingly small. These reactions are also chemically irreversible.

The four generally-accepted criteria of electrochemical reversibility are:-

i) The half-wave potential $\mathbf{E_{½}}$ has to be independent of scan speed v;

ii) The separation ($\mathbf{E_{Pa}}$-$\mathbf{E_{Pc}}$) between the peak potentials ΔE must be constant and equal to 59/n mV or less at 25°C. ΔE must also be independent of scan rate;

iii) Anodic and cathodic peak currents must be equal i.e. $\mathbf{i_{Pa}/i_{Pc}}$=1;

iv) The peak current must be directly proportional to the root of the scan rate i.e. $\mathbf{i_p}/v^{½}$=constant.

If one or more of the above conditions are not obeyed then the reaction is deemed to deviate from complete reversibility. The process, therefore, exhibits electrochemical quasi-reversibilty or irreversibility.

1.1.2 Apparatus

All electrochemical experiments were carried out using a standard-design glass three-electrode cell. Platinum wire working and counter (auxiliary) electrodes were used, whilst the reference electrode was either an Ag/AgCl system (Metrohm EA 441/5) or a pseudo reference system comprising a platinum wire electrode and a salt bridge. All redox potentials given were cross-referenced using the ferrocene-ferrocenium couple as a calibrant. The oxidation of $Fecp_2$ occurs at +0.50V with respect to Ag/AgCl. A Metrohm E506 potentiostat and Metrohm E612 VA scanner were used to produce and apply the potential to the electrochemical cell.

In order to ensure the reliability and reproducibility of results, certain procedures had to be followed to maintain the apparatus in a contaminant-free condition. The glass cell was stored in a clean oven at 40°C. All platinum electrodes were cleaned at regular intervals according to the method suggested by Geiger et al[8]:-

i) Electrodes are refluxed in concentrated nitric acid for one hour, rinsed with clean water and wiped;

ii) Refluxing is followed by overnight soaking in a saturated solution of ammonium ferrous sulphate in 1 mol dm^{-3} sulphuric acid;

iii) After rinsing with distilled water and careful drying, the electrodes are placed in dichloromethane and held first at -1.0V and then +1.0V until a steady-state current was achieved.

Once clean, all electrodes were kept in the rigorously moisture-free environment of a desiccator, to minimise adsorption of water.

1.1.3 Solvents

Three solvent systems - dichloromethane, acetonitrile and tetrahydrofuran - were used. All were purified before use.

Dichloromethane was subjected to preliminary drying over potassium hydroxide pellets. All storage containers were wrapped in aluminium foil to minimise photodecomposition of the solvent. Immediately before use, the dichloromethane was refluxed over and distilled from calcium hydride under a constant stream of dry nitrogen gas.

Tetrahydrofuran was purified by refluxing over and finally distillation from Na/benzophenone under a constant stream of nitrogen gas, to ensure a moisture-free product. It was used immediately after distillation.

In order to obtain acetonitrile of sufficiently high quality for use in voltammetric experiments, several stages of purification were followed to remove the small, but significant, contaminants (e.g. water, acetamide, acrylonitrile). The method of purification developed by Walter and Ramaley[9] was followed.

The solvent (1000 cm^3) is refluxed for one hour under nitrogen over anhydrous aluminium trichloride (15.0 g), which had been dried for two days in an oven at 100° C. Following rapid distillation, the acetonitrile is added to a mixture of potassium permanganate (10.0 g) and lithium carbonate (10.0 g) and allowed to reflux for 15 minutes under nitrogen before being rapidly distilled onto potassium hydrogen sulphate (15.0 g). After refluxing under nitrogen for one hour, the acetonitrile is rapidly distilled. The final step of the process involves refluxing the solvent over calcium hydride (2.0 g) under nitrogen for one hour and fractional distillation, retaining only the middle 80% fraction. The purified acetonitrile is stored under an inert atmosphere.

1.1.4 Electrolyte

The electrolyte used in all experments was tetra-n-butylammonium tetrafluoroborate. It was prepared according to the following reaction:-

$$(C_4H_9)_4NOH + HBF_4 \rightarrow (C_4H_9)_4NBF_4 + H_2O$$

Tetra-n-butylammonium hydroxide (50 g; 40% aqueous solution; 0.0771 mol) was placed in a 1000 cm^3 beaker and the volume made up to 400 cm^3 with distilled water. Fluoroboric acid (40% aqueous solution) was added dropwise to the stirred solution until pH 7 was achieved. The resulting copious white precipitate was removed by filtration and washed with large amounts of cold distilled water. After being allowed to dry on the sinter for some minutes, the solid was dissolved in a minimum volume of warm methanol and water (100-200 cm^3) was added to precipitate the electrolyte. Before use the electrolyte was dried for 6-8 hours under vacuum at 100°

C and subsequently stored in a desiccator (Typical yield=12.39 g; 48.8%).

Microanalysis:-			
Calculated:-	C=58.36%	H=11.02%	N=4.25%
Found:-	C=58.36%	H=11.51%	N=4.25%
	C=58.47%	H=11.10%	N=4.29%

To minimise the risk of contamination, the electrolyte was prepared using equipment reserved for that purpose only.

All electrochemical and spectroelectrochemical experiments in the three solvent systems were carried out using 0.2 mol dm^{-3} supporting electrolyte.

1.2 Infrared Spectroelectrochemistry

1.2.1 Infrared Spectroscopy

Vibrational spectroscopy is used extensively to study the vibrations of the constituent nuclei in molecules and thus learn more about molecular structure and chemical bonding.[10-14] The frequencies of the vibrational transitions occur in the infrared region of the spectrum (10 000 - 10 cm^{-1}) and are determined by the masses of the nuclei involved, the molecular geometry and the interatomic forces.

Chemical bonds in diatomic molecules conform to Hookes' Law of springs for small displacements. A spring requires a force, **F**, to restore it to its equilibrium length, $\mathbf{r_e}$, from a displaced length, **r**, according to the equation:-

$$F = -k(r-r_e)$$

where the proportionality constant, **k**, is known as the force constant and is a direct measure of the strength of the spring. The potential energy of a diatomic molecule, with atoms of mass m_1 and m_2, acting as a harmonic oscillator, is given by:-

$$V = \tfrac{1}{2}k(r-r_e)^2$$

and frequency:-

$$\nu = \sqrt{k/4\pi^2\mu}$$

$1/\mu$=reduced mass=$(1/m_1)+(1/m_2)$

The parabolic potential energy function is a good approximation only for very small displacements from the equilibrium bond length. An improved approximation is one which allows for deviation from anharmonicity, such as the empirical expression derived by Morse:-

$$V = D_e e^{-2\beta(r-re)} - 2\beta e^{-\beta(r-re)}$$

D_e=dissociation energy

$\beta=2\pi^2\nu\mu D_e$

The energies of the vibrational levels are therefore given by:-

$$E(v) = (v+½)h\nu - (v+½)^2h\nu x_e + (v+½)^3h\nu y_e \ldots$$

v=vibrational quantum number $\Delta v=\pm1, \pm2, \pm3 \ldots$

x_e, y_e = anharmonicity constants

Analysis of polyatomic molecules is significantly more complicated. Each non-linear molecule has 3N-6 (N=number of atoms in the molecule) **normal vibrations.** A **normal vibration** is defined as a molecular motion in which all the atoms which move do so with the same frequency.[14] There is no longer a simple relationship between force constants and vibrational frequencies, since the vibrations are not independent and are affected by other vibrational modes in the molecule. Correlations between vibrational frequencies and molecular force constants can be obtained by carrying out normal coordinate, or **F** and **G** matrix, analysis. Potential energy is given by the equation[11]:-

$$2V = \Sigma_{ij}F_{ij}S_iS_j + \Sigma_{ijk}F_{ijk}S_iS_jS_k + \ldots$$

S_i=displacements of internal coordinates from equilibrium positions

F_{ij}=quadratic force constants

F_{ijk}=cubic force constants

The energy of the vibrational levels to second order is given by:-

$$E(v) = \Sigma_i\omega_i(v_i+\tfrac{1}{2}d_i)+\Sigma_i\Sigma_{j\geq i}X_{ij}(v_i+\tfrac{1}{2}d_i)(v_j+\tfrac{1}{2}d_j)+W(l_i,l_j\ldots)$$

ω_i=fundamental vibrational frequency at infinitesimal amplitude

d_i=degeneracy of ω_i

X_{ij}=anharmonic constant

l_i, l_i=internal angular momentum quantum numbers ($l_i=v_i, v_i-2, \ldots 1$)

W=function of l_i, l_j ...

Many of the normal vibrations are not infrared active, since the absorption of radiation involves the interaction of the oscillating electric field vector of the radiation with the oscillating dipole of the molecule. Absorptions can, therefore, only be observed if there is a change in the dipole moment of the molecule during vibration. The dipole moment can be expressed as:-

$$\mu_k = \mu_o + (d\mu/dQ_k)\Delta Q_k$$

μ_o=permanent dipole moment

Q_k=normal coordinate describing molecular motion

If $d\mu/dQ_k=0$ then $\mu_k=\mu_o$ and no infrared absorption can occur. In order for the vibration to be spectroscopically observed in the infrared, $d\mu/dQ_k$ (or at least one of its components $d\mu_x/dQ_k$, $d\mu_y/dQ_k$ or $d\mu_z/dQ_k$) must be non-zero. Many allowed vibrations are not easily observed because of the low intensity of the band.

$$\text{Intensity } \alpha \ (d\mu_x/dQ_k)^2 + (d\mu_y/dQ_k)^2 + (d\mu_z/dQ_k)^2$$

If two of the terms equal zero and the remaining term is very small, then the band is very weak.

Normal vibrations can arbitrarily be sub-divided into two categories - **skeletal** and **group** vibrations. In the former, many atoms undergo displacement during the vibration, and modification of substituents may often result in substantial change to a number of normal modes. The spectral bands can only be assigned to individual vibrational modes with great difficulty. For certain normal modes, a single pair of atoms may exhibit large displacements whilst the remainder of the molecule is stationary. The frequencies of these modes are almost independent of the structure of the molecule as a whole and the spectral bands arising from them tend to occur in regions above or below those of the skeletal modes. The frequencies of the bands are characteristic of the group and are widely used in analysis. For example, $-NH_2$, -C=O, and -C≡N groups generally give rise to bands at 3400 cm^{-1}, 1750-1600 cm^{-1} and 2100-2250 cm^{-1} respectively.[14]

1.2.2 Fourier Transform Infrared Spectroscopy

For many years, the only widely available spectrometers for the collection of infrared data were grating instruments. With the advent of more sophisticated computer systems Fourier Transform Infrared Interferometers, with all their inherent advantages, have become more feasible alternatives to the conventional instrumentation.[15] An FTIR interferometer possesses several advantages over dispersive systems :-

i) SPEED - FTIR is N times faster and $\sqrt{N}$ times more sensitive than dispersive spectrophotometers (N=number of resolution elements in the spectrum), because all frequencies are measured simultaneously (*Felgett's Advantage*).

ii) HIGH ENERGY THROUGHPUT - The lack of slits enables all the energy to reach the sample and detector (*Jacquinot's Advantage*).

iii) ACCURACY - An FTIR system encorporates a He-Ne laser for wavelength calibration (*Conne's Advantage*).

iv) SPECTRAL MANIPULATION - Powerful data systems, which perform the Fourier transform, also allow extensive manipulation of the data.

v) STRAY LIGHT - Each frequency of the incident radiation is modulated by the interferometer (at a different but proportional frequency to ν). Since stray light is unmodulated it can make no contribution to the interferogram.

The fundamental part of the instrument is the interferometer, one type of which is the Michelson interferometer (**Fig. 1.2**). This consists of one fixed and one moving mirror, and a beamsplitter, which splits infrared radiation from a broadband source into two beams of equal intensity. Both beams are reflected back to the beamsplitter by the mirrors, where they are recombined either constructively or destructively depending on the relative displacement δ of the moving mirror to the stationary one. The resulting intensity is proportional to **sin**δ/δ and conforms to the following equation:-

$$I(\delta) = \tfrac{1}{2}I(0) + \int_0^{+\infty} I(\sigma)\cos(2\pi\delta\sigma)d\sigma$$

δ=optical path difference
I(0)=intensity at zero path difference
σ=wavenumber
I(σ)=intensity at wavenumber σ

The second term of the equation is known as the *interferogram function*:-

$$F(\delta) = \int_0^{+\infty} I(\sigma)\cos(2\pi\delta\sigma)d\sigma$$

and yields the spectrum upon Fourier transformation :-

$$I(\sigma) = \int_{-\infty}^{+\infty} f(\delta)\cos(2\pi\delta\sigma)d\sigma$$

In addition to the infrared beam, the Bruker IFS 113v interferometer used for all experiments has two other beams incorporated into the interferometer. A He-Ne

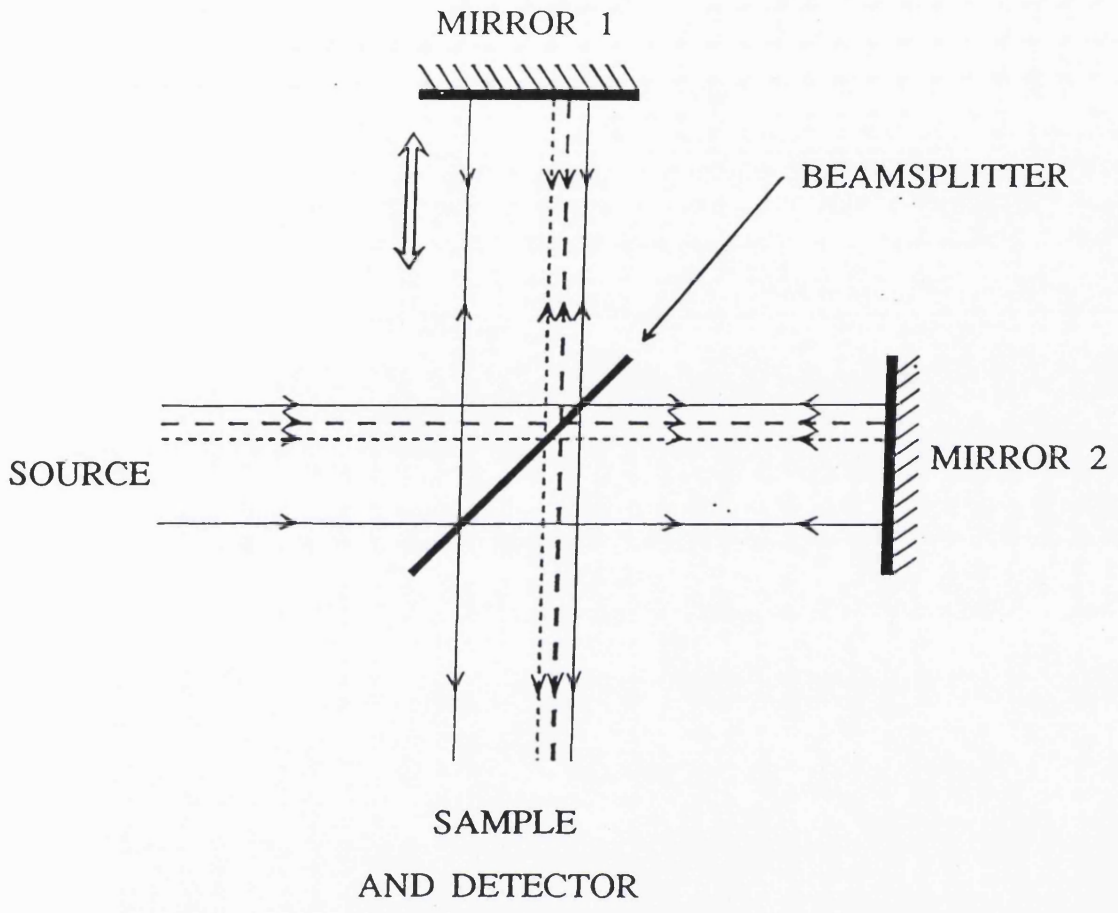

Fig. 1.2 Michelson Interferometer

laser of known wavelength ensures extremely high accuracy of frequency calibration. A beam of white light interferes constructively at the zero path difference (δ=0). This is detected and converted into a digital signal, which is used to synchronise data

collection.

The interferometer is designed in such a way that the zero path difference of the white light beam coincides with the start of the motion of the moving mirror. The scanning mirror is in constant backward and forward motion, even when spectral data is not being collected. These movements are short and rapid (a complete cycle lasts approximately 0.45 s), but lengthen during data-collection scans. The latter comprise a long, slow outward travel of the scanning mirror, during which data acquisition occurs, followed by a faster return to the starting position. For example, for a resolution of 0.5 cm^{-1}, the outward and return mirror travel are complete in 1.5 s. The digital signal from the white light interferometer is also detected every 1.5 s, since it occurs only once during each scanning motion - at the very start.

A Globar source and liquid nitrogen-cooled MCT (mercury-cadmium-telluride) detector were used for all infrared experiments. A germanium-coated potassium bromide beamsplitter was used for investigations in the mid-infrared spectral region.

1.2.3 IRRAS Cell

Work has been carried out to design and modify an IRRAS (infrared reflection absorption spectroscopy) cell, (**Fig. 1.3**) based on the standard three-electrode systems used in electrochemistry, for use with the Bruker IFS 113v evacuable Fourier Transform interferometer. Since its original conception,[16] the cell has undergone several stages of alterations, leading to improved reliabilty, air-tightness and ease of handling.

The cell is positioned on the interferometer (**Fig. 1.4**) such that the IR beam passes through an alkali halide window into a thin layer of solution, before being reflected from a highly-polished disc of platinum. It then passes through the solution again and is finally directed onto the detector using the set of mirror attachments shown in **Fig. 1.4**. The platinum disc acts both as a reflector and the working electrode of the system.

The main body of the cell (**Fig. 1.3**) is constructed from Teflon with a centrally-located sample chamber. A thin film of solution is created betwen the cell window and the base of the vertically-held working electrode. The micrometer attachment, fixed to the cell body with steel posts, allows fine control of the height

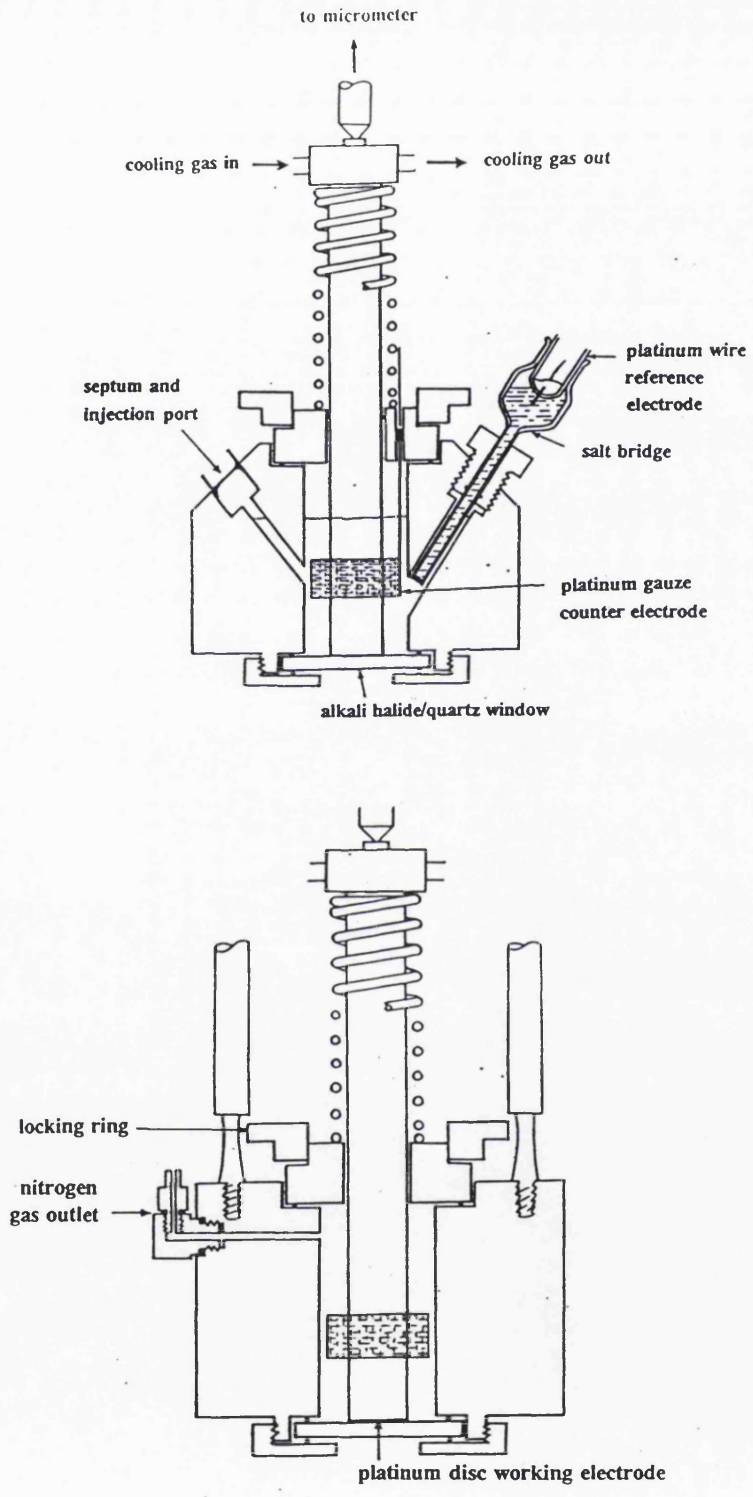

Fig.1.3 IRRAS cell, shown from two angles

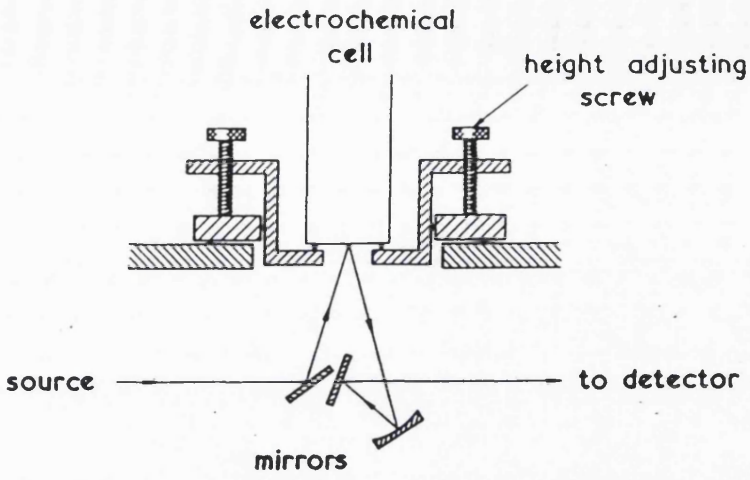

Fig.1.4 Mirror mounting arrangement present in FTIR spectrometer, directing the infrared beam onto the IRRAS cell and detector

of the electrode above the window - the film thickness can thus be accurately known to within 0.5 μm. Uniform film thickness is guaranteed by holding the working electrode firmly, using Teflon locking rings, such that it is always perpendicular to the alkali halide window.

The working electrode (**Fig. 1.5**) itself consists of a disc of platinum welded onto a brass pin, encased in a very close-fitting sleeve of Teflon to prevent bleeding of solution past the platinum disc. A tight seal can be achieved by cooling the brass pin to liquid nitrogen temperatures and push-fitting it into a warmed Teflon sleeve. Channels cut into the pin enable the electrode to be cooled by the passage of cold nitrogen gas for low temperature spectroelectrochemical studies. Initial experiments were carried out using a 5 mm diameter platinum disc electrode. However, the enhanced reaction rates obtained with smaller electrodes led to the use of 2 mm and 1 mm diameter discs.

The critical nature of the working electrode to the success of the experiments encouraged a strict regime of storage, cleaning and polishing to be followed, in order to ensure optimum results. All working electrodes were stored in a desiccator and rinsed only with distilled solvents. In order to obtain a highly-smooth and flat surface for efficient reflection of the beam, the electrodes were regularly subjected to polishing using 0.075 μm aluminium oxide (as an aqueous slurry). If the imperfections

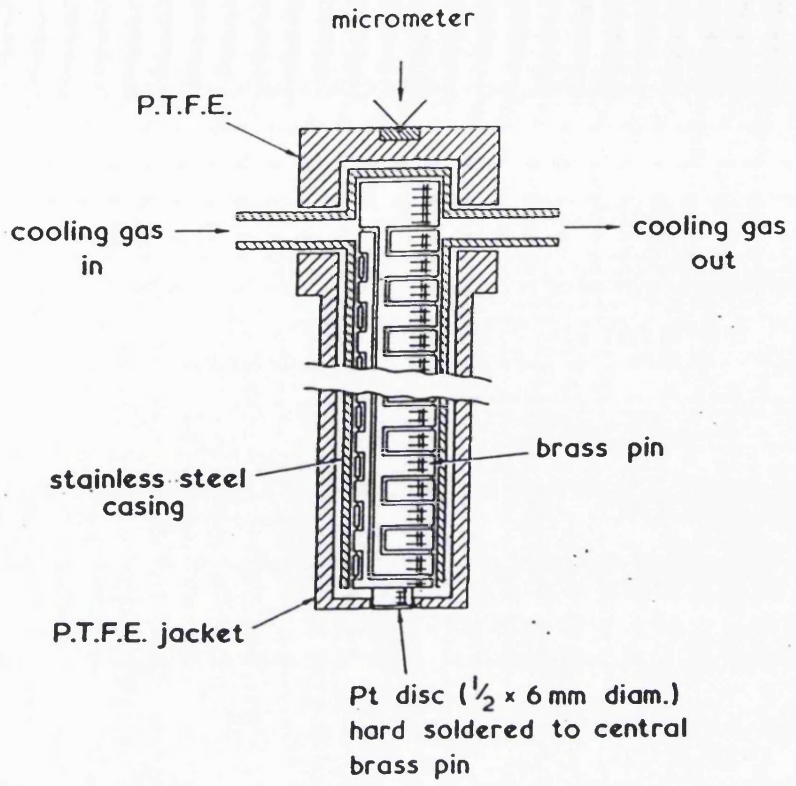

Fig.1.5 Working electrode of IRRAS cell

were judged to be more serious, this was preceded by polishing with coarser grade 1 μm cerium oxide (also as an aqueous slurry). The routine was completed by a brief period of sonication (as suggested by Armstrong et. al.[17]) to remove any adhered polishing medium.

The counter electrode consists of a circular platinum gauze surrounding the shaft of the working electrode. The gauze is spot-welded onto platinum wire, which slots into a brass socket on the underside of the Teflon retaining ring. The connection to the potentiostat is made by via a socket on the top of the ring.

The reference electrode is, effectively, a scaled-down version of the pseudo-reference system described in section 1.1. It comprises a platinum wire electrode and a salt-bridge, which fits into an adaptor, the screw-thread of which enables it to be fitted into an angled port in the body of the cell.

A significant modification was to bore another access port into the sample compartment, with a wider entrance to allow the insertion of a size B10 Subaseal. As

well as forming an air-tight seal, the septum also allows injection of air- or moisture-sensitive solutions directly into the sample chamber. The syringe needle also doubles as an entry port for the nitrogen gas used to flush the system before injection of solution and degas samples in situ. A port for the exiting gases is also provided.

The alkali halide window used for most experiments was sodium chloride. This is more resistant to chemical oxidation than potassium bromide or caesium iodide. Calcium fluoride windows were used when the compounds being examined did not have bands of interest below 1000 cm^{-1}. Quartz was substituted for the fragile alkali halide windows in ultra-violet/visible studies. All windows were carefully cleaned and polished to leave uncontaminated, flat surfaces.

1.2.4 Normal Spectroelectrochemistry

Until the 1960's, information about the mechanism and kinetics of electrode processes and the nature of the electrode-electrolyte solution interface could only be obtained from current, potential and charge measurements. Kuwana et al.[18] were the first to carry out spectroscopic investigations of the interface, when they studied the electro-oxidation of o-toluidine in aqueous hydrochloric acid. This was a transmission technique and required the use of an optically transparent electrode (OTE), such as an antimony-doped tin oxide film on a glass substrate. Three years later, Murray et al.[19] reported a different cell configuration, in which the optically transparent thin-layer electrode (OTTLE) comprised a gold minigrid sealed between two glass slides.

Both the above techniques were of use primarily in the ultra-violet/visible region of the spectrum. The advances in the infrared detection of electrochemically-generated species have occurred in the last fifteen years[20,21] and signalled a departure from transmission spectroscopic methods. The first technique to be developed was EMIRS (electrochemically modulated infrared spectroscopy),[21,22] which was designed to detect a small a.c. component of the reflection radiated from an electromodulated electrode surface.

A second technique, IRRAS (infrared reflection-absorption spectroscopy),[23] was originally developed to study gases and films on surfaces. Its major advantage over EMIRS was that a "normal" infrared spectrum was produced, whereas the results of an EMIRS experiment are displayed as a "difference" spectrum between the spectra

collected at the modulation potentials.[21]

Pons et al.[20,24] subsequently developed SNIFTERS (subtractively normalised interfacial Fourier transform infrared spectroscopy). This technique involves the repeated cycling of the potential between two values. An interferogram is collected at each change of potential. The interferograms are then coadded to give two spectra, with enhanced signal-to-noise, each representing the species in solution at one of the potentials. Although EMIRS and IRRAS experiments can be carried out using grating spectrometers, the use of a Fourier Transform Interferometer is an essential requirement of SNIFTERS.

Spectroelectrochemical experiments are generally preceded by preliminary cyclic voltammetric investigation of the compound being studied. In this way, the reversibility of the electrochemical reaction can be determined and any following reactions and other electroactive species present in solution monitored. With this knowledge, the half-wave redox potentials, $\mathbf{E_{1/2}}$, and the initial and final potentials, $\mathbf{V_i}$ and $\mathbf{V_f}$, of the electrochemical reaction can be selected. $\mathbf{V_i}$ is chosen to be a reference potential whilst $\mathbf{V_f}$ is a potential at which an electrochemical process occurs and takes a value beyond the half-wave redox potential, $\mathbf{E_{1/2}}$, of the reaction.

Normal spectroelectrochemistry, as practised here, involves the bulk electrogeneration of the oxidised/reduced species, closely resembling the investigations carried out using OTTLE's. The potential is initially held at $\mathbf{V_i}$, for a reference spectrum to be collected. It is then switched to $\mathbf{V_f}$ and spectral data is collected at regular intervals as the interconversion takes place (**Fig. 1.6a-c**)).

The usual procedure, when using the 5mm diameter working electrode, is to record a series of sixteen spectra, each spectrum being computed from ten coadded interferograms (for improved signal-to-noise). Each spectrum takes an average of 20s to collect. The first spectrum represents the initial compound and subsequent spectra show the changes gradually ocurring on oxidation/reduction, with the increase in concentration of the new electrochemically-generated species.

The timescale of experiments of this type proved to be too long to detect the shorter-lived species formed in rapidly-occuring reactions or for experiments involving the use of the smaller 2 mm diameter working electrode, where the timescale of the electrogeneration is much reduced. In these situations, spectra were computed from

a single interferogram. Careful time control of the data collection scans enabled spectra to be acquired at regular, preset intervals, of between two and ten seconds. The only disadvantage to this approach was a reduction in spectral quality, due to reduced signal-to-noise.

1.2.5 Modulation Technique

In the course of several spectroelectrochemical experiments, it was noticed that many rapid changes were occuring as the compound under investigation underwent oxidation or reduction. Often, a series of chemical reactions seemed to be initiated by the electron transfer. In some instances, following chemical reactions were observed even though cyclic voltammetric studies indicated that the reactions were electrochemically reversible. In order to study reactive oxidation/reduction products, it was necessary to develop a technique, which only required the reactive species to be present in solution for very short periods of time and at low concentrations.

In the "Modulation Technique" a potential of V_i is applied to the working electrode for a specified time, t_1. The potential is then switched to V_f and maintained at that value for time t_2. The times, t_1 and t_2, need not be the same, and may be varied according to the requirements of the experiment. This cycle of changes of potential is repeated as many times as necessary to improve the signal-to-noise ratio of the spectra and test the chemical reversibility of the reaction. The sequence of events is shown in **Fig. 1.6d-f)** and compared with normal spectroelectrochemistry (**Fig. 1.6a-c**)). It is estimated that 5-10% of the complex undergoes electrochemical reaction at each change of potential.

The repeated stepping of the potential applied to the electrode between a reference value, V_i, and a value, V_f, at which the electroactive compound undergoes reaction, closely resembles the electrochemical technique known as double potential step chronoamperometry.[2] The "Modulation Technique" is similar to Pons' method SNIFTERS,[20,24] described above.

An interferogram is collected just before every change of potential. The resulting data can be analysed in two different ways - individually computing all interferograms into spectra and examining them separately (e.g. 20 interferograms thus giving rise to a series of 20 spectra), or coadding all the interferograms collected at

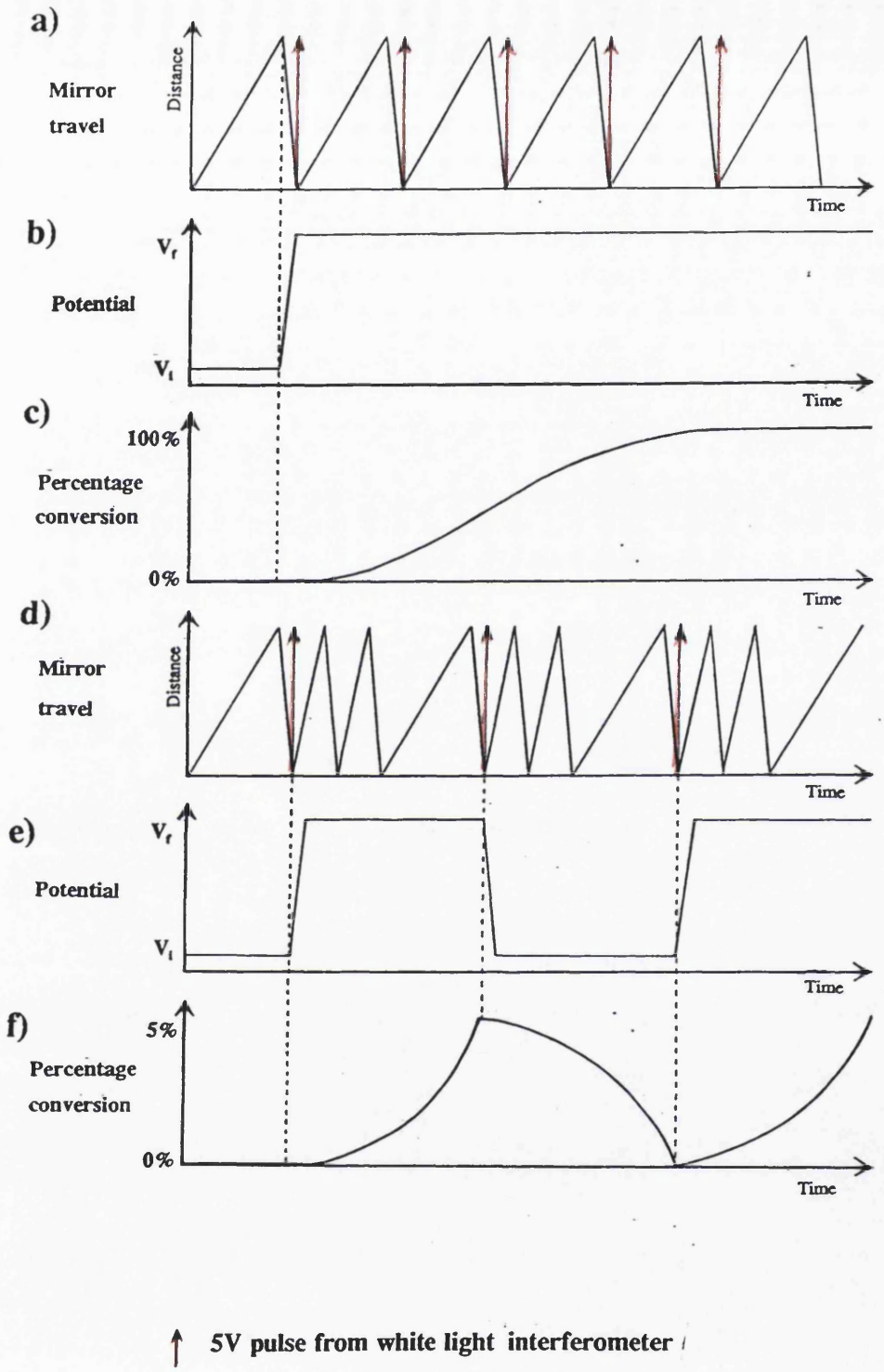

Fig.1.6 Diagram showing the synchronisation of infrared spectral data acquisition with changes of potential

V_i and computing them into one spectrum and comparing this with the result of the coaddition and computation of all the interferograms collected at V_f (e.g. 20 interferograms, 10 collected at V_i and 10 at V_f, giving rise to 2 spectra, one representing the species in solution at V_i and the other at V_f). The second approach yields spectra with better signal-to-noise, but only in chemically well-behaved systems. When the spectral changes occuring on each cycle are not repeatable, this method of analysis is unsuitable since the resultant interferograms are not of a well-defined product. Indeed, in most other cases it is preferable to analyse each interferogram individually.

The precise synchronisation necessary for this type of experiment requires the potentiostat to be interfaced with the FTIR interferometer. A BBC microcomputer is used for this purpose. The 5 V pulse derived from the white light interferometer at the commencement of every scan is detected by the BBC microcomputer and the time separation between consecutive pulses monitored. A change of potential is initiated by the computer program only after the detection of a longer, data-collection scan. The short, non data-collection scans of the interferometer are ignored. A listing of the BASIC computer program written to perform this task is given in **Appendix I**. The BASIC program used to control normal spectroelectrochemical experiments is also listed (**Appendix II**).

The hardware configuration of the experiment is as follows:- The white light interferometer, emitting regular 5 V pulses, is connected to the microcomputer using the printer port. Once the trigger is detected, the microcomputer sends out a signal to the potentiostat via a digital-to-analogue converter, which is connected to the 10MHz bus. The circuit diagram of the digital-to-analogue converter and its amplifier are given in **Appendix III**.

A gas chromatography software package, with time-resolved spectroscopy capabilities is included in the Bruker data system, and this provides the software interface necessary to control the timing of interferogram acquisitions. By constructing a variety of macro programs within this software, the times between consecutive data-collection scans can be controlled.

It is often found that the spectral data obtained in "modulation" spectroelectrochemical experiments have poor signal-to-noise ratios, which may make

subsequent analysis of the spectra difficult. This is ameliorated by using a BASIC computer program to simulate the spectral bandshapes. In this way, heights, full widths at half-height, positions and Gaussian/Lorentzian ratios can be determined for all peaks. A listing of this program is included (**Appendix IV**).

The behaviour of the current, as a function of the potential applied to the working electrode, was monitored using a Y-T chart recorder. This provided valuable additional information related to the spectroelectrochemical experiments. The current-time graph had two features of interest - the charging current and the reaction current. The former represents the amount of current required to charge the working electrode to the necessary potential and is a function of the size of the electrode; its time dependence is a function of the current output and compliance voltage of the potentiostat. The latter is a function of the current flowing in the cell as a result of the electrochemical reaction taking place. Both observations are useful in determining whether a particular reaction is proceeding in a chemically-reversible fashion. This is indicated by reproducible behaviour by each.

1.3 Ultra-violet/visible Spectroelectrochemistry

1.3.1 Ultra-violet/visible Spectroscopy

Ultra-violet/visible spectroscopy provides a powerful tool with which to probe the structure of transition metal complexes.[13] In cases where there is partial d-orbital occupancy, many of the visible spectral features are due to crystal field bands. The more intense of these are spin-allowed transitions and the less intense spin-forbidden transitions. Virtually all compounds, however, absorb in the ultra-violet region, such that spectroscopy in this region is a generally applicable technique. Most charge-transfer bands (electronic transitions between the metal and the ligand) and transitions within the ligand itself (usually $\pi \rightarrow \pi^*$ or $\sigma \rightarrow \sigma^*$ transitions) occur in the ultra-violet region of the spectrum.

Transition metal spectra were initially explained in terms of crystal field and, subsequently, ligand field theory. These state that the imposition of a non-spherical field of charge around a metal ion results in the removal of the d-orbital degeneracy.

However, crystal field theory treats ligands only as point charges. Metal-ligand interactions are taken into consideration in Molecular Orbital theory. The geometry of the ligand field determines the nature of the d-orbital splitting, whilst the ligand itself will have a significant effect upon the magnitude of this splitting. The latter phenomenon is the basis of the spectrochemical series of ligands.

The intensities of spectroscopic bands conform to the Beer-Lambert Law:-

$$\text{Absorbance} = \log(I/I_0) = \varepsilon cl$$

I_0=incident intensity
I=transmitted intensity
ε=molar decadic extinction coefficient ($dm^3mol^{-1}cm^{-1}$)
c=concentration ($moldm^{-3}$)
l=path length (cm)

ε is a measure of the probability of the electronic transition. Spin-forbidden crystal field transitions will have molar decadic extinction coefficients of the order 1-500 $dm^3mol^{-1}cm^{-1}$; the more intense, charge transfer bands have values ranging from 1000 to 10 000 $dm^3mol^{-1}cm^{-1}$.

1.3.2 Instrumentation

An Oriel Instaspec III system, incorporating multi-channel diode array detection, was used for all measurements in the ultra-violet/visible region. Light was channelled into a 0.25 m monochromator, using fibre optic light guides, and dispersed onto a 1024 pixel diode array. A spectrum could be recorded over 700 nm, if a 150 lines per millimetre grating is used, in a minimum of 0.016 s. The instrumentation was controlled from an IBM-compatible computer with 386sx processor and an enhanced graphics monitor. The computer also allowed a considerable degree of spectral manipulation as well as flexibility in data collection. The source was a 50 W/12 V tungsten lamp, normally operated at 8-9 V.

The IRRAS cell described above (**section 1.2.3**) was used without further modification, and in an analogous fashion, for ultra-violet/visible studies. However,

a different set of apparatus was necessary to direct the beam from the source onto the cell and then into the detector (**Fig. 1.7**).

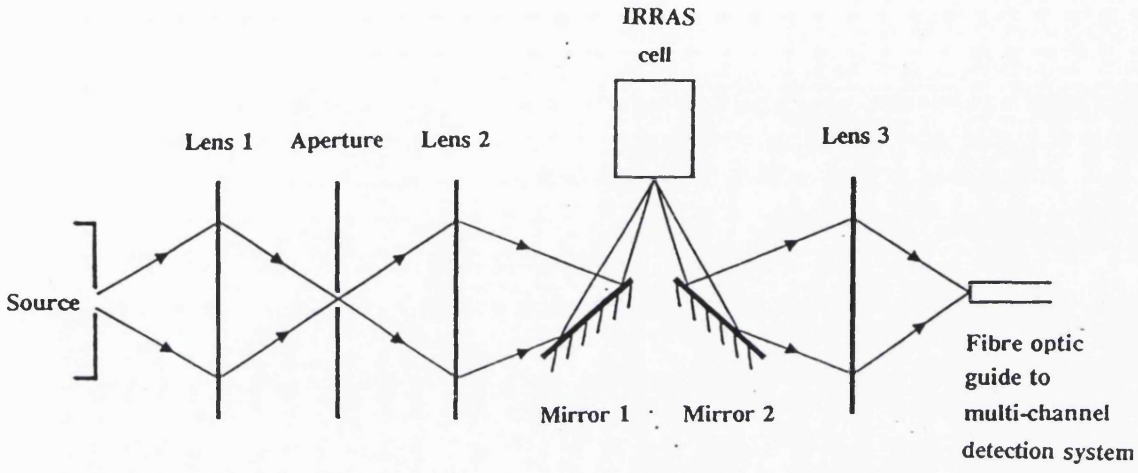

Fig.1.7 Optical path of beam ultra-violet/visible spectroscopic studies

Light from the tunsten lamp source was focussed onto a 0.5 mm aperture to create a beam of well-defined diameter. The beam was reflected from a mirror onto the working electrode of the cell. Another lens, placed between the aperture and the mirror, brought the beam to a focus at the electrode surface. The cell was rigidly held in a horizontal position by a purpose-built holder. The reflected light was collected at another mirror and focussed, using a third lens, onto an optical fibre leading into the monochromator. 25 μm slits were used throughout. Initially, optical fibres consisting of a 3.0 mm diameter bundle of fibres was used. Subsequently, a single-strand 100 μm, polymer-coated fibre was shown to be more than adequate for the requirements of the experiment.

Most of the spectra collected were computed from ten coadded scans, each recorded with an integration time of 16 ms, the delay between spectra being specified beforehand.

References

1. A. R. Denaro, "Elementary Electrochemistry", 2nd. ed., Butterworth & C., London (1979)

2. W. E. Geiger, *Prog. Inorg. Chem.*, (1985), **33**, 275

3. G. A. Mabbott, *J. Chem. Ed.*, (1983), **60**, 697

4. P. T. Kissinger, W. R. Heineman, *J. Chem. Ed.*, (1983), **60**, 702

5. D. H. Evans, K. M. O'Connell, R. A. Petersen, M. J. Kelly, *J. Chem. Ed.*, (1983), **60**, 290

6. J. T. Maloy, *J. Chem. Ed.*, (1983), **60**, 285

7. K. J. Laidler, *J. Chem. Ed.*, (1970), **47**, 600

8. W. E. Geiger, P. H. Rieger, B. Tulyathan, M. D. Rausch, *J. Am. Chem. Soc.*, (1984), **106**, 7000

9. M. Walter, L. Ramaley, *Anal. Chem.*, (1973), **45**, 165

10. K. Nakamoto, "Infrared Spectra of Inorganic and Coordination Compounds", Wiley, New York, (1963)

11. L. H. Jones, "Inorganic Vibrational Spectroscopy", Marcel Dekker, New York, (1971)

12. H. A. Szymanski, "Theory and Practice of Infrared Spectroscopy", Plenum, New York, (1964)

13. M. Orchin, H. H. Jaffé, "Symmetry, Orbitals and Spectra", Wiley-Interscience, New York, (1971)

14. C. N. Banwell, "Fundamentals of Molecular Spectroscopy", McGraw-Hill, London, (1972)

15. S. F. Johnston, *Chem. in Br.*, (1990), **26**, 573

16. S. P. Best, R. J. H. Clark, R. C. S. McQueen, R. P. Cooney, *Rev. Sci. Instrum.*, (1987), **58**, 2071

17. F. A. Armstrong, A. M. Bond, H. A. O. Hill, B. N. Oliver, I. S. M. Psalti, *J. Am. Chem. Soc.*, (1989), **111**, 9185

18. T. Kuwana, D. K. Darlington, D. W. Leedy, *Anal. Chem.*, (1964), **36**, 2023

19. R. W. Murray, W. R. Heinemann, G. W. O'Dom, *Anal. Chem.*, (1967), **39**, 1666

20. S. Pons, *J. Electroanal. Chem.*, (1983), **150**, 495

21. A. Bewick, *J. Electroanal. Chem.*, (1983), **150**, 481

22. H. Raether, "Physics of Thin Films", Vol. 7, G. Hass, M. H. Francombe, R. W. Hoffmann (eds.), Academic Press, New York, (1977)

23. E. Kretschmann, *Z. Phys.*, (1971), **241**, 313

24. S. Pons, T. Davison, A. Bewick, *J. Electroanal. Chem.*, (1984), **160**, 63

Chapter 2

Spectroelectrochemical Studies of Tris-Maleonitriledithiolate Complexes

The discovery of metalloenzymes in many biological systems generated significant interest in the properties and behaviour of related transition metal complexes. Although iron was shown to be the predominant transition metal in numerous systems, molybdenum also began to attract attention as the only second row transition metal to be essential to living organisms,[1] despite its low natural abundance compared to that of metals of the first transition series. The properties of molybdenum complexes with sulphur-donor ligands were of particular interest, as examination of many molybdoenzymes had indicated that the metal atom was bonded to the ligand system via sulphur atoms.[2] For example, the molybdenum cofactor, **Mo-co**, of the oxo-transferases exists as a molybdopterin structure (**Fig. 1** in **Introduction**). The unsaturated backbone of the pterin ligand gives rise to significant delocalisation of charge over both itself and the metal atom centre.

Accordingly, considerable effort has been directed towards the study of model complexes of all transition metals with similar, but much simpler, ligand systems with an aim to mimicking the spectroscopic and chemical characteristics of metalloenzymes.[2-4] Of particular interest are the "dithiolenes" - ligands containing the grouping $R_2C_2S_2$ (R=H, alkyl, aryl, CF_3, CN). Most transition metals react readily with dithiolene ligands to form complexes, invariably characterised by intense absorptions in the visible region and having a very rich and varied redox chemistry. In a number of cases, it is possible to isolate the complex in several oxidation states.[5-7] It is presumed that the overlap between the metal and ligand orbitals facilitates the delocalisation of charge throughout the molecule and this underlies the redox chemistry. Under these circumstances, any assignment of formal oxidation state for the metal atom is a purely notional exercise.

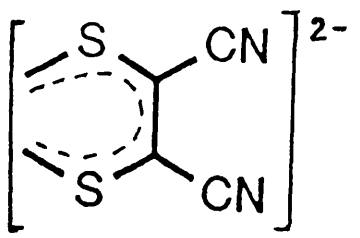

Fig. 2.1 Maleonitriledithiolate ligand

One of the most widely studied of these ligands is maleonitriledithiolate (mnt) (**Fig. 2.1**). Whereas four-coordinate bis-mnt species are well-known[8,9] (e.g. $Ni(mnt)_2^{2-}$,[10-12] $Co(mnt)_2^{2-}$,[11,13] $Pd(mnt)_2^{2-}$), the majority of metals form six-coordinate tris-mnt complexes[5,7,14,15] (e.g. $Mo(mnt)_3^{2-}$, $Fe(mnt)_3^{2-}$, $Cr(mnt)_3^{3-}$) with structures intermediate between octahedral and trigonal prismatic. These dithiolate compounds are, in fact, examples of the few compounds with molecular six-coordination which do not exhibit octahedral geometry. (Prior to this, trigonal prismatic coordination had only been reported for non-molecular, extended lattice systems such as molybdenite (MoS_2) and tungstite (WS_2)).[1] The precise nature of the coordination geometry depends upon the magnitude of the negative charge carried by the complex and the d-electron occupancy. It is generally assumed that neutral species tend towards trigonal prismatic geometry while increasing the negative charge on the complex favours an octahedral stereochemistry.[1]

X-ray crystal studies[16] have shown that the neutral species $Re(S_2C_2Ph_2)_3$ contains a virtually perfect trigonal prismatic array of sulphur atoms with a D_{3h} coordination geometry. The average intra- and inter-ligand sulphur-sulphur separations are 3.04 and 3.05 Å respectively. Other neutral complexes also have trigonal prismatic structures - $V(S_2C_2Ph_2)_3$ [17] is slightly distorted away from the trigonal prismatic to the octahedral by a trigonal twist of 8.5°; $Mo(S_2C_2H_2)_3$ has C_{3h} symmetry,[18] the $S_2C_2H_2$ rings deviating by 18° from planar. The tetramethylammonium salt of $V(mnt)_3^{2-}$, however, adopts a structure with D_3 symmetry intermediate between trigonal prismatic and octahedral,[19] whilst the tetraphenylarsonium salt of $Fe(mnt)_3^{2-}$ is octahedral.[20]

Extensive spectroelectrochemical studies have been carried out on these complexes by Best et al..[21] The mono-, di- and trianionic species of various tris-mnt complexes $M(mnt)_3^{n-}$ (n=1, 2, 3; M=V, Cr, Mn, Fe, Mo, W, Re) have been identified and the spectral data correlated with changes in structure, charge and electronic configuration. Although cyclic voltammetry indicates a second reduction wave for a

number of the complexes, leading to the formation of a tetra-anionic species, none had been detected spectroscopically.

Using the modulation technique, and the improved cell design, described in **Chapter 1**, the infrared spectra of several of the tetra-anionic tris-mnt species have been observed. Owing to the reactivity of the reduction products, the spectral changes are only reversible when smaller-diameter working electrodes are employed, and experiments conducted at reduced temperatures. Despite these precautions, it was not possible to prevent $W(mnt)_3^{4-}$ from undergoing further decomposition reactions.

2.1 Electronic Structure

A qualitative description of the electronic structure of $Re(S_2C_2Ph_2)_3$ has been proposed by Stiefel et al.[22] assuming D_{3h} symmetry for the complex (**Fig. 2.2**). The six sp^2 hybrid orbitals on the sulphur atoms, pointing towards the metal centre, interact with the d_{xz} and d_{yz} metal d orbitals (e″ symmetry). This gives rise to strongly bonding σ orbitals(2e″) localised predominantly on the ligand orbitals and strongly antibonding σ^* orbitals(4e″) localised primarily on the metal orbitals. Similarly, the six sp^2 hybrids, in the plane of the chelate ring, at 120° to the σ orbitals overlap with the d_{z^2} metal orbital (a_1') to give a ligand-based bonding π orbital ($2a_1'$) and a metal-based antibonding π^* orbital ($3a_1'$).

The mnt ligand has four ligand π orbitals lying parallel to the plane of the ring and delocalised over the S-C-C-S framework - $1\pi_v$, $2\pi_v$, $3\pi_v$ and $4\pi_v$. In the dianionic formulation of the ligand, all the levels up to and including the $3\pi_v$ are filled. Of these, the $3\pi_v$ orbital is comparable in energy to the metal d orbitals and interacts with the d_{xy} and $d_{x^2-y^2}$ orbitals to give two molecular orbitals (4e′ and 5e′). They are highly delocalised, with both metal and ligand character. The remaining $3\pi_v$ orbital (2a′) is not of a symmetry to combine with any metal orbitals and, therefore, remains non-bonding.

The $2a_1'$ and 4e′ orbitals stabilise the trigonal prism, whilst occupancy of the $3a_1'$ and 5e′ levels results in an overall destabilisation of the trigonal prism relative to the octahedron. The 4e′ and $2a_2'$ levels are completely filled in all the complexes

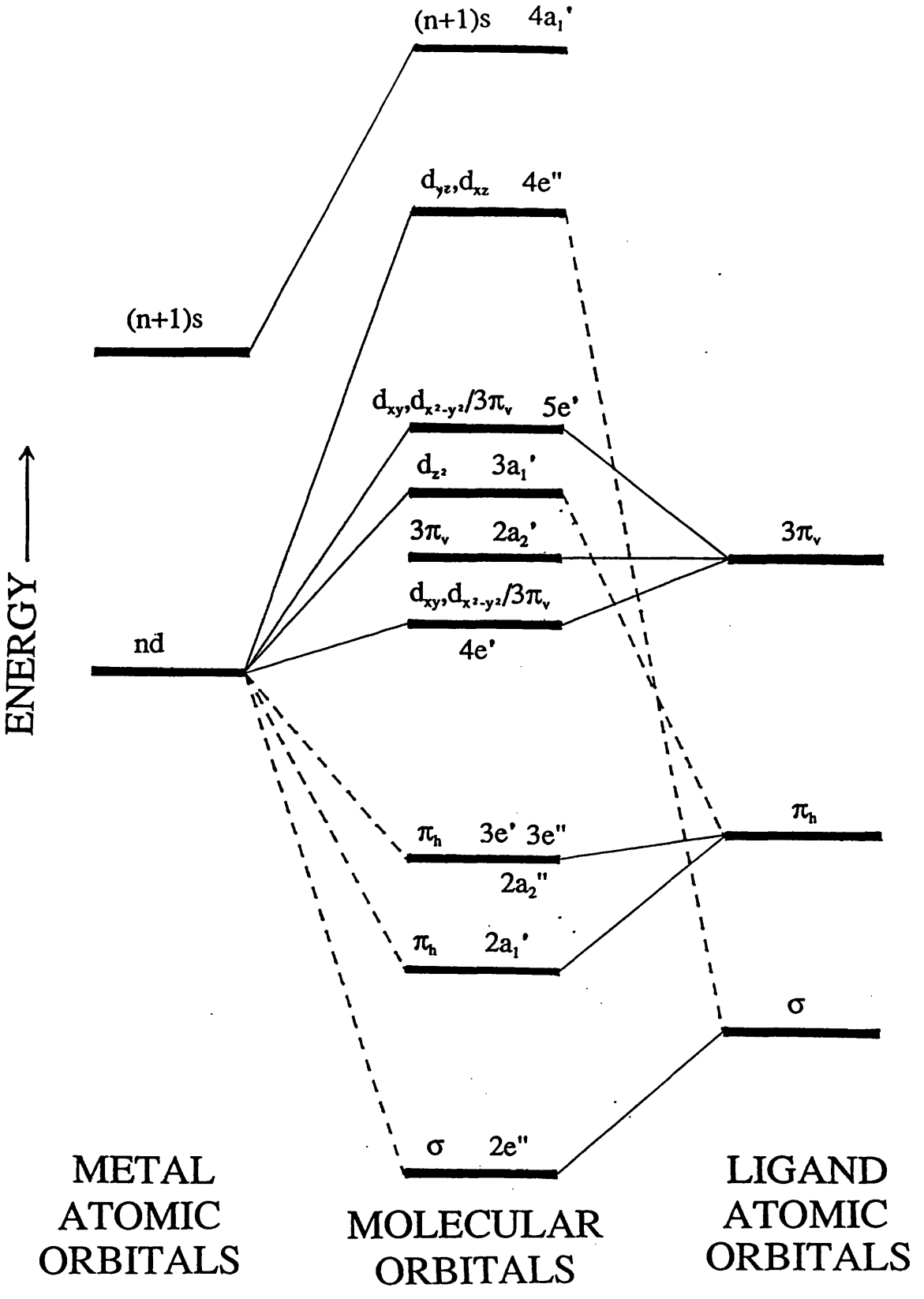

Fig. 2.2 Molecular orbital scheme for $M(mnt)_3^{2-}$ complexes

studied and occupancy of subsequent levels is dependent upon the identity of the metal involved and the overall charge of the complex.

The trigonal prismatic complex $Re(S_2C_2Ph_2)_3$ has only one electron in the antibonding $3a_1'$ orbital, which destabilises the trigonal prism, whereas $Mo(mnt)_3^{2-}$ has the ground state $(4e')^4$ $(2a_1')^2$ $(3a_1')^2$. The doubly-occupied $3a_1'$ level causes the stabilisation of octahedral geometry relative to trigonal prismatic and, as a consequence, the molecule adopts an intermediate structure. At the other extreme, octahedral geometry arises from the filling of the $5e'$ antibonding orbitals, for example in the case of $Fe(mnt)_3^{2-}$.

This model has been successful in explaining earlier Raman and e.s.r. spectroscopic results for this and other complexes.[23,24] However, assumptions were made regarding the relative energies of the metal and ligand orbitals specifically for D_{3h} geometry. These relative energies are altered as the complex deviates from D_{3h} geometry, which tends to occur as the negative charge on the complex increases, necessitating a re-evaluation of the molecular orbital scheme. As a result, an analysis of trianionic complexes has been put forward by Best et al.[21] (**Fig. 2.3**). This scheme also takes into consideration the increased metal-to-ligand π charge transfer, which results from the increased negative charge on the complex.

The energies of the metal d orbitals increase as the $M(mnt)^{n-}$ species is reduced and more electrons are fed into the system. As a result, the possibilty arises of π back-bonding from the metal $d\pi$ to the ligand $4\pi_v$ orbitals. The ligand π-acceptor orbital, $4\pi_v$, is a cyanide antibonding orbital. The molecular orbitals of interest are, therefore, $4e''$ (. delocalised orbitals with both ligand and metal character), $5e'$ (non-bonding metal orbitals), $3a_1'$ (a metal-based, antibonding orbital), a_1'' (a non-bonding ligand orbital) and $5e''$ (delocalised, strongly antibonding orbitals).

The ultra-violet/visible spectra of tris-mnt complexes are very sensitive to the formal oxidation state and the identity of the metal atom. All complexes of the first row transition metals have a band near 15 000 cm^{-1}, and complexes of metals adjacent to one another in the periodic table have at least one other band in common. However, electronic transitions are very sensitive to the stereochemistry of the complex and the electronic spectra are, at best, difficult to interpret and, at worst, ambiguous.

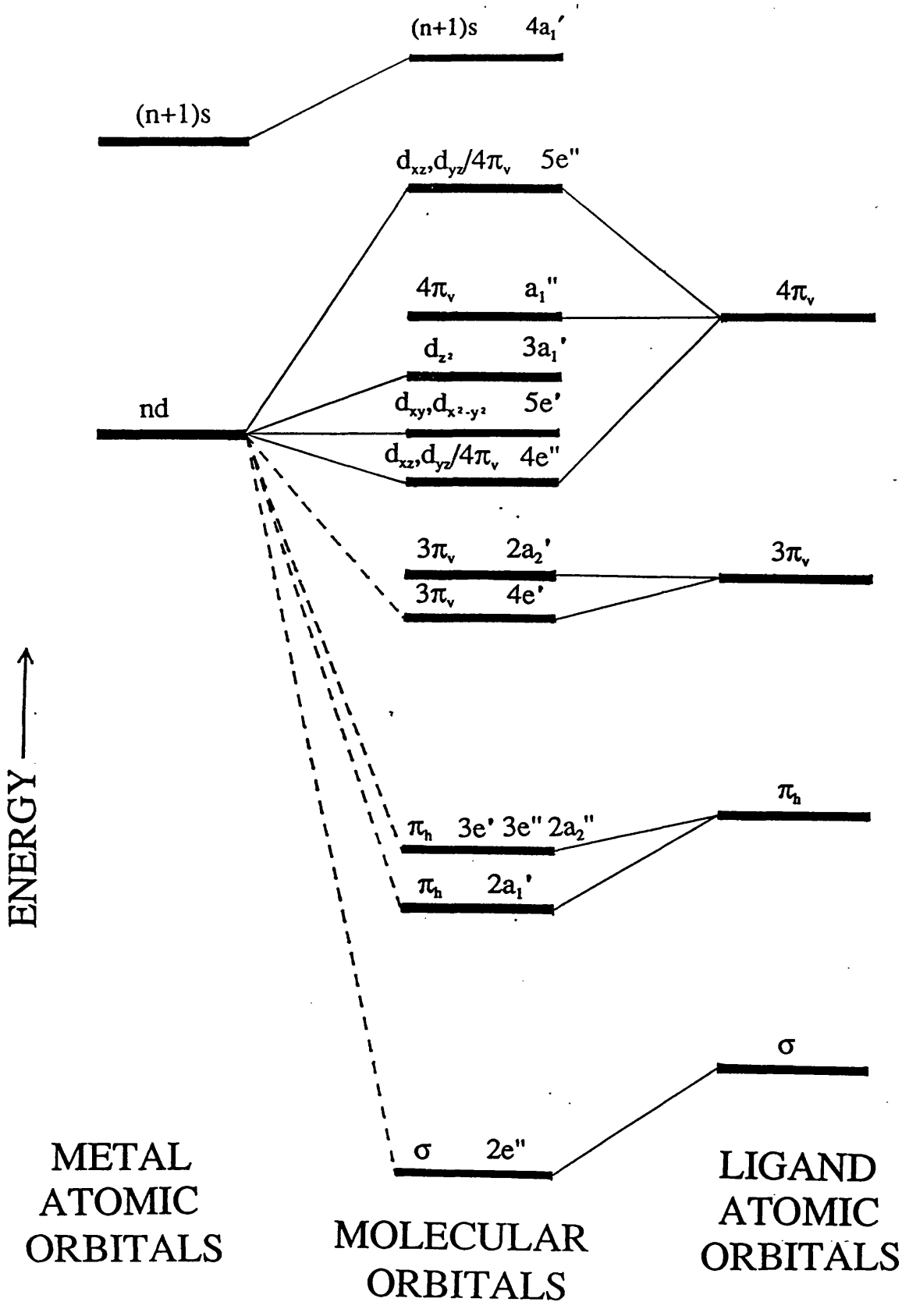

Fig. 2.3 Molecular orbital scheme for $M(mnt)_3^{3-}$ complexes

Another way of examining these complexes is to use vibrational spectroscopy. Most vibrational modes are usually highly mixed, which makes assignment to spectral bands difficult. Local vibrational modes, however, are virtually independent of the remainder of the molecule and more easily interpreted. Their spectral bands generally occur at wavenumbers above or below skeletal vibrational modes. The cyanide stretching vibration, ν(CN), is an excellent example of this type of mode.

The cyanide groups of the mnt ligand give rise to very intense absorption bands in the infrared spectrum between 2150 and 2220 cm^{-1}. The wavenumber and intensity of this band are very sensitive to the charge on the complex - the more reduced or negatively-charged the molecule, the greater the extent of metal dπ to ligand π back-bonding. This entails partial or complete filling of ligand $4\pi_v$ orbitals (antibonding with respect to cyanide) with the resultant effect of lengthening the carbon-nitrogen bond. As a consequence, ν(CN) is seen to shift to a lower wavenumber. Mono-, di- and trianionic tris-mnt species have been shown to display this type of behaviour.[21]

Further information can be obtained about frontier molecular orbitals from the intensities of cyanide stretching bands. From his study of transition metal hexacyano complexes, Jones[25] has shown that the intensity of the band is directly proportional to the extent of metal-to-ligand back-bonding. These conclusions have been upheld by the work of Best et al.[21]

2.2 Electrochemistry

The electrochemistry of tris-mnt complexes has been studied both in dichloromethane and acetonitrile.[5,21] Each compound undergoes at least two reversible redox steps, many undergo three, and molybdenum and rhenium both undergo two oxidations and two reductions. The results are given in **Table 2.1**. Most redox couples are reversible in cyclic voltammetry experiments. The second reductions of the tungsten and rhenium complexes occur at very negative potentials and are, therefore, observable only in acetonitrile, which has a larger negative potential range than dichloromethane.

Table 2.1 Redox potentials of $M(mnt)_3^{n-}$ complexes

Metal	0/1-	1-/2-	2-/3-	3-/4-
V		+0.70	-0.35	-1.65
Cr		+0.66‡	+0.17	-1.13
Mo	+1.28	+0.73	-0.95	-1.78
W		+0.68‡	-1.16	-1.76
Re	*+0.95**	+0.17	-0.59	*-2.09**

*Data from reference *5* in acetonitrile vs Ag/Ag^+

‡Irreversible at 20 °C; reversible at -20 °C

2.3 Synthesis

2.31 Molybdenum

The compound was prepared according to the method of Stiefel et al.[5] A solution of molybdenum (V) chloride (1.46 g; $5.35x10^{-3}$ mol) in absolute ethanol (10.5 cm^3) was added gradually, with stirring, to a suspension of sodium maleonitriledithiolate (2.79 g; 0.015 mol) in absolute ethanol (20.5 cm^3). Almost immediately, the solution began to turn dark green. After 30 minutes, tetra-n-butylammonium bromide (1.62 g; $5.04x10^{-3}$ mol) was added with the resultant

formation of a precipitate. The mixture was allowed to stand for a further 10 minutes before the solid was removed by filtration. The dark green crystalline solid was recrystallised twice from dry dichloromethane/absolute ethanol and washed thoroughly with absolute ethanol and ether before being vacuum dried.

Yield of $(Bu_4N)_2Mo(mnt)_3$:- 2.22 g; 45%

Elemental analysis:-

Calculated:-	C=52.77%	H=7.25%	N=11.19%	S=19.21%
Found:-	C=52.56%	H=7.23%	N=11.07%	S=19.57%

2.32 Vanadium

This compound was prepared according to the method of Davison et al.[26] Anhydrous vanadium (III) chloride (0.54 g; 3.43×10^{-3} mol) was added to a suspension of sodium maleonitriledithiolate (2.01 g; 0.011 mol) in tetrahydrofuran (50 cm^3). The solution was stirred for 30 minutes, filtered, and a solution of tetraphenylarsonium chloride (4.30 g; 0.010 mol) in ethanol (45 cm^3) was added. The resulting precipitate was removed by filtration and washed with ethanol. The black crystalline solid was recrystallised from acetone/water, washed with ethanol and dried under vacuum.

Elemental analysis of $(AsPh_4)_2V(mnt)_3$:-

Calculated:-	C=58.20%	H=3.26%	N=6.79%	S=15.54%
Found:-	C=58.03%	H=3.14%	N=6.78%	S=15.04%

2.33 Chromium

The chromium complex was prepared using Davison's procedure.[26] A solution of chromium (III) chloride hexahydrate (1.25 g; 4.69×10^{-3} mol) in water (30 cm^3) was added to an aqueous solution of sodium maleonitriledithiolate (2.71 g; 0.0146 mol). After heating for 20 minutes, a solution of tetraphenylarsonium chloride (6.03 g; 0.144 mol) in ethanol (60 cm^3) was added. The resulting dark brown solid was filtered off and recrystallised twice from hot dimethylformamide/water.

Elemental analysis of $(Ph_4P)_3Cr(mnt)_3$:-

Calculated:-	C=62.18%	H=3.73%	N=5.18%
Found:-	C=65.12%	H=4.04%	N=5.60%

2.34 Tungsten

This compound was prepared according to the method of Stiefel et al.[5] A solution of tungsten (VI) chloride (0.92 g; 2.32×10^{-3} mol) in ethanol (15 cm^3) was added to a solution of sodium maleonitriledithiolate (1.42 g; 7.63×10^{-3} mol) in ethanol (20 cm^3). The solution was allowed to stand for 20 minutes and tetrabutylammonium bromide (1.65 g; 2.92×10^{-3} mol) was added. The mixture was cooled and the resulting crystals collected, recrystallised from dichloromethane/ethanol, washed with ether, and vacuum dried.

Elemental analysis of $(Bu_4N)_2W(mnt)_3$:-

Calculated:-	C=48.51%	H=6.66%	N=10.29%
Found:-	C=48.39%	H=6.49%	N=8.89%

2.35 Rhenium

The rhenium tris-maleonitriledithiolate complex was prepared according to the method of Stiefel et al.[5] The synthesis was carried out under anaerobic conditions. Sufficient ethanol (ca. 50 cm^3) was added to sodium maleonitriledithiolate (1.70 g; 9.15×10^{-3} mol) under nitrogen for it to dissolve. Tetraphenylarsonium chloride (2.01 g; 4.80×10^{-3} mol) was added to the solution, followed by rhenium (V) chloride (0.90 g; 2.48×10^{-3} mol). The mixture was stirred under nitrogen for 1 hour and 45 minutes and filtered. The dark green solid was washed with ethanol and recrystallised twice from acetone/ethanol. It was finally washed with cold ethanol and ether and dried under vacuum. A side-product of the reaction is the oxo complex $ReO(mnt)_2^-$.

Elemental analysis of $(AsPh_4)_2Re(mnt)_3$:-

Calculated:-	C=52.47%	H=2.94%	N=6.12%
Found:-	C=53.63%	H=3.07%	N=5.82%

2.4 Infrared Spectroelectrochemistry

2.41 Molybdenum

The complex $Mo(mnt)_3^{2-}$ undergoes two reversible one-electron oxidations and two reversible one-electron reductions (**Table 2.1**). While the first oxidation and reduction give well-defined products, which have already been characterised using standard spectroelectrochemical techniques (**Table 2.2**; **Fig. 2.4**), the remaining processes give ill-defined results.

Table 2.2 Infrared band maxima (ν(CN)) for $M(mnt)_3^{n-}$ complexes

Metal	$M(mnt)_3^{1-}$	$M(mnt)_3^{2-}$	$M(mnt)_3^{3-}$
V	2216.1 2224.0 (sh)	2203.1 2215.0 (sh)	2188.1
Cr	2213.7	2202.6	2190.5
Mo	2215.6 2224.0 (sh)	2202.6 2213.0 (sh)	2177.5
W	2216.9 2225.0 (sh)	2202.4 2213.0 (sh)	2169.8 2193.0 (sh)
Re	2216.6 2226.0 (sh)	2202.7 2218.0 (sh)	2178.8 2200.0 (sh)

Following the one-electron oxidation to the monoanion:-

$$Mo(mnt)_3^{2-} \rightleftharpoons Mo(mnt)_3^{1-} + e^-$$

the cyanide stretching mode at 2202.6 cm^{-1} (with a shoulder at 2213.0 cm^{-1}) shifts to 2215.6 cm^{-1} (with a shoulder at 2224.0 cm^{-1}) via an isosbestic point, suggesting a one-step reaction with no intermediates (**Fig. 2.4a**).

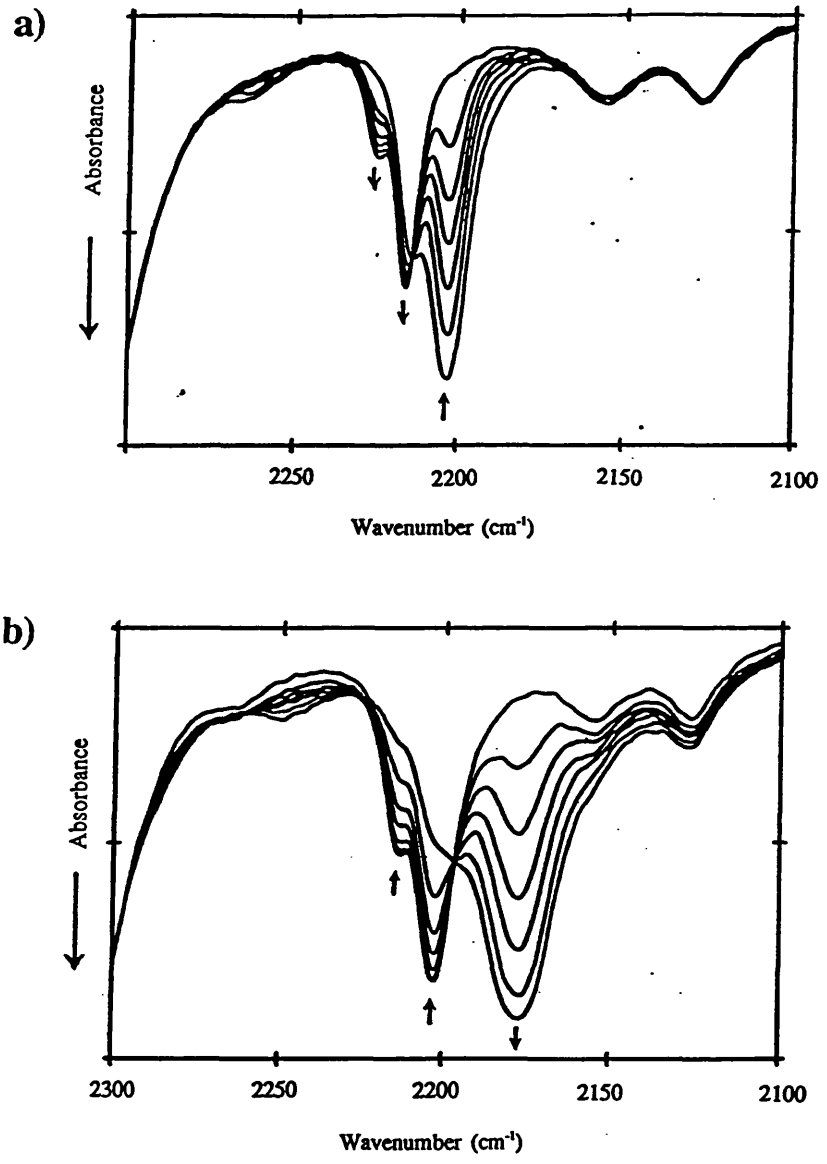

Fig. 2.4 Changes observed in ν(CN) during normal spectroelectrochemistry
a) on oxidation to $Mo(mnt)_3^{1-}$ **b)** on reduction to $Mo(mnt)_3^{3-}$

On one-electron reduction to the trianion:-

$$Mo(mnt)_3^{2-} + e^- \rightleftharpoons Mo(mnt)_3^{3-}$$

ν(CN) moves to lower wavenumbers (2177.5 cm^{-1}) (**Fig. 2.4b**). Both reactions are chemically reversible, the starting material being regenerated completely on switching the potential back to V_i (0.0 V in each case). The intensities of the bands are seen to increase progressively with increasing negative charge on the anion.

These results show that the well-behaved first oxidation and first reduction are ideally suited for use as test reactions during the development and testing of the modulation technique. In this way, the optimum experimental conditions were achieved. The first spectra were obtained using solutions of comparable concentration to those used in standard spectroelectrochemistry, a 5 mm diameter working electrode and films between 10 and 20 μm thick. 200 scans were recorded (100 at V_i=0.2 V; 100 at V_f=1.2 V) at time intervals of 3.3 s and coadded to give two spectra with improved signal-to-noise. In the difference spectrum for the oxidation (**Fig. 2.5a**) the negative peak is indicative of the extent of depletion of the dianionic species, whilst the positive peak is due to the generation of the monoanion. The decrease in intensity of the ν(CN) band on oxidation is sharply emphasised.

Similarly, by cycling the potential applied to the 5 mm working electrode of the cell between V_i=-0.5 V and V_f=-1.4 V every 1.1 s, a comparable spectrum was obtained for the one-electron reduction to the trianionic species (**Fig. 2.5b**). Once again, the two negative peaks are due to the depletion of the starting material, and the more intense positive peak at 2177.5 cm^{-1} is evidence of the formation of $Mo(mnt)_3^{3-}$.

The high spectral quality of these results is an indication of chemical, as well as electrochemical, reversibilty of the reaction. If the proportions of the species in solution undergoing redox reaction at each change of potential are comparable, assuming negligible decomposition, then all scans collected at a certain potential are virtually identical. The resultant spectrum, upon coaddition of the individual scans, has enhanced signal-to-noise and distinct peaks. In the case of irreversible reactions the starting material is gradually depleted as the experiment progresses, giving rise to scans with a large variety of peak intensities. As a result, the spectra obtained upon

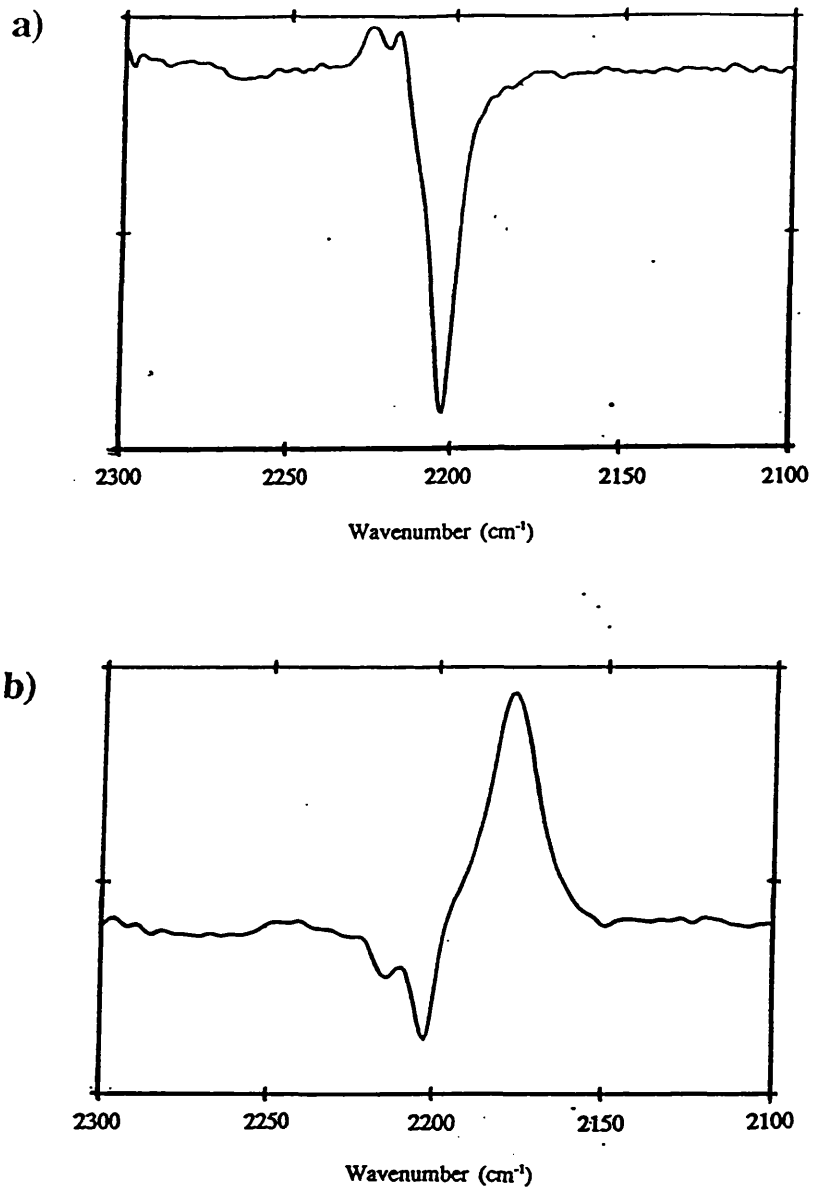

Fig. 2.5 Difference absorbance spectra modulated spectroelectrochemical studies **a)** reduction to $Mo(mnt)_3^{3-}$ **b)** oxidation to $Mo(mnt)_3^{1-}$

coaddition have very low signal-to-noise quality and very indistinct, and often spurious, peaks.

In subsequent experiments each scan of the series was computed into an individual spectrum and examined separately. All spectra acquired at V_i are superimposable and differ from those collected at V_f, which are themselves

superimposable (**Fig. 2.6**). Approximately 5-10% of $Mo(mnt)_3^{2-}$ undergoes oxidation/reduction at each potential step.

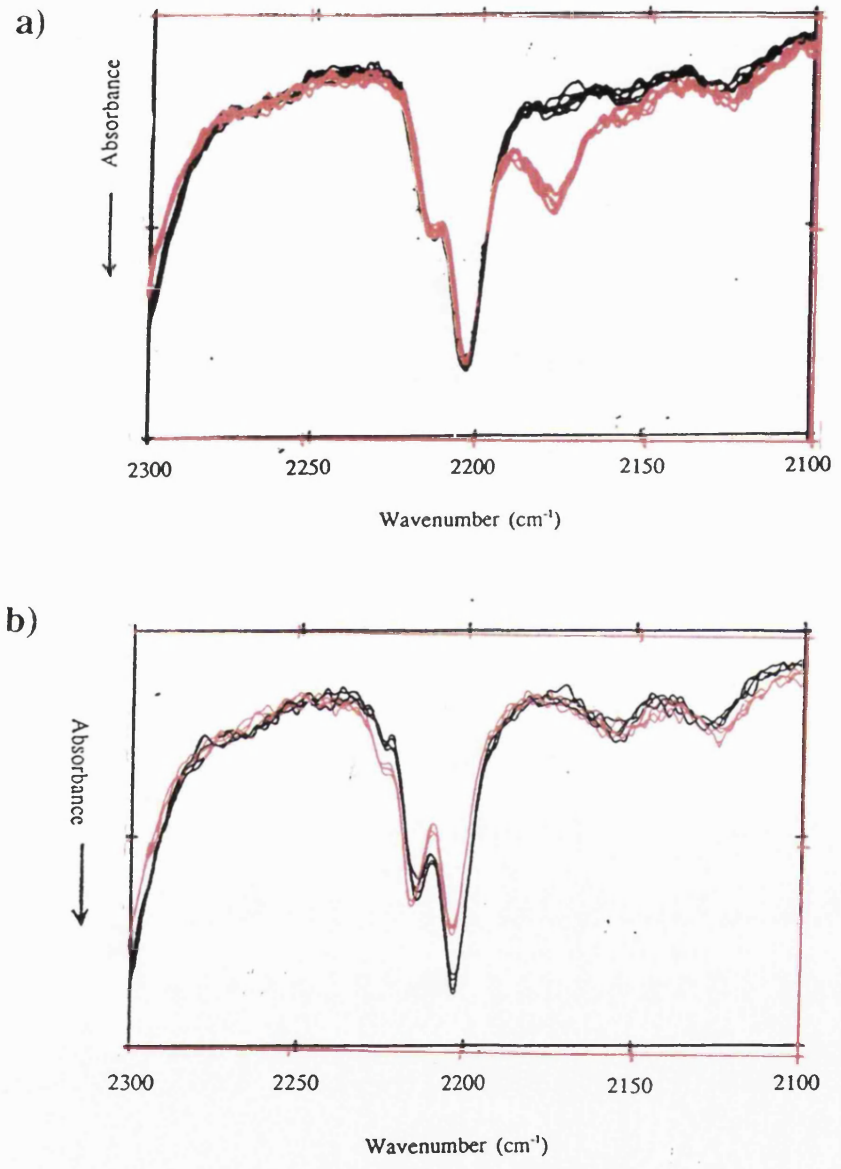

Fig. 2.6 Modulated spectroelectrochemical studies, showing changes in ν(CN) **a)** oxidation to $Mo(mnt)_3^{1-}$ **b)** reduction to $Mo(mnt)_3^{3-}$

Further analysis revealed that little or no redox chemistry occurred on the first potential cycle and fully reversible behaviour was not attained until at least the second cycle. This explains the observation that improved spectral quality resulted not only

from coadding an increased number of scans, but also from discarding the first two or four scans of a series. Analogous effects are often observed in cyclic voltammetric studies, where the initial scan is similarly rejected.

Examination of the second reduction of $Mo(mnt)_3^{2-}$ by modulation techniques gave some indication of a chemically reversible transformation. The electrogenerated species was found to be insufficiently stable at room temperature for the acquisition of spectral data, and the reduced reaction rate associated with larger working electrodes effectively precluded their use in these circumstances. However, experiments carried out using the smaller, 2 mm diameter, working electrode at reduced temperatures enabled spectra of the tetra-anionic species to be collected. A very broad band was observed at 2134.0 cm^{-1} when the potential was switched between -1.3 and -1.9 V every 3 s (**Fig. 2.7**). Although relatively small amounts of $Mo(mnt)_3^{4-}$ are generated, there is evidence to show that ν(CN) is very much more intense than for the trianionic species. Under these conditions, the reaction is both electrochemically and chemically reversible.

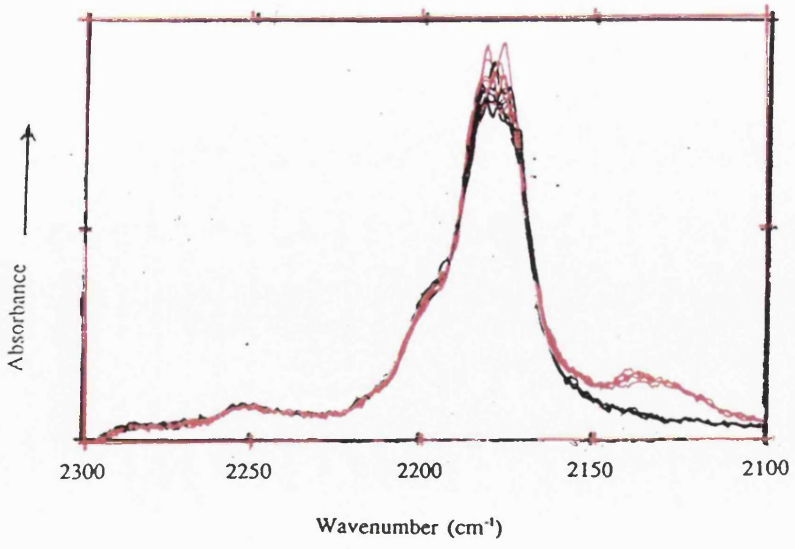

Fig. 2.7 Series of spectra obtained using modulated spectroelectrochemical techniques, indicating the formation of a ν(CN) band for $M(mnt)_3^{4-}$

2.42 Vanadium

Cyanide stretching frequencies have already been determined for the mono-, di- and trianionic complexes of $V(mnt)_3^{2-}$,[21] but there had been little success in identifying the tetra-anionic species. The second one-electron reduction of the vanadium complex occurs at -1.65 V - only the chromium complex $Cr(mnt)_3^{2-}$ undergoes the second reduction at a less negative potential (**Table 2.1**). As a result, $V(mnt)_3^{4-}$ can be generated at room temperature in dichloromethane. $\mathbf{V_i}$ was taken to be -0.6 V; $\mathbf{V_f}$ was -1.8 V.

The modulation technique produced spectra with a peak at 2164.0 cm^{-1}, much broader and more intense than that of the trianion (**Fig. 2.8**). The reaction is completely reversible and proceeds via an isosbestic point. Reducing the temperature of the experiment increases the lifetime of the tetra-anion, but also seems to promote the formation of a film of solid on either the surface of the cell window or the working electrode, indicated by a marked increase in overall absorbance and simultaneous loss of signal-to-noise.

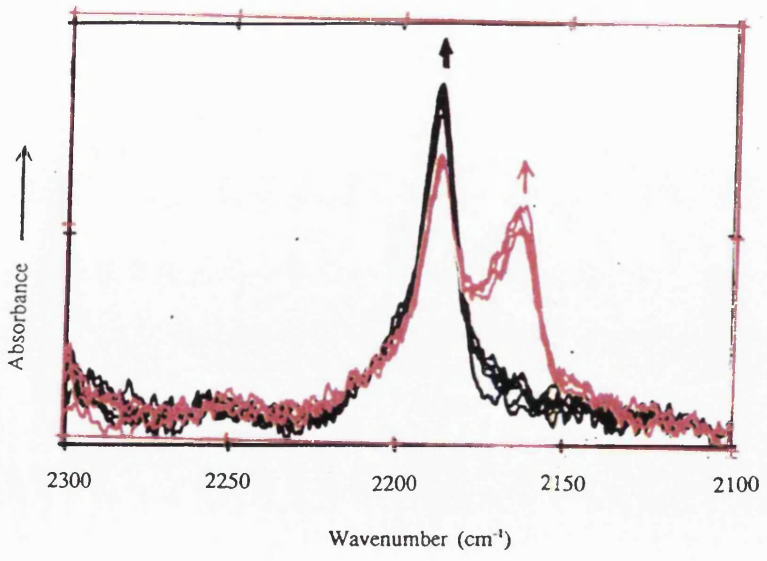

Fig. 2.8 Series of spectra obtained using modulation spectroelectrochemical techniques, indicating the formation of a ν(CN) band for $V(mnt)_3^{4-}$

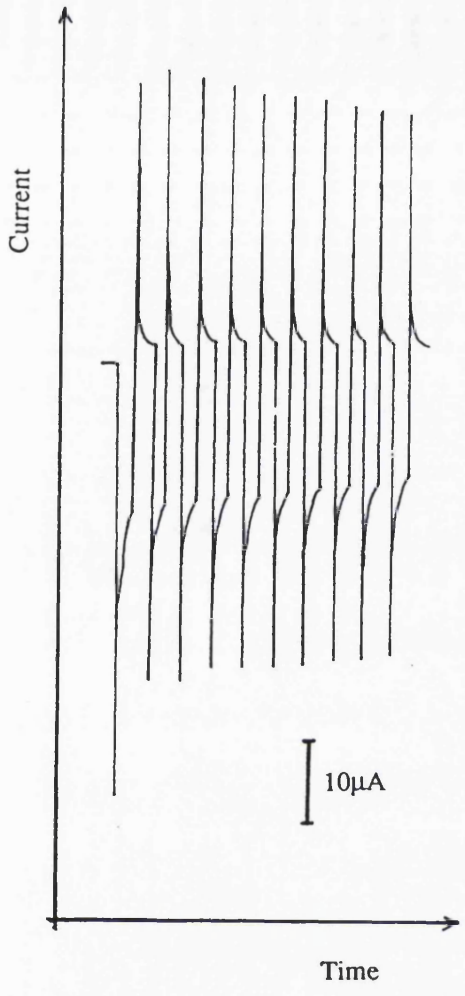

These results were corroborated by the current versus time graphs recorded (**Fig. 2.9**) during the course of the experiment. After the initial 2-4 scans, both the charging and reaction currents adopt a uniform pattern, at both potentials V_i and V_f, which is maintained for the duration of the experiment.

Fig. 2.9 Current response for the modulated spectroelectrochemical reduction to $V(mnt)_3^{4-}$

2.43 Chromium

Despite having a relatively positive half-wave redox potential for the reduction to the tetra-anion, spectroelectrochemistry could only be successfully carried out on acetonitrile solutions. When dichloromethane is used as the solvent, the spectral changes which occur on reduction are too small and indistinct to be easily monitored.

As the temperature at which the experiment is carried out is reduced, the lifetime of the tetra-anion $Cr(mnt)_3^{4-}$ in acetonitrile solution increases, but the chemical reversibilty of the reaction is not improved. The best results are obtained when only

3 s are allowed for the reduction to the tetra-anion, but 10 s are allowed for the re-oxidation to the trianion. This suggests that the complex undergoes a significant chemical transformation following electron transfer.

Of all the metal compounds studied, only the chromium tetra-anionic complex exhibits a multiplicity of cyanide stretching bands; a broad band at 2171.2 cm^{-1} and a second, less intense, one at 2163.0 cm^{-1} (**Fig. 2.10**).

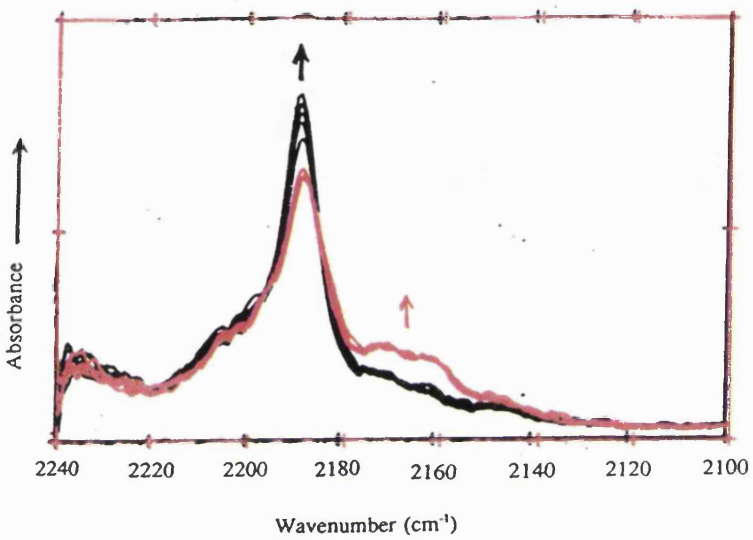

Fig. 2.10 Series of spectra obtained using modulated spectroelectrochemical techniques, indicating the formation of a ν(CN) band for $Cr(mnt)_3^{4-}$

2.44 Rhenium

The rhenium complex $Re(mnt)_3^{4-}$ is one of the more reactive tetra-anionic compounds studied. Use of the 2 mm diameter working electrode combined with reduced temperatures and acetonitrile solvent are required to record spectra of the electrogenerated species. However, under these conditions, the spectroelectrochemical results indicate that reaction to the tetra-anion is completely reversible (**Fig. 2.11**). The reaction proceeds via an isosbestic point. The new peak was observed at 2133.0 cm^{-1}.

Confirmation of reversibilty was obtained from current-time graphs (**Fig. 2.12**), which showed uniform behaviour of the charging and reaction currents.

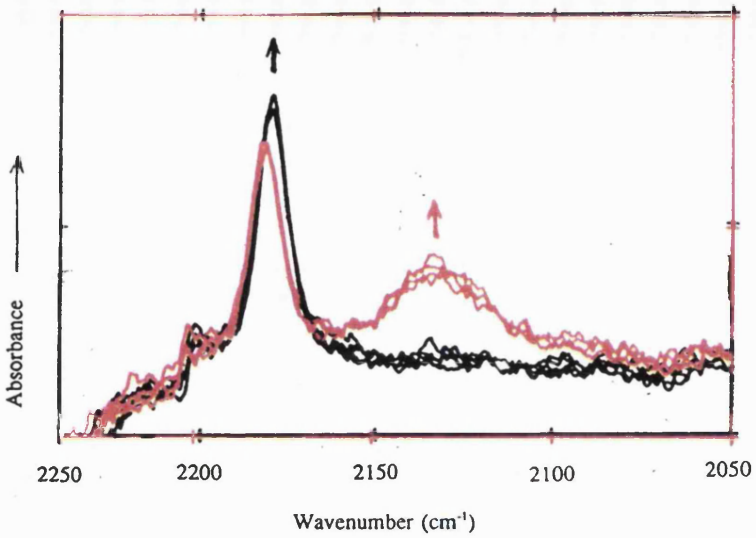

Fig. 2.11 Series of spectra obtained using modulated spectroelectrochemical techniques, indicating the formation of a ν(CN) band for $Re(mnt)_3^{4-}$

2.45 Tungsten

The second reduction wave occurs at the most negative potential (-2.19 V) of all the tris-mnt complexes studied when the metal involved is tungsten (**Table 2.1**). As a result, spectroelectrochemistry can only be carried out on acetonitrile solutions. Most of the modulation experiments carried out on $W(mnt)_3^{2-}$ were done so at reduced temperatures in an attempt to stabilise the reactive tetra-anionic species. Despite these precautions, the reactions following electron transfer are probably the most complicated observed for a molecule in this series.

As the potential is switched to $\mathbf{V_f}$, the ν(CN) peak of the trianionic species at 2169.8 cm^{-1} is seen to collapse and a new band simultaneously grows at 2054.0 cm^{-1} (**Fig. 2.13**). The new band has approximately twice the width at half-height of the parent peak, and is extremely intense. However, even when the reaction is monitored using "asymmetric" timescales (e.g. maintaining the potential at $\mathbf{V_f}$ for 2 s and at $\mathbf{V_i}$ for 10 s) at -20 °C no regeneration of the trianionic complex was observed. Spectra obtained at $\mathbf{V_f}$ are superimposable with respect to the changes associated with the 2054.0 cm^{-1} peak, which collapses at $\mathbf{V_i}$, but all spectra, including those collected at $\mathbf{V_i}$, show a steady, and apparently irreversible, depletion of the 2169.8 cm^{-1} band. The

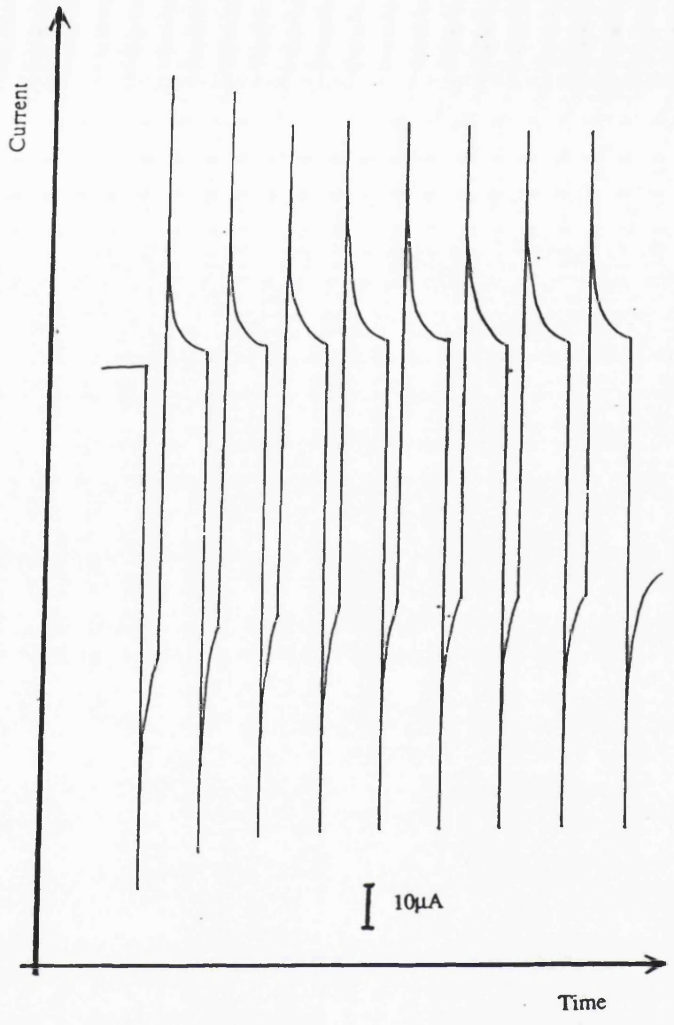

Fig. 2.12 Current response for the modulated spectroelectrochemical reduction to $Re(mnt)_3^{4-}$

absence of any solid formation is indicated by good spectral quality throughout the experiments, the absence of baseline shifts and the lack of any effect as a result of cleaning the working electrode.

Closer examination reveals a group of small, indistinct peaks below 2200 cm^{-1}, which appear and disappear in concert with the band at 2054.0 cm^{-1}. When the potential is set at V_f, the 2054.0 cm^{-1} peak is at its maximum intensity and the small bands are not apparent; as the potential is switched and the former collapses, a peak at 2194.4 cm^{-1}, with shoulders at 2202.6 and 2183.8 cm^{-1}, grows into the spectrum. Modulation experiments suggest that chemical reversibility, on this timescale, is

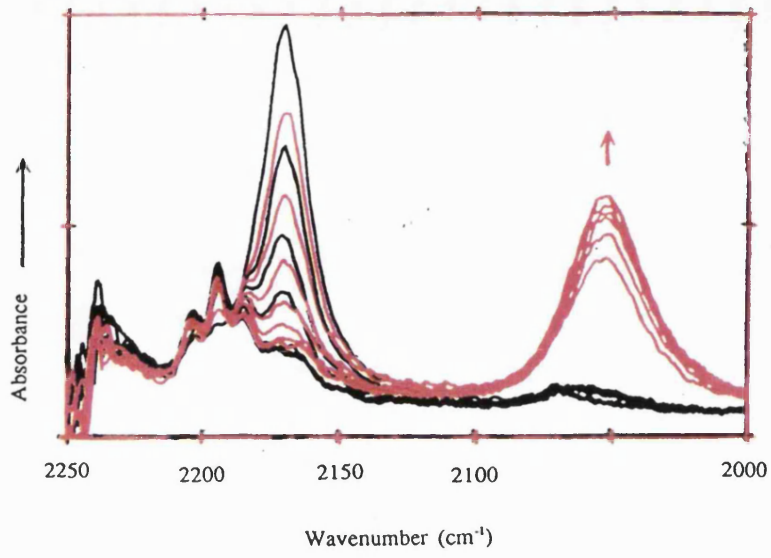

Fig. 2.13 Series of spectra obtained using modulated spectroelectrochemical techniques for the one electron reduction of $W(mnt)_3^{3-}$

between the species responsible for the 2054.0 and 2194.4/2202.6/2183.8 cm^{-1} bands, and not between the 2054.0 and 2169.8 cm^{-1} ones. It is also noted that the 2054.0 cm^{-1} band loses intensity slightly at the end of the experiment when all the $W(mnt)_3^{3-}$ complex had been consumed (as indicated by the disappearance of the parent 2169.8 cm^{-1} band).

When spectroelectrochemical experiments are conducted in acetonitrile, the associated current-time graphs show very large charging and reaction currents at V_f, which decrease sharply as the experiment proceeds (**Fig. 2.14**). Although this effect becomes less pronounced with the use of the "asymmetric" timescale, it does not at any point disappear. This is usually an indication of the general chemical irreversibility of a reaction.

2.5 Discussion

Both the conventional electrochemistry and the modulation experiments are consistent with chemical and electrochemical reversibilty for the second reduction, forming the tetra-anionic species of molybdenum, vanadium, chromium and rhenium,

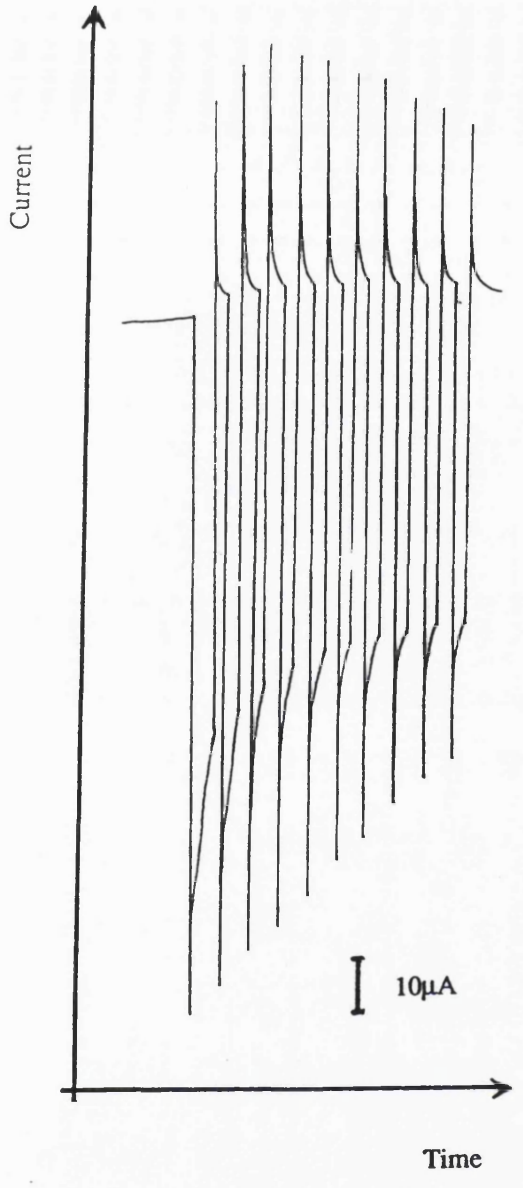

Fig. 2.14 Current response for the modulated spectroelectrochemical reduction of $W(mnt)_3^{3-}$

whereas for $W(mnt)_3^{3-}$ the reduction was found to be chemically irreversible. The starting material is regenerated completely in a time comparable, or identical, to that allowed for the prior reduction. This suggests that no chemical transformation occurs on electron transfer, which is fast, and that the electrogenerated product is sufficiently stable not to undergo decomposition on the timescale of the modulation experiment.

With the repeated stepping of the potential between V_i and V_f, a reproducible cycle of behaviour was established, such that all spectra collected at each potential were superimposable. Use of the modulation technique also provided proof of the relationship of the new peak to that of the trianion, i.e. the two species were interconvertible, and the reduced product could not be produced in the absence of the trianion.

Current versus time graphs, which provide a measure of the current response of the system, analysed in conjunction with spectroelectrochemical data, proved to be complementary probes of chemical reversibility. Although the time dependence of the charging current is a function of the electrode surface area and the electrical characteristics of the potentiostat, the reaction current is directly proportional to the current flowing in the solution and, therefore, to the amount of substrate undergoing redox chemistry.

Constant reaction currents at V_i and V_f are indicative of equal amounts of the compound being oxidised/reduced at each cycle. This factor, in turn, is a requirement of chemical reversibilty.

The tetra-anionic species are invariably found to be extremely air-sensitive. Even under strictly anaerobic conditions, at -20 °C or below, most of the tetra-anions studied have lifetimes of the order of seconds. The modulation technique provides an excellent means of studying this type of short-lived species, minimising the extent of decomposition.

The only tetra-anionic species studied which could not be stabilised sufficiently to allow collection of infrared spectra is $W(mnt)_3^{4-}$. However, with the use of modulation techniques, the cyanide stretching bands of the decomposition product(s) can be distinguished. As a result, it can be shown that a chemically reversible reaction is taking place between the decomposition products and the first observable product of the reduction. It is not possible, nevertheless, to suggest a structure for the decomposition product(s) without additional investigation. The bands observed cannot be definitely assigned to the immediate product(s) of the decomposition and may be due to a species generated in subsequent reactions.

The continuous depletion of the trianionic cyanide band suggests that $W(mnt)_3^{3-}$ is being consumed in a chemical reaction even at a potential of V_i. The probability of dimerisation between two $W(mnt)_3^{4-}$ units, or $W(mnt)_4^{4-}$ and $W(mnt)_3^{3-}$, is small, because the electrostatic repulsion involved in bringing such two highly-charged molecules close together would be considerable. A more feasible proposition entails the possible loss of a $(mnt)^{2-}$ ligand from the system, and its replacement by two solvent molecules to give $W(mnt)_2(MeCN)_2^{2-}$. The possibility of dimerisation between $W(mnt)_3^{3-}$ and $W(mnt)_3^{4-}$ or $W(mnt)_2(MeCN)_2^{2-}$ cannot be ruled out and more than one species may be responsible for the very indistinct peaks seen in the spectrum.

All the metal complexes studied showed a shift to a lower wavenumber on reduction from the trianion to the tetra-anion. Although this followed the general trend observed previously, the shift for each individual metal was significantly greater than that noted for the reduction from the dianion to the trianion - ν(CN) for the tetra-anion is even more sensitive to the identity of the metal than is that of the trianion.

The tungsten complex displayed the largest shift - 2169.8 cm^{-1} (trianion) to 2054.0 cm^{-1} (tetra-anion), a vast change of over 100 cm^{-1}, although it has to be taken into consideration that the product of this reaction may be chemically different from other tetra-anionic species. The range of ν(CN) values for all the $M(mnt)_3^{4-}$ complexes spanned 39 cm^{-1} (excluding the tungsten complex). In addition, as the complex became more negative, the intensity of the band increased.

The large shifts to lower wavenumber observed in ν(CN), on reduction to the tetra-anion, are indicative of a significant decrease in the force constant of the C≡N bond, as a result of the population of the ligand π_v^* orbitals by electrons from the metal dπ orbitals. Similar conclusions can be drawn from the substantial increase in the intensities and widths of the new bands, compared to those of the trianionics. In general, it was found that first row transition metal complexes exhibited the smallest shifts and the least change in intensity on reduction, suggesting that back-donation was a less important factor in their bonding than in compounds of second and third row transition metals. For example, the ν(CN) band for first observable reduction product of $W(mnt)_3^{3-}$ is much more intense than the corresponding peak for the molybdenum complex, which is, in turn, more intense than that for $Cr(mnt)_3^{4-}$.

As the group of transition metals is descended, the spatial extent of the d orbitals increases. This enhances the π-overlap between them and the $4\pi_v$ π-acceptor orbitals of the ligand, such that back-bonding can occur to a more substantial degree. The increase in intensity and shift in ν(CN) exhibited by the mnt complexes of the chromium triad on reduction is evidence of this. On the other hand, as the radii of the metal orbitals decrease from left to right across a row, the π-overlap decreases and a resultant increase in ν(CN) is noted, such as for $V(mnt)_3^{4-}$ compared to $Cr(mnt)_3^{4-}$ (**Fig. 2.15**).

As the negative charge on the complex increases, the d orbitals are raised in energy, until they approach that of the unoccupied cyanide π^* orbitals. The molecular orbital scheme proposed by Stiefel et al. for dianionic complexes has, therefore, been modified to take into account the accessibility of the $4\pi_v$ orbital and emphasise the increased likelihood of back-bonding. According to this scheme, the 4e″ molecular orbital is fully occupied in all $M(mnt)_3^{3-}$ complexes. On undergoing the second reduction, the 5e′ orbital becomes singly occupied in the case of $V(mnt)_3^{4-}$ and doubly

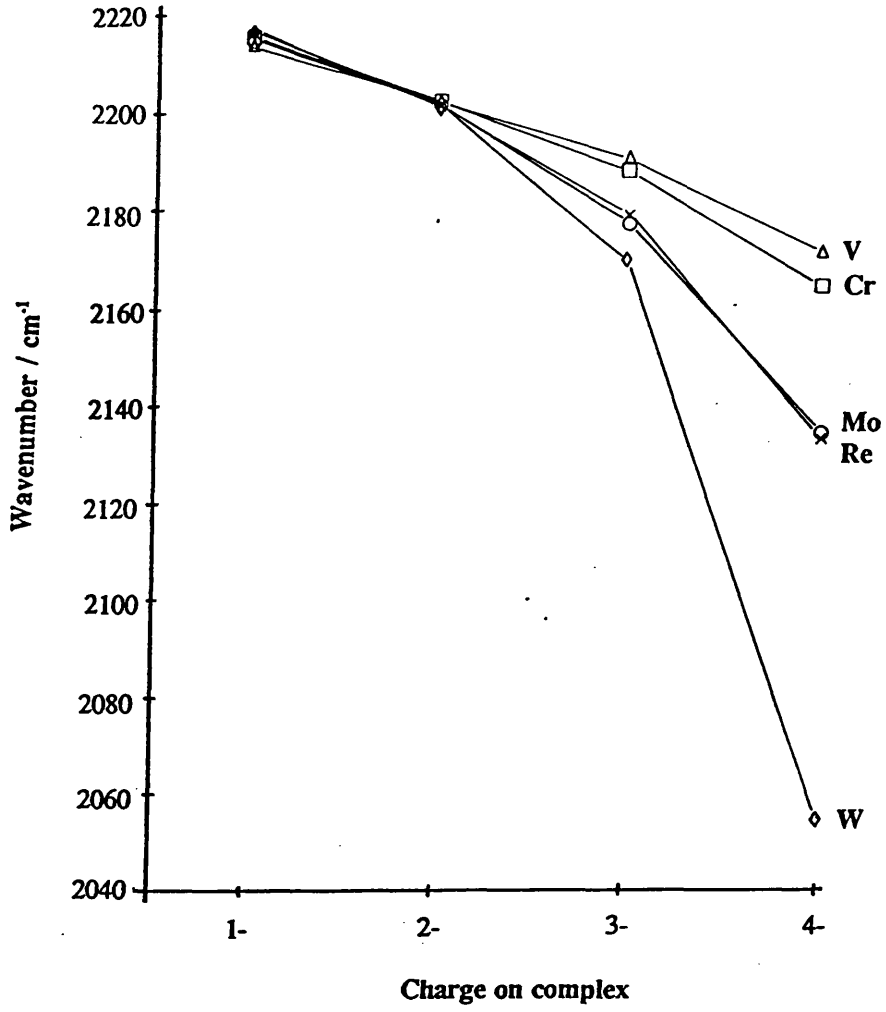

Fig. 2.15 Correlation of the cyanide stretching frequency with the charge on the $M(mnt)_3^{n-}$ complex

occupied for $Cr(mnt)_3^{4-}$, $Mo(mnt)_3^{4-}$ and $W(mnt)_3^{4-}$. Formation of the rhenium tetra-anion involves addition of a third e^- to the 5e′ orbital. These propositions could be verified by carrying out e.s.r. experiments.

The only exception to the tendency of the heavier, second and third row transition metal complexes to exhibit larger shifts on reduction to the tetra-anion, is the rhenium tetra-anion $Re(mnt)_3^{4-}$, the cyanide stretch of which occurs at a much higher wavenumber than expected. In both its tri- and tetra-anionic forms, it closely resembles the analogous molybdenum complexes rather than those of its neighbour tungsten. The rhenium tetra-anion is the only complex under scrutiny for which the

triply
5e′ orbital is occupied. This is a molecular orbital based essentially on the metal, which is not of a symmetry to interact with the ligand π^* orbital. As a result, any electron entering the 5e′ level will have minimal participation in back-bonding to the cyanide antibonding orbitals, explaining the comparatively small shifts observed in ν(CN).

It also has to be taken into consideration that population of the higher-energy molecular orbitals necessarily leads to a considerable destabilisation of the trigonal prismatic geometry with respect to the octahedral. Theoretically, it is possible to deduce the structure of the compound by monitoring the number of cyanide stretching fundamental bands in the infrared and Raman spectra. Trigonal prismatic structures with D_{3h} symmetry have $\Gamma_{CN}=a_1'+a_2''+2e'$, of which a_2'' and e' are infrared-active. O_h symmetry gives rise to $\Gamma_{CN}=a_{1g}+e_g+t_{1u}$, of which only t_{1u} is predicted to be an infrared-active mode. A lowering of molecular symmetry would result in an increase in the number of infrared- and Raman-active modes.

In practice, however, bands in Raman spectra have been found to be very weak and obscured by fluorescence. Although virtually all mono- and dianionic species studied had two bands in their infrared spectra, the interpretation placed upon the second, weaker peak is uncertain. For example, $Fe(mnt)_3^{2-}$ has been shown to be octahedral and yet its infrared spectra reveal the presence of two ν(CN) bands. As the complexes became more negatively charged, the spectra revealed a gradual diminution in the size of the second peak until its apparent disappearance in the spectra of trianionic complexes, only $Mo(mnt)_3^{3-}$ and $W(mnt)_3^{3-}$ retaining small shoulders at higher wavenumbers. All $M(mnt)_3^{4-}$ species (bar $Cr(mnt)_3^{4-}$) exhibit only one band in the cyanide stretching region of the spectrum.

According to the above interpretations, our results imply a gradual change from predominantly trigonal prismatic geometries for mono- and dianions, to octahedral ones for tetra-anions. It is doubtful, without further exhaustive studies, whether this effect could be used as a definitive test for distinguishing the geometry of compounds, especially in the absence of other corroborating data.

2.6 Conclusions

The aim of this work was to study highly-reduced transition metal tris maleonitriledithiolate complexes with a view to verifying current theories about the frontier molecular orbitals of the systems and, if necessary, adapting them to meet the requirements of the more negatively-charged species. From an experimental point of view, considerable advances had to be made in operational techniques and equipment, without which most of the tetra-anionic species could not have been observed.

Just as the metal-sulphur σ bonding, predominant in $M(mnt)_3^{1-}$ and $M(mnt)_3^{2-}$, governs the properties and behaviour of these ions, so the spectra of the tri- and tetra-anionic complexes can be largely explained in terms of an increasing tendency for the electron-rich metal centres to donate $d\pi$ electrons to the empty cyanide-based π antibonding orbitals. The extent of back-donation can be approximately deduced from the position of the cyanide stretching mode and its intensity. The greater the charge on the anion, the larger the spread of ν(CN) for all the metal complexes and the more intense the bands.

Although some tentative predictions can be made as to the geometries of complexes, infrared spectroscopy alone does not allow for structures to be established unambiguously. Complementary techniques, such as Raman spectroscopy, and ultra-violet/visible studies, in conjunction with existing results, would elucidate matters further.

References

1. J. E. Huheey, "Inorganic Chemistry", 3rd.ed., Harper, New York, (1983)

2. T. G. Spiro, ed. "Molybdenum Enzymes", Wiley-Interscience, New York (1985)

3. A. G. Wedd, "Studies in Inorganic Chemistry", Vol.5, Elsevier, Amsterdam

4. I. G. Dance, *Polyhedron*, (1986), **5**, 1037

5. E. I. Stiefel, L. E. Bennet, Z. Dori, T. H. Crawford, C. Simo, H. B. Gray, *Inorg. Chem.*, (1970), **9**, 281

6. J. A. McCleverty, J. Locke, E. J. Wharton, M. Gerloch, *J. Chem. Soc. (A)*, (1986), 816

7. J. A. McCleverty, N. M. Atherton, N. G. Connelly, C. J. Winscom, *J. Chem. Soc. (A)*, (1969), 2242

8. A. Davison, N. Edelstein, R. H. Holm, A. H. Maki, *Inorg. Chem.*, (1963), **2**, 1227

9. A. Davison, R. H. Holm, *Inorg. Synth.*, (1967), **10**, 9

10. W. E. Geiger, T. E. Mines, F. C. Senftleber, *Inorg. Chem.*, (1975), **14**, 2141

11. H. B. Gray, R. Williams, I. Bernal, E. Billig, *J. Am. Chem. Soc.*, (1962), **84**, 3596

12. D. Coucouvanis, J. P. Fackler, *Inorg. Chem.*, (1967), **6**, 2047

13. I. G. Dance, *Inorg. Chem.*, (1973), **12**, 2381

14. C. H. Langford, E. Billig, S. I. Shupack, H. B. Gray, *J. Am. Chem. Soc.*, (1964), **86**, 2958

15. N. G. Connelly, C. J. Jones, J. A. McCleverty, *J. Chem. Soc. (A)*, (1971), 712

16. R. Eisenberg, J. A. Ibers, *J. Am. Chem. Soc.*, (1965), **87**, 3776

17. R. Eisenberg, H. B. Gray, *Inorg. Chem.*, (1967), **6**, 1844

18. A. E. Smith, G. N. Schrauzer, V. P. Mayweg, W. Heinrich, *J. Am. Chem. Soc.*, (1965), **87**, 5798

19. E. I. Stiefel, Z. Dori, H. B. Gray, *J. Am. Chem. Soc.*, (1967), **89**, 3353

20. A. Sequiera, I. Bernal, Abstracts, American Crystallographic Association Meeting, Minneapolis, Minnesota, (1967), 75

21. S. P. Best, R. J. H. Clark, R. C. S. McQueen, J. R. Walton, *Inorg. Chem.*, (1988), **27**, 884

22. E. I. Stiefel, R. Eisenberg, R. C. Rosenberg, H. B. Gray, *J. Am. Chem. Soc.*, (1966), **88**, 2956

23. W. L. Kwik, E. I. Stiefel, *Inorg. Chem.*, (1973), **12**, 2337

24. R. J. H. Clark, P. C. Turtle, *J. Chem. Soc., Dalton Trans.*, (1978), 1714

25. L. H. Jones, *Inorg. Chem.*, (1963), **2**, 777

26. A. Davison, N. Edelstein, R. H. Holm, A. H. Maki, *J. Am. Chem. Soc.*, (1964), **86**, 2799

Chapter 3

Spectroelectrochemical Studies of Oxomolybdenum bis (maleonitriledithiolate)

The close resemblance of the maleonitriledithiolate ligand (**Fig. 2.1** in **Chapter 2**) to the unsaturated sulphur-donor pterin backbone coordinated directly to the metal centre of **Mo-co**, has already been noted in **Chapter 2**. This relationship has stimulated a wide study of mnt complexes with many transition metals. However, these were of the general form $M(mnt)_3^{n-}$ or $M(mnt)_2^{n-}$ and it was not until 1969 that McCleverty et al. first reported the preparation of oxo-metal dithiolenes $(Ph_4P)_2VO(mnt)_2$ and $X_2MoO(mnt)_2$ ($X=PPh_4^+$, NEt_4^+, $N(Bu^n)_4^+$).[1] These complexes bear a significant similarity to the **Mo-co** of oxotransferases, in which a terminal oxo group and a pterin ligand system are coordinated to the central molybdenum atom (**Fig. 1** of **Introduction**).

For $MoO(mnt)_2^{2-}$, as with the tris-mnt complexes, overlap between the ligand and metal orbitals gives rise to an extensive π-bonding network which may result in considerable delocalisation of charge throughout the molecule. The effect of changes in the occupancy of the metal-ligand π molecular orbitals is transmitted, via the π-orbital of the ligand, to the CN groups of the mnt ligand. An increase in the occupancy of the ligand π orbitals results in a shift in the wavenumber of the ν(CN) band and a variation in its intensity. Oxidation of the molecule, involving the removal of an electron(s) from the system, will, in general, lessen the tendency for dπ-pπ back-bonding, decreasing the population of cyanide π^* antibonding orbitals. This increases the force constant for the C≡N bond and shifts ν(CN) to higher wavenumbers. Reduced back-donation is usually accompanied by a decrease in intensity of the band due to ν(CN).

An attractive feature of $MoO(mnt)_2^{2-}$ is the opportunity to simultaneously monitor two vibrational modes in spectroelectrochemical experiments, viz the Mo=O

stretching vibration in addition to ν(CN). The bands due to ν(Mo=O) are generally observed at 900-1000 cm^{-1} - a region of the spectrum free of solvent bands. These vibrational modes are diagnostic of the molybdenum-oxygen bond order, which itself depends upon the electron distribution within the molecule and especially at the metal centre.[2-5] A decrease in the charge density on the metal atom centre, resulting from electrochemical oxidation, decreases the extent of π back-donation into metal-ligand antibonding orbitals. The increased force constant of the Mo=O bond is manifest by an increase in the frequency of the stretching vibration.

In common with all the tris-mnt transition metal complexes, $MoO(mnt)_2^{2-}$ is highly coloured.[6] However, unlike the tris-mnt complexes, which undergo several redox steps, the molybdenyl complex undergoes only one electrochemical reaction - a reversible one-electron oxidation[1] - within the electrochemical range of the solvent. Standard spectroelectrochemical experiments revealed that this oxidation was far from simple. A complex series of irreversible chemical reactions was initiated by the electron transfer, involving radical changes in molecular structure. The analysis of these results, in conjunction with the data from ultra-violet/visible and time-resolved studies, using the modulation technique, resulted in the identification of several intermediate species and, ultimately, the formulation of a possible reaction scheme.

3.1 Electronic Structure

Many early transition metal ions have a tendency to form remarkably stable oxocations of the form MO^{n+}.[2,3] One of the most widely known and best characterised is the vanadyl ion VO^{2+}.[7,8] Much of the research into other metal oxo complexes has been based on the results obtained from the study of the vanadyl ion. For example, the molecular orbital scheme proposed by Gray and Hare for $MoOCl_5^{2-}$ [9] was founded upon preliminary work by Ballhausen and Gray based on $VO(H_2O)_5^{2+}$.[10]

$MoO(mnt)_2^{2-}$ adopts a square pyramidal geometry (of C_{2v} symmetry), the metal lying above the basal plane of the ligands, in common with compounds of the vanadyl ion with bidentate ligands[1] (**Fig. 3.1**). The apical position of the pyramid is occupied

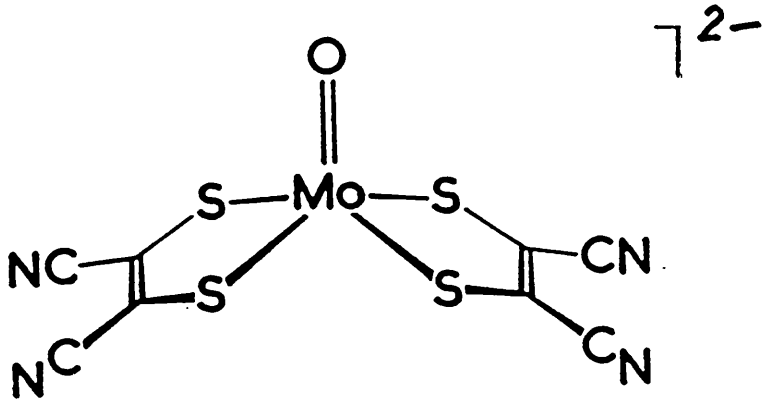

Fig. 3.1 Structure of $MoO(mnt)_2^{2-}$

by the oxo group, forming an extremely short (1.67Å)[11] and strong multiple bond to the molybdenum atom. Coordination to the trans position by a sixth, usually nitrogen-donor, ligand is possible and results in a lengthening of the metal-oxygen bond and decrease in the (M-O) stretching frequency.

The molecular orbital scheme devised by Hare and Gray for $MoOCl_5^{2-}$ [9] was used to analyse $MoO(mnt)_2^{2-}$. Although the coordination numbers of the molecules differ, their symmetries are approximately the same (C_{4v}) and the coordination of the chlorine atom trans to the oxo group in $MoCl_5^{2-}$ is weak. A set of coordinates was utilised where the z-axis coincides with the apical oxo group. The strongest bond in the complex is the Mo=O multiple bond; the four chlorides in the square plane are equivalent, and form stronger bonds to the metal centre than the axial chloride trans to the oxo (**Fig. 3.2**).

The oxygen sp_σ orbital (formed by the hybridisation of 2s and $2p_z$) combines with the molybdenum ($5s+4d_{z^2}$) hybrid orbital to give a strong σ bond (bonding and antibonding) of a_1 symmetry. Two π bonds, of e symmetry, are formed by the interaction of oxygen $2p_x$ and $2p_y$ orbitals and metal $4d_{xz}$ and $4d_{yz}$ orbitals, thus giving a total bond order of three for MoO^{2+}. The donor atoms located in the equatorial positions utilise $3p_z$ and nsp_σ orbitals (chlorine and oxygen/sulphur respectively) for bonding. They overlap with metal ($5s-4d_{z^2}$), $5p_x$, $5p_y$ and $4d_{x^2-y^2}$ orbitals, yielding four σ bonding and four σ antibonding orbitals - $2a_1$, 1e, 1e and $2b_1$ respectively. The

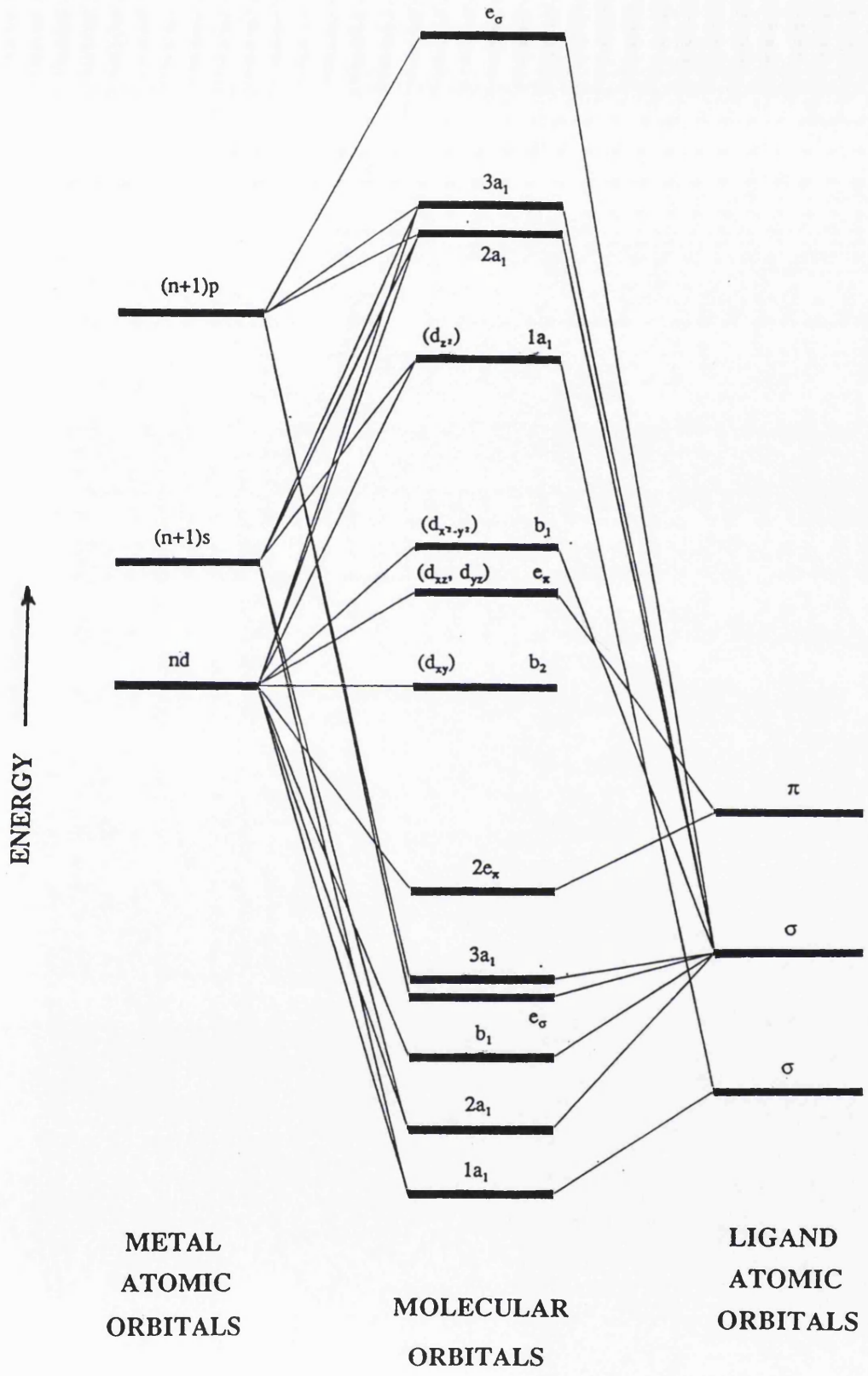

Fig. 3.2 Molecular orbital scheme for $MoOCl_5^{2-}$

σ bonding of the sixth ligand involves ligand sp_σ and metal $5p_z$ orbitals (a_1). π-bonding between the chloride ligands and molybdenum was assumed to be negligible. The remaining metal orbital $4d_{xy}$, of symmetry b_2, is non-bonding.

It has been shown that optical spectra of vanadyl complexes are minimally affected by the occupation of the sixth coordination site trans to the multiply-bonded oxo ligand.[10] This indicates that the orbital energies remain relatively unaltered on changing from five- to six-coordination providing that the bonding to the sixth ligand is fairly weak. The absence of a sixth ligand would lower the energy of the $1a_1$ level (an antibonding orbital with significant metal d_{z^2} character), such that it approaches the $2e_\pi$ molecular orbital.

Further work[8] seems to indicate that splitting of the $2e_\pi$ term occurs when the degeneracy is removed as a result of the equatorial coordination of bidentate ligands. However, the ground states of the isoelectronic VO^{2+} and MoO^{3+} are virtually identical - $(1a_1)^2\ (2a_1)^2\ (b_1)^2\ (1e)^4\ (3a_1)^2\ (2e_\pi)^4\ (b_2)^1$. According to this molecular orbital scheme, three electronic transitions can be predicted - $b_2 \rightarrow 2e_\pi^*$, $b_2 \rightarrow b_1^*$ and $b_2 \rightarrow 1a_1^*$.

The electronic structure of MoO^{2+} is expected to be simply related to that of MoO^{3+}, involving the double-filling of the non-bonding b_2 molecular orbital. Some authors[11] have also suggested that the stability of the MoO^{2+} ion may be due, in part, to back-bonding from the $1b_2$ orbital into ligand π^* orbitals. The presence of mnt ligands, and their ability to accept π electrons from the metal centre, decreases the extent of back-donation to the oxo group. This results in a strengthening of the oxomolybdenum bond and an increase in ν(Mo=O).

Oxidation of the complex involves the removal of an electron from the non-bonding b_2 orbital. The decrease in the charge density on the metal atom centre enhances its σ and π accepter properties, thereby strengthening the molybdenum-oxygen bond. The effect is to shift ν(MoO) to a higher wavenumber. The converse is expected for a reduction of the complex, which involves the population of the e_π Mo=O antibonding orbital, since this results in a decrease of the effective Mo=O bond order to 2.5.

The argument used to explain the behaviour of the cyanide stretching frequency on oxidation/reduction is analogous to that put forward in the discussion of tris-mnt complexes (**Chapter 2**). The decrease in the energies of the metal d orbitals, as

electrons are removed from the system, increases the energy difference between them and the $4\pi_v$ ligand antibonding orbitals. The probability of $d\pi$-$p\pi$ back-bonding is, therefore, significantly reduced, resulting in an increase in the frequency of ν(CN). The converse applies for reduction processes. The intensity of cyanide stretching bands should follow a similar pattern to that exhibited by $M(mnt)_3^{n-}$ complexes, although the effect is expected to be less pronounced, because back-bonding is not as important a factor in the bonding of $MoO(mnt)_2^{2-}$ as in the tris-mnt complexes.

3.2 Electrochemistry

The complex, $MoO(mnt)_2^{2-}$ undergoes only a reversible one-electron oxidation, with a half-wave redox potential in dichloromethane of +0.475 V versus ferrocene (**Fig. 3.3**), within the potential range of the solvent.

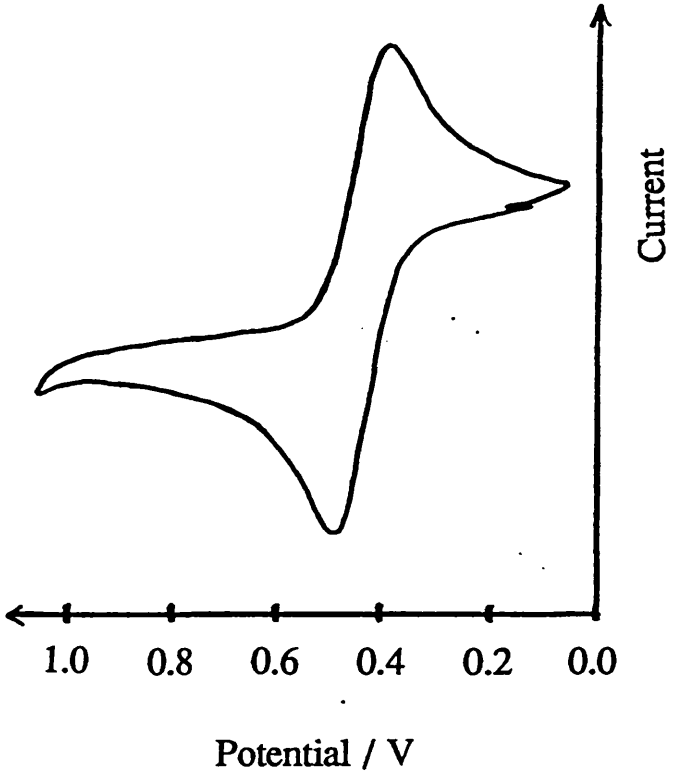

Fig. 3.3 Cyclic voltammogram of $MoO(mnt)_2^{2-}$

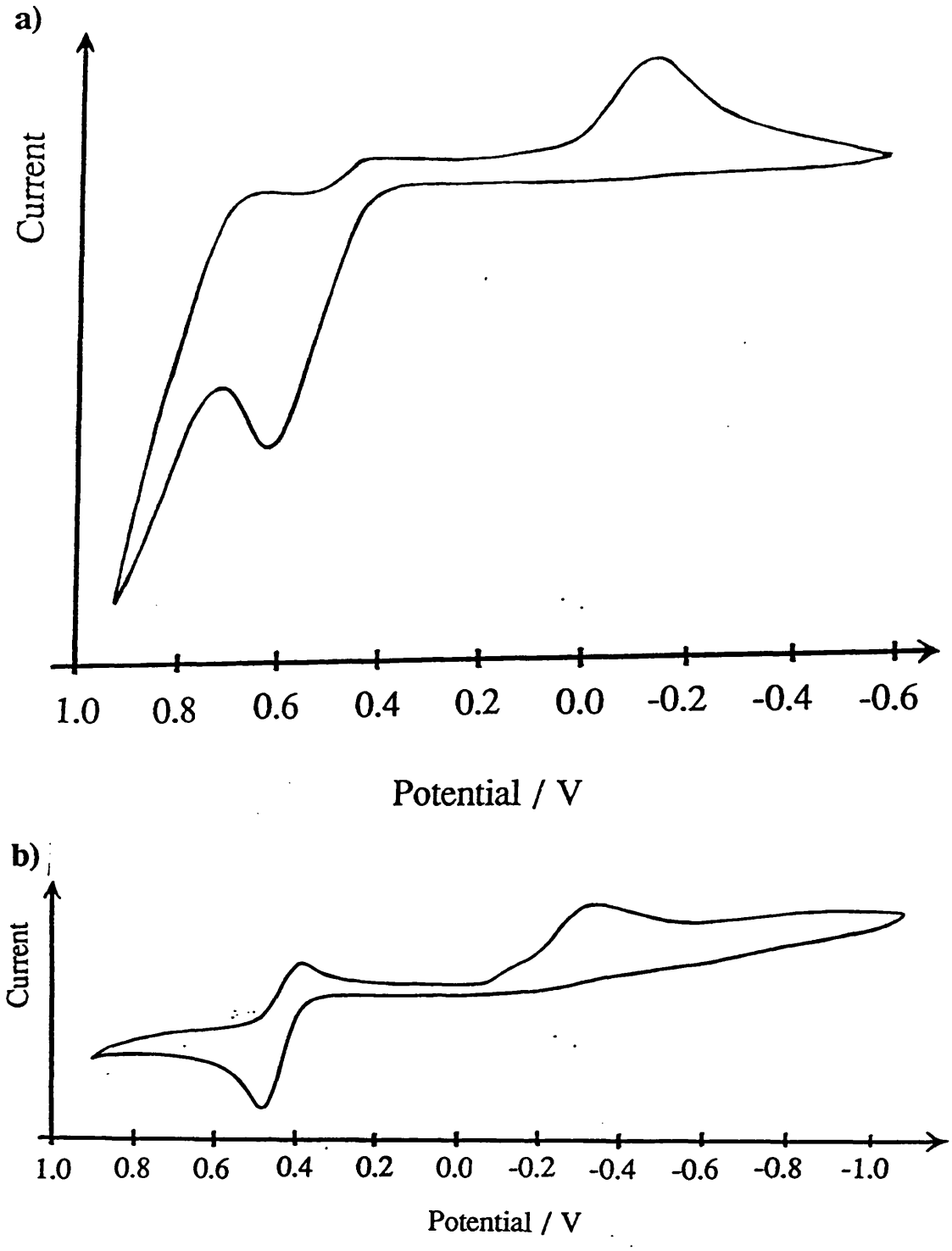

Fig. 3.4 Cyclic voltammogram of $MoO(mnt)_2^{2-}$ in the presence of excess:-
a) chloride ions
b) bromide ions

The effect of the occupation of the vacant sixth coordination position of the complex on the $MoO(mnt)_2^{2-}/MoO(mnt)_2^{1-}$ couple has also been studied. The use of coordinating solvents, such as acetonitrile, or the addition of coordinating ligands, such

as chloride or bromide ions, results in the loss of electrochemical reversibilty. The shape and position of the anodic peak remains unchanged (**Fig. 3.4**), but the cathodic peak shifts to more negative potentials (in all cases removed by over 0.5 V from its original value). In all instances where chloride or bromide were added to dichloromethane solutions of the complex, the value of i_{P_c} was less than half that of i_{P_a}.

Coordination by chloride and bromide ions shifted the cathodic peak to -0.19 and -0.11 V respectively in dichloromethane. Cyclic voltammetry of $MoO(mnt)_2^{2-}$ with triphenyphosphine in dichloromethane showed a cathodic peak at -0.35 V, with some indication of a shift to more negative potentials as the temperature was lowered (**Fig. 3.5**). Acetonitrile appeared to coordinate less strongly to the complex than either of the halide ions, since a cathodic peak, diminished in size, was observed at the potential expected for the cathodic wave of $MoO(mnt)_2^{2-}$ in dichloromethane (+0.41 V). However, a small cathodic peak at approximately -0.10 V indicated that coordination of the halide to a small amount of the complex had occurred.

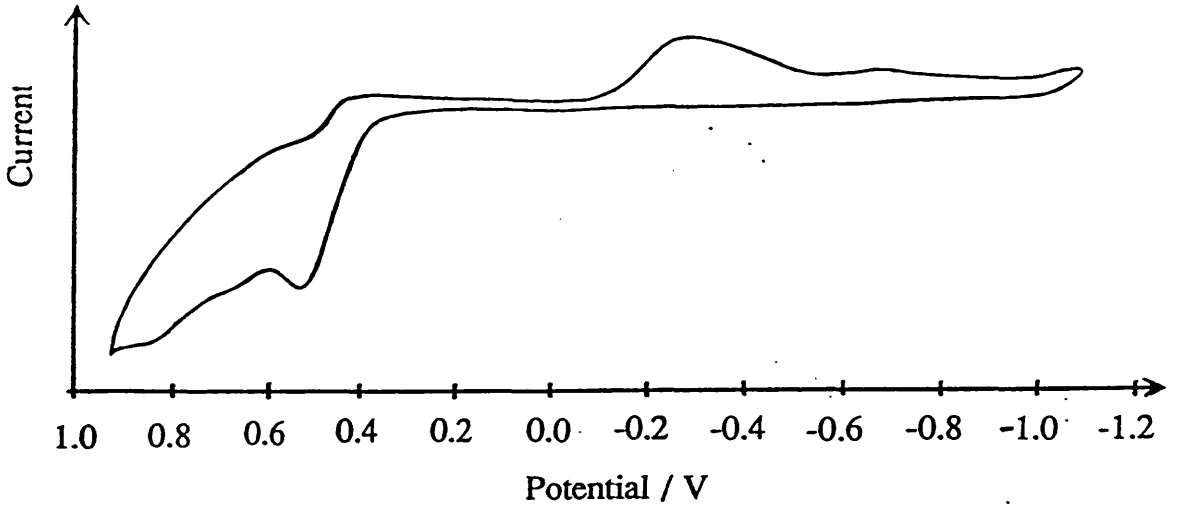

Fig. 3.5 Cyclic voltammogram of $MoO(mnt)_2^{2-}$ in the presence of triphenylphosphine

3.3 Synthesis

The complex was prepared according to the method of McCleverty et al.[1] Ammonium paramolybdate (2.03 g; 1.65×10^{-3} mol) was dissolved in water (40 cm^3) and warmed gently until all the solid had dissolved. A solution of sodium maleonitriledithiolate (4.25 g; 0.0229 mol) in ethanol (63.5 cm^3) was added. The solution was heated on a steam bath for 3½ hours. Tetra-n-butylammonium bromide (6.34 g; 0.020 mol), dissolved in the minimum volume of ethanol, was added, causing the immediate precipitation of brown crystals. The mixture was allowed to cool, the solid was removed by filtration and washed with methanol until the washings were colourless. The green-brown crystalline solid was recrystallised four times from acetone/methanol and dried in a desiccator.

Yield of $(Bu_4N)_2MoO(mnt)_2$:- 2.47 g; 25%

Elemental analysis:-

Calculated:-	C=54.77%	H=8.27%	N=9.58%	S=14.62%
Found:-	C=54.75%	H=8.58%	N=9.63%	S=14.61%

3.4 Infrared Spectroelectrochemistry

The molybdenum-oxygen stretching mode ν(MoO) for $MoO(mnt)_2^{2-}$ occurs at 931.1 cm^{-1}. $\mathbf{V_i}$ and $\mathbf{V_f}$ are taken to be 0.0 V and 1.0 V for all experiments. In standard spectroelectrochemical experiments, using a 5 mm diameter working electrode, this band shifts by 26.5 cm^{-1} to 957.6 cm^{-1}, as the potential is changed to $\mathbf{V_f}$ (**Fig. 3.6a**). However, after several seconds, the new peak collapses giving rise to several small, indistinct peaks. On switching the potential to $\mathbf{V_i}$, very broad, ill-defined bands appear (**Fig. 3.6b**). None of the previously-observed peaks are regenerated.

Similarly complicated behaviour is noted for the cyanide stretching vibrations, which occurs at 2194.5 and 2205.5 cm^{-1} in the starting material. The removal of an electron from the complex appears to initiate a two-step process, the ultimate product

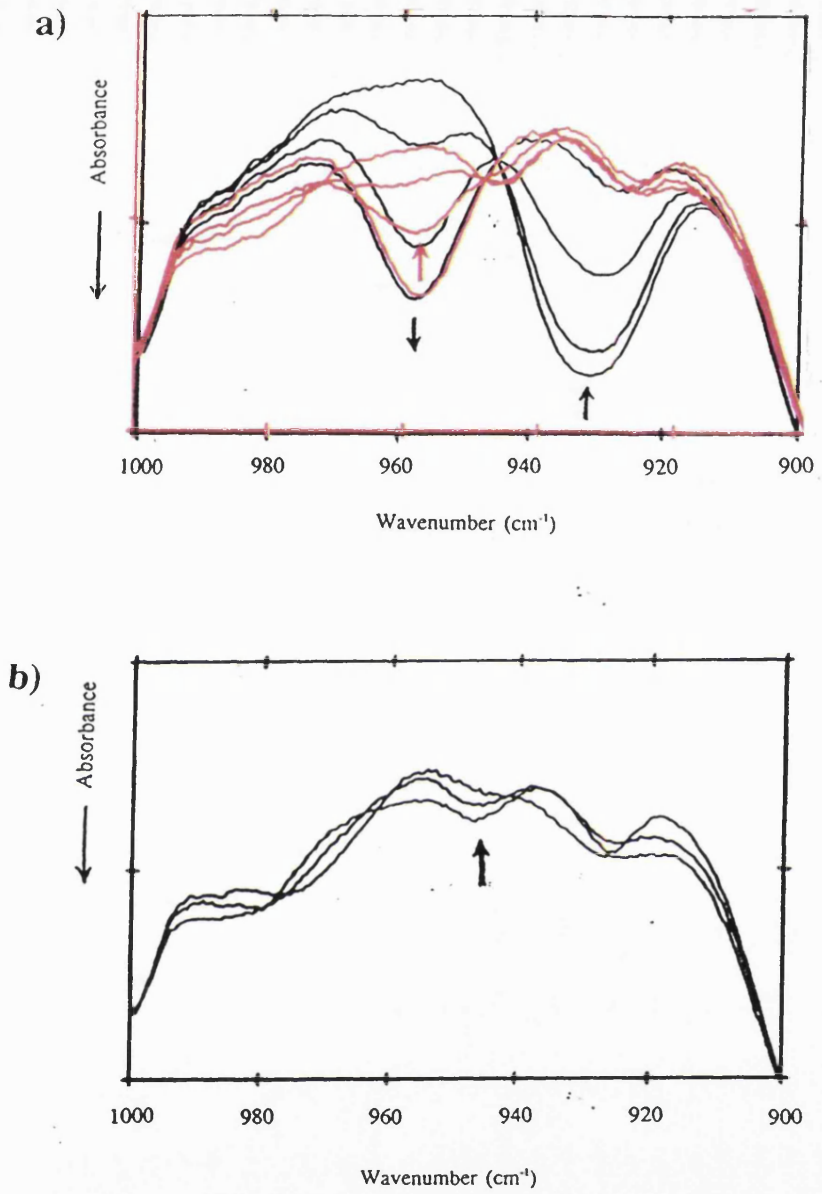

Fig. 3.6 Changes observed in ν(MoO) of $MoO(mnt)_2^{2-}$ during normal spectroelectrochemistry
a) on oxidation
b) on re-reduction

of which has a ν(CN) of 2215.6 cm^{-1} with a shoulder at 2223.8 cm^{-1} (**Fig. 3.7a**). The reaction proceeds via an intermediate, the ν(CN) band of which occurs at 2210.0 cm^{-1} (with a shoulder at 2220.4 cm^{-1}). Neither of the intermediate peaks, nor those of the starting material, are regenerated on switching the potential to $\mathbf{V_i}$. Instead, an intense

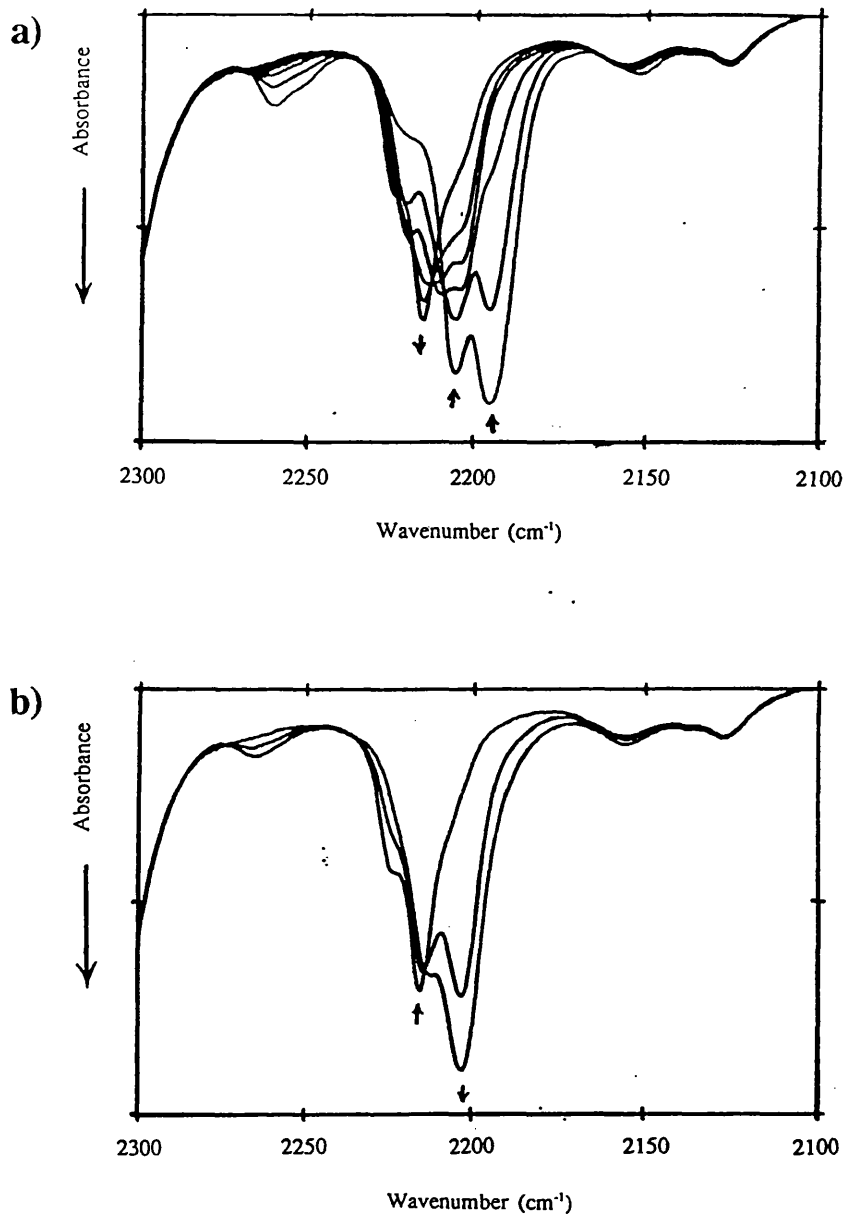

Fig. 3.7 Changes observed in ν(CN) of $MoO(mnt)_2^{2-}$ during normal spectroelectrochemistry
a) on oxidation
b) on reduction

band is observed at 2202.6 cm^{-1}, with a shoulder at 2213.0 cm^{-1} **(Fig. 3.7b)**. The formation of the bands at 2210.0 and 2220.4 cm^{-1} coincides with the appearance of the 957.6 cm^{-1} peak in the region of the molybdenyl stretching mode.

In an attempt to clarify the course of the reaction, several experiments were

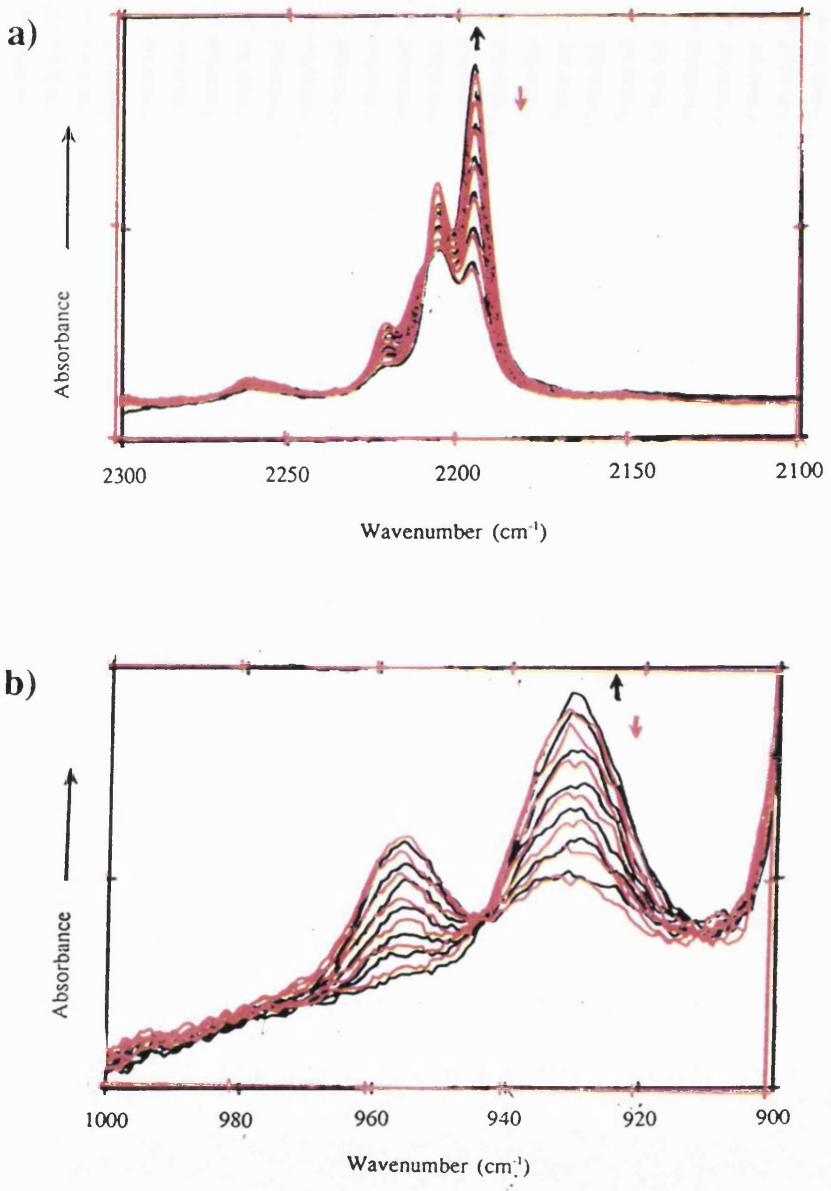

Fig. 3.8 Changes observed in **a)** ν(CN) **b)** ν(MoO) during 2.0 s/2.0 s modulated spectroelectrochemical oxidation of $MoO(mnt)_2^{2-}$

carried out using the modulation technique descibed in **Chapter 1**. Initially, the potential was switched between $\mathbf{V_i}$ and $\mathbf{V_f}$ every 2 s at room temperature (using the 5 mm diameter working electrode). Very small quantities of $MoO(mnt)_2^{2-}$ undergo oxidation at $\mathbf{V_f}$ on this timescale, with new peaks appearing at 957.7 cm^{-1}, 2210.0 and 2220.4 cm^{-1} at the expense of those at 931.1 cm^{-1}, 2194.5 and 2205.5 cm^{-1} respectively (**Fig. 3.8**). There is, however, little change in the intensities of either of the ν(MoO) bands on switching back to $\mathbf{V_i}$, and the intensities of the bands due to ν(CN) at 2194.5

and 2205.5 cm^{-1} indicate continued depletion. Overall, the series of spectra obtained from this experiment indicate a gradual consumption of the starting material, resulting in almost total conversion to the relatively unstable intermediate by the end of the experiment.

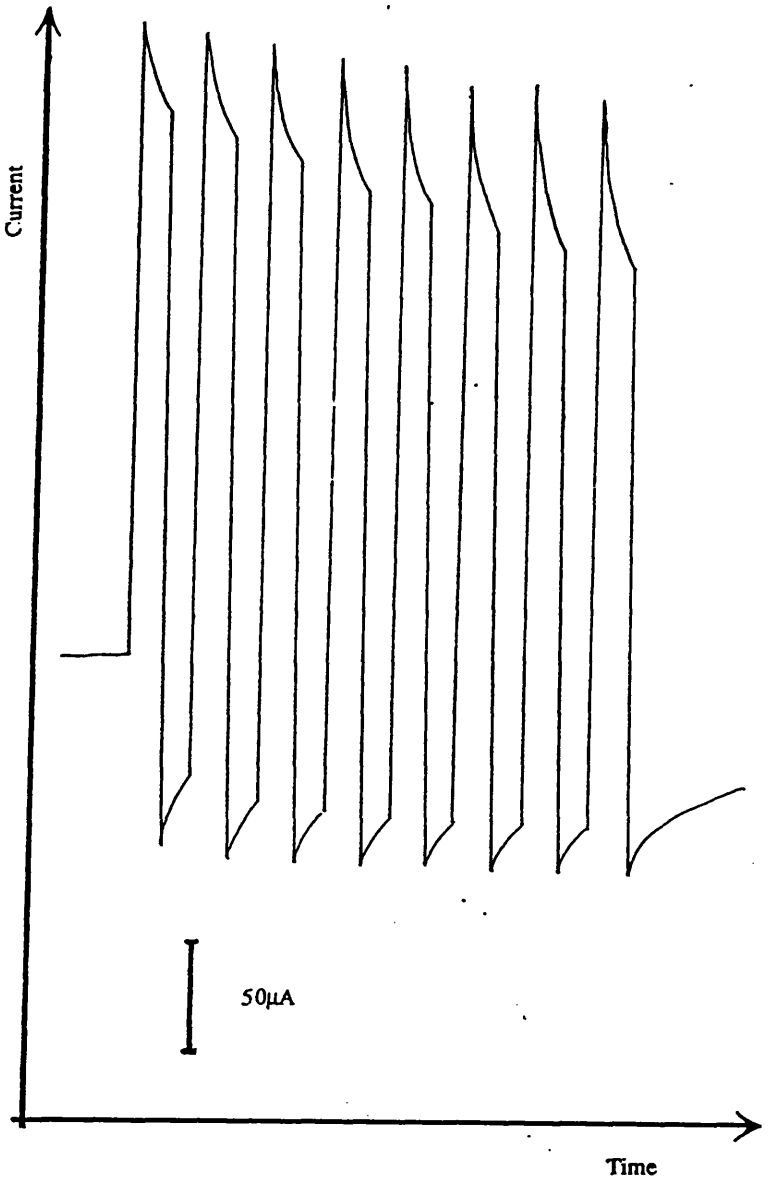

Fig. 3.9 Current response for the 2.0 s/2.0s modulated spectroelectrochemical oxidation of $MoO(mnt)_2^{2-}$

Examination of current versus time graphs (**Fig. 3.9**) for the experiment further emphasises the lack of both chemical and electrochemical reversibility for this reaction. The reaction current at V_i decreases with each cycle, whilst that at V_f

increases dramatically as the experiment proceeds, almost doubling in size. Similarly irregular behaviour can be seen with respect to the charging currents at both potentials.

Two likely explanations of these observations are that the reaction is chemically irreversible, or that it is chemically reversible, but with a very slow rate of re-reduction to the starting material. Although experiments were performed, in which 2-3 s were allowed for oxidation, followed by 20-60 s for reduction, the slow response times of the larger working electrodes gave rise to minimal changes in spectral bands, which were very difficult to analyse and suffered from poor reproducibilty.

The enhanced response time of the 2 mm diameter working electrode, in comparison with the larger electrode, led to a significant increase in the proportion of the reactant at the electrode surface undergoing conversion at each potential change. The combination of a smaller-diameter working electrode and reduced temperatures in experiments, permitted the stabilisation of more reactive species, giving rise to spectral changes which could be more easily interpreted.

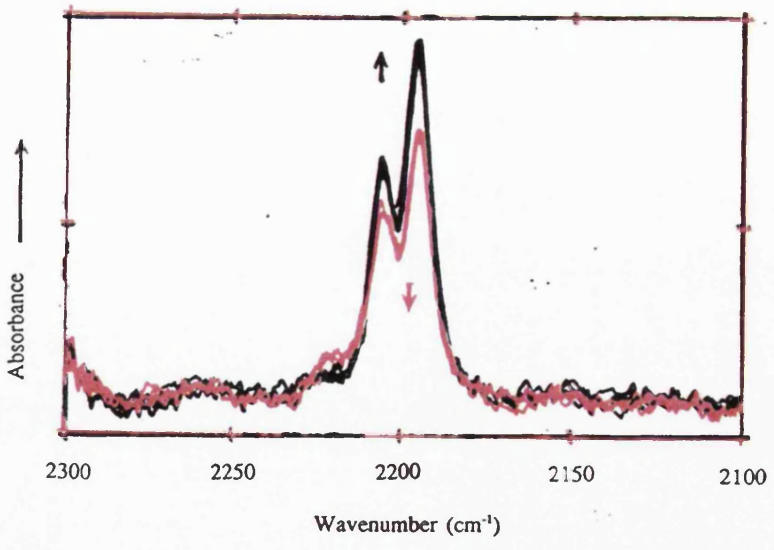

Fig. 3.10 Changes observed in ν(CN) for the 2.0 s/60.0 s modulated spectroelectrochemical oxidation of $MoO(mnt)_2^{2-}$ at -5.0 °C

The best evidence of chemical reversibility for the oxidation of $MoO(mnt)_2^{2-}$ was obtained at -12 °C, by maintaining the potential at $\mathbf{V_f}$ for 2 s and at $\mathbf{V_i}$ for 60 s

(**Fig. 3.10**). It was noted that no changes occurred during the first potential cycle, but that all spectra collected at V_i were superimposable and showed peaks at 2194.5 and 2205.5 cm^{-1}. The ν(CN) bands in the spectra collected at V_f were less intense, but equally superimposable. They had additional features of a shoulder at 2210.0 cm^{-1} and a small peak at 2220.4 cm^{-1}.

Reference to current versus time graphs confirmed these conclusions (**Fig. 3.11**). The charging and reaction currents, at both V_i and V_f, followed an invariant pattern throughout the repeated cycles of potential - one of the criteria of a chemically reversible reaction.

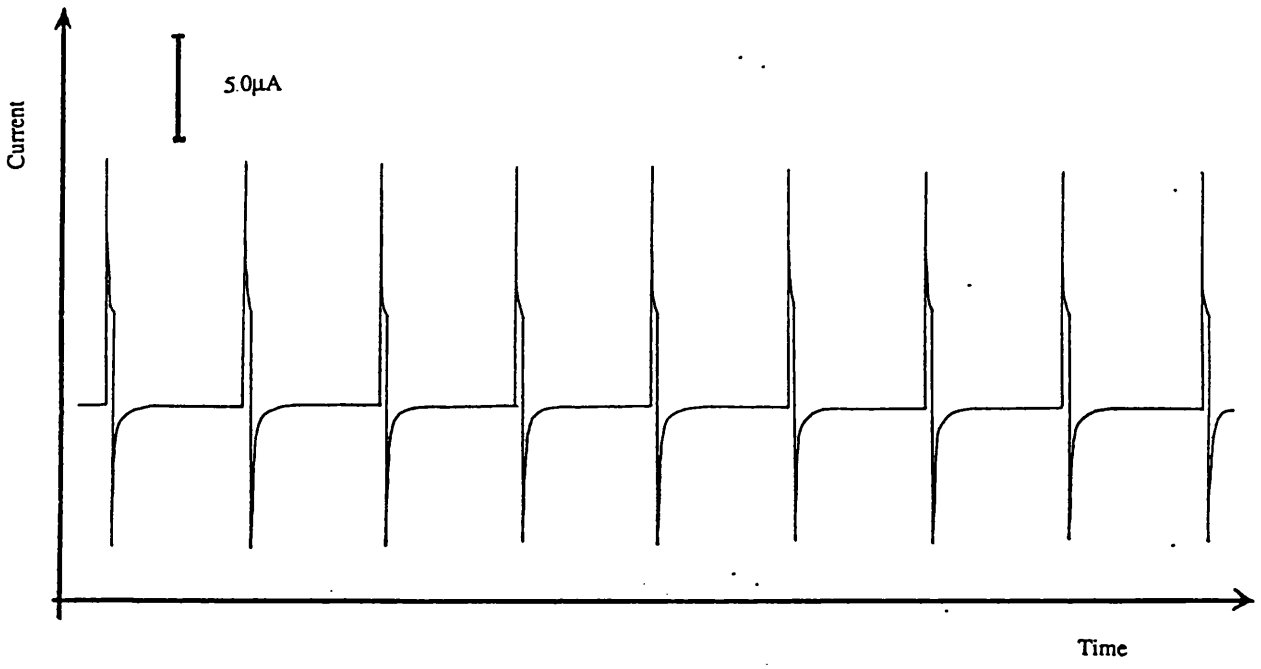

Fig. 3.11 Current response for the 2.0 s/60.0 s modulated spectroelectrochemical oxidation of $MoO(mnt)_2^{2-}$ at -5.0°C

In order to stabilise any reactive square pyramidal intermediates and reduce the possibility of dimer formation, tetra-n-butylammonium bromide was added in order to fill the vacant sixth coordination site in the complex. The initial cyanide (2194.5 and 2205.5 cm^{-1}) and the oxomolybdenum (931.0 cm^{-1}) stretching modes remain unchanged, indicating that coordination by the bromide ion to the starting material - $MoO(mnt)_2^{2-}$ - does not occur to a significant extent.

As the potential is switched to V_f, the molybdenyl band at 931.1 cm^{-1} shifts to

976.0 cm^{-1} (**Fig. 3.12a**). The latter band does not lose intensity as the experiment proceeds, even at room temperature, suggesting that the electrogenerated product is relatively stable and undergoes little decomposition. The new band was slightly less intense than that of the original compound with decreased full-width at half-height. The starting material was partially regenerated (approximately 50%) when the potential was changed to one beyond the new cathodic wave seen at -0.11 V in the cyclic voltammograms (**Fig. 3.12b**).

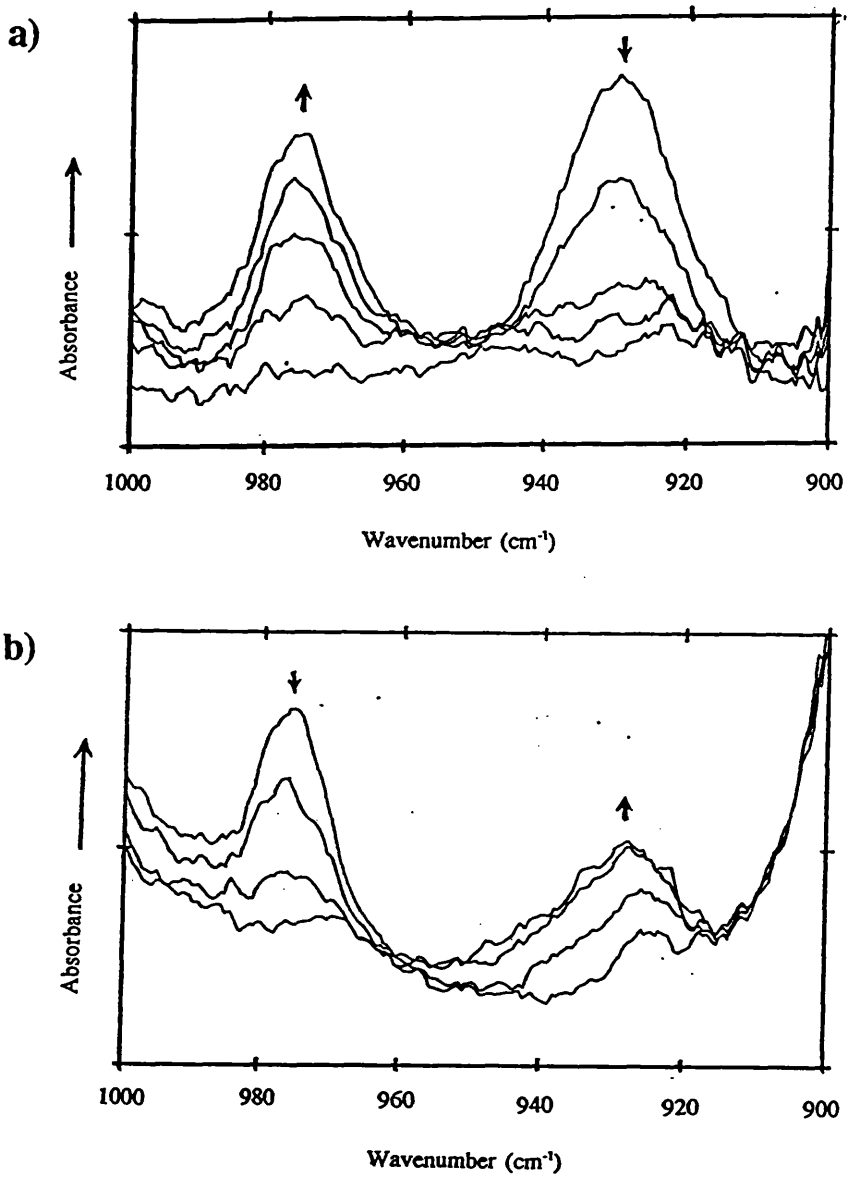

Fig. 3.12 Changes observed in ν(MoO) during normal spectroelectrochemistry in the presence of bromide ions
a) on oxidation **b)** on reduction

The bands at 2194.5 and 2205.5 cm^{-1}, which are due to cyanide stretching vibrations, gradually collapse as the potential is switched from V_i to V_f (**Fig. 3.13a**). New, weak bands appear at 2210.8 and 2221.9 cm^{-1}. The ν(CN) bands of the starting material reappear, with significantly lower intensities, on switching the potential to V_i (**Fig. 3.13b**). This is comparable to the behaviour observed in the 900-1000 cm^{-1} region.

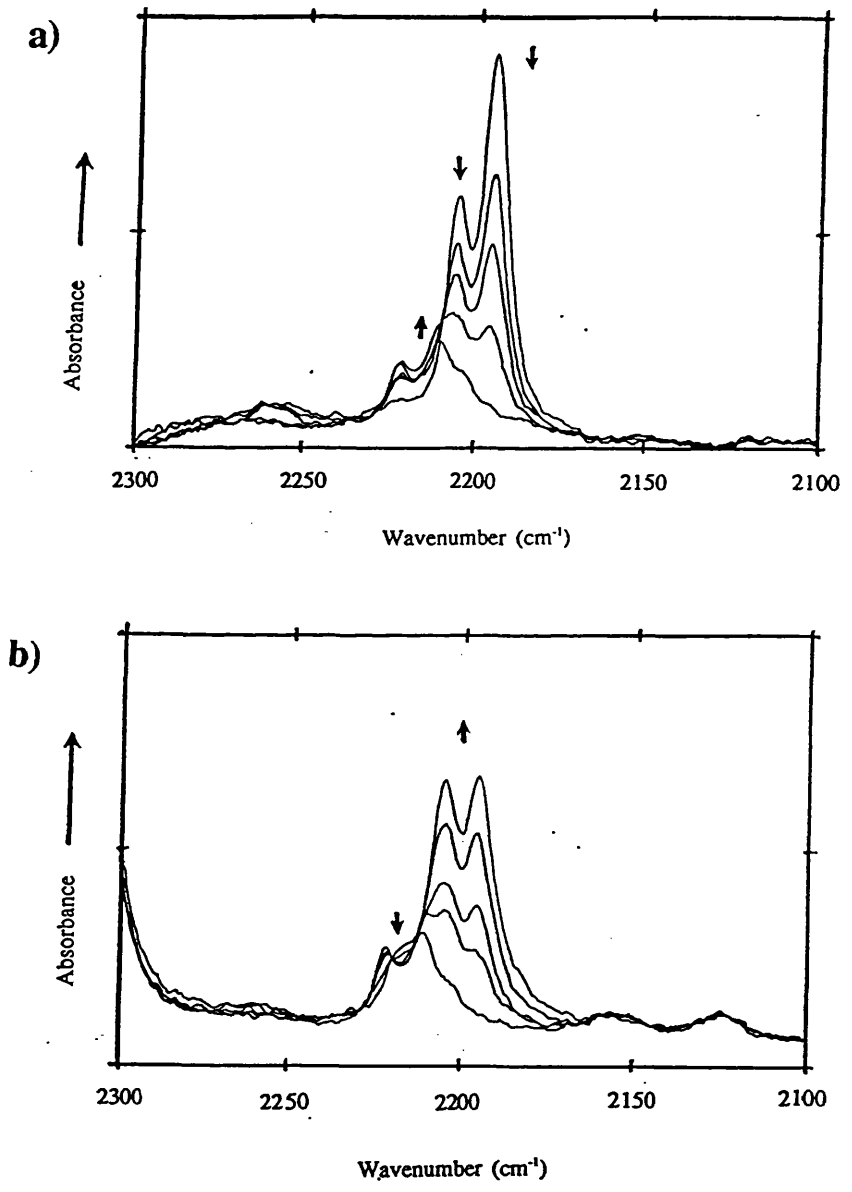

Fig. 3.13 Changes observed in ν(CN) during normal spectroelectrochemistry of $MoO(mnt)_2^{2-}$ in the presence of halide ions
a) on oxidation
b) on reduction

3.5 Ultra-violet/visible Spectroelectrochemistry

Within the spectral region studied (1000-400 nm), the electronic spectrum of $MoO(mnt)_2^{2-}$ consists of two very weak bands at 605 nm and 494 nm. Their molar decadic extinction coefficients are 150 $dm^3mol^{-1}cm^{-1}$ and 240 $dm^3mol^{-1}cm^{-1}$ respectively. An additional band at 667 nm reported by McCleverty et al.[1] is not apparent in the spectrum. This feature is strongly suspected to arise from a trace impurity of the tris-mnt species $Mo(mnt)_3^{2-}$ in their sample. As the spectroelectrochemical experiment progresses, new bands initially appear at 565 and 779 nm (**Fig. 3.14a**). Both the peaks are significantly more intense than those of the starting material. However, the species responsible for these features is short-lived and decomposes with a half-life of approximately 15-20 s. The 565 nm and 779 nm band are replaced by intense bands at 495 nm and 696 nm. These spectral changes proceed via an isosbestic point, suggesting that the the second stage of the reaction is a simple interconversion process between two species and does not involve the formation of intermediates.

On returning the potential to V_i, none of the original peaks, or those of the intermediate species are regenerated (**Fig. 3.14b**). Instead, the band at 495 nm decreases in intensity, while remaining at the same position; the 696 nm peak shifts to 672 nm with a loss of intensity.

Examination of the spectra reveal that the electronic bands at 779 and 565 nm are at their maximum intensity approximately 20-30 s after the commencement of the experiment. For the corresponding infrared experiment, the appearance of these bands coincides with the appearance of peaks at 2210.0 and 2220.4 cm^{-1} in the cyanide stretching region and the 957.6 cm^{-1} band in the molybdenyl region. It is, therefore, concluded that all the spectral features observed are due to the same species. The infrared and electronic bands of the final products of the reactions can similarly be proved to arise from one species.

The addition of a source of bromide ions to a solution of the compound in dichloromethane does not alter the spectral bands in the electronic spectrum of the starting material. On changing the potential to V_f, a new, more inten se peak was observed to develop at 774 nm, whilst the bands at 605 and 494 nm shifted to 609 and

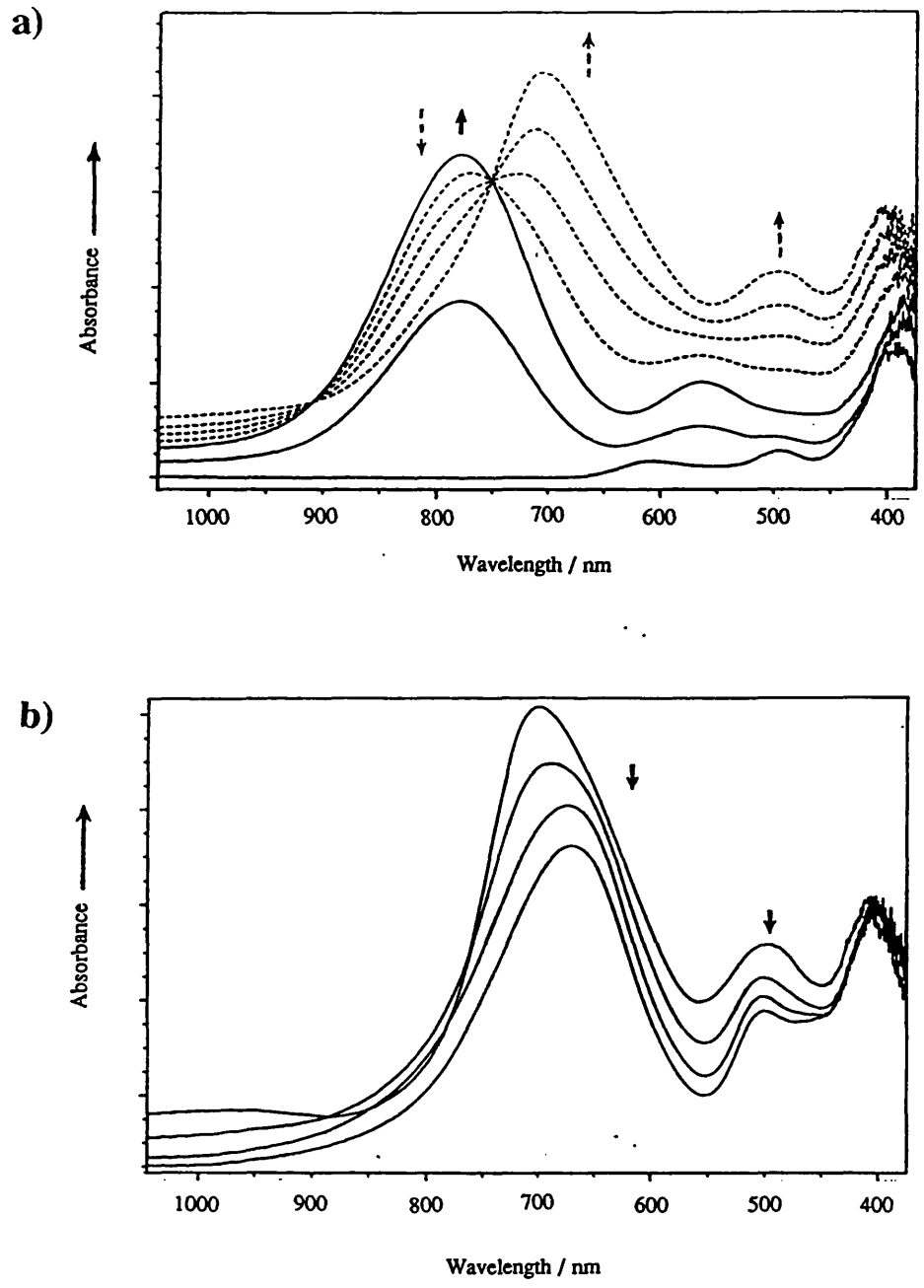

Fig. 3.14 Changes observed during ultra-violet/visible spectroelectrochemistry of $MoO(mnt)_2^{2-}$
a) on oxidation **b)** on reduction

473 nm respectively (**Fig. 3.15a**). However, this appeared to be an intermediate species, for the 774 nm peak subsequently moved to 662 nm and the 475 nm band greatly increased in intensity. Bands at 630 and 479 nm were observed after switching the potential to V_i (**Fig. 3.15b**).

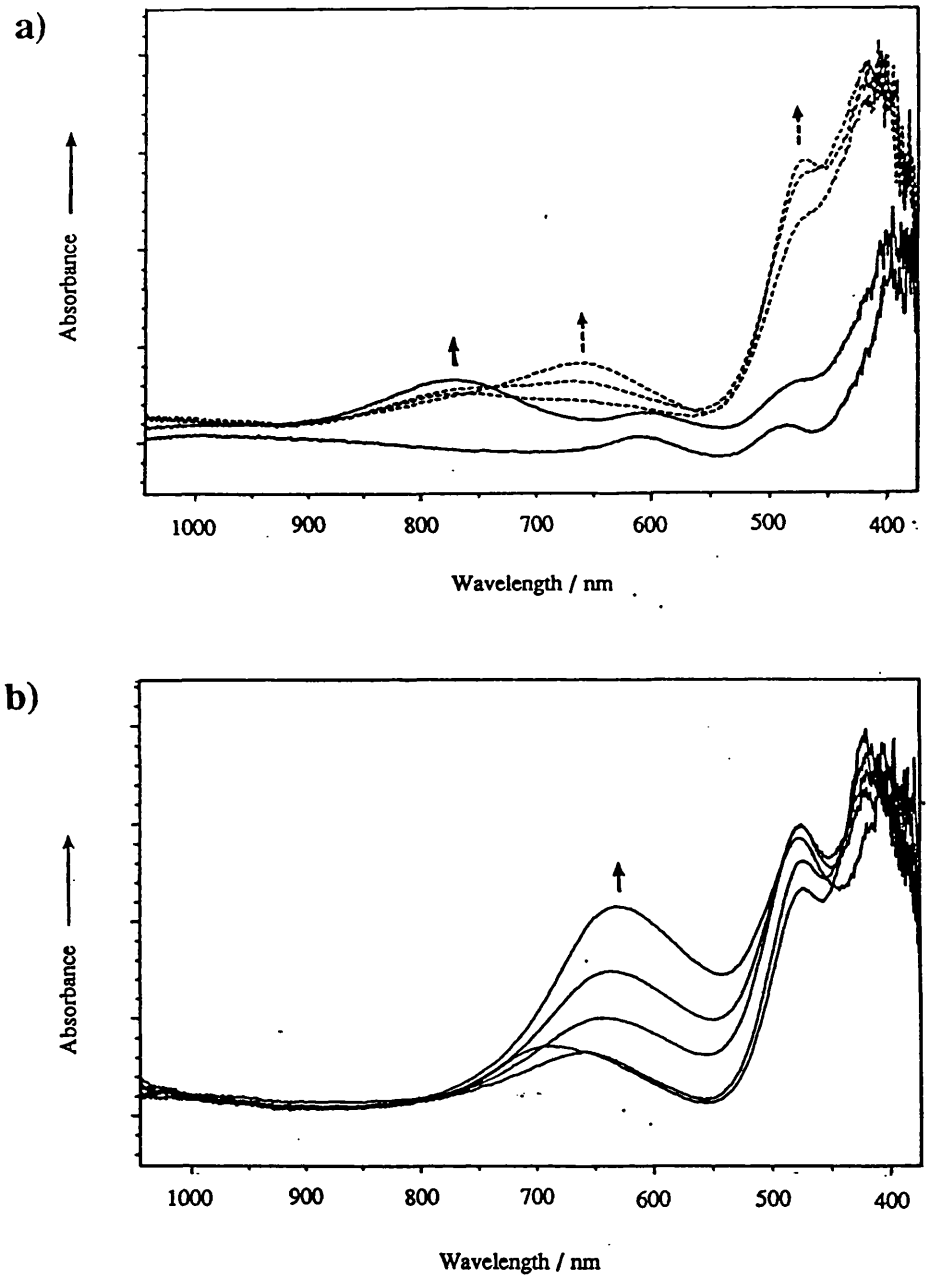

Fig. 3.15 Changes observed during ultra-violet/visible spectroelectrochemisty in the presence of bromide ions
a) on oxidation **b)** on reduction

3.6 Discussion

The most striking feature of both the infrared and electronic spectroelectrochemical results is the total chemical irreversibility of the reaction. This was especially unexpected behaviour, when considered in the light of the well-behaved

electrochemical reversibility exhibited in the preliminary cyclic voltammetry experiments (**Fig. 3.1**). A possible reaction scheme, shown in **Fig. 3.16**, is suggested to explain the spectral and electrochemical observations.

Species **A** is almost certainly $MoO(mnt)_2^{2-}$, because the differences between solid state and solution infrared and ultra-violet/visible spectra are minimal - the solid state structure of the compound is well-characterised. It can, therefore, be deduced that the sixth coordination position in the complex remains vacant in dichloromethane solutions and the square pyramidal geometry is retained.

During cyclic voltammetry an oxidised species **B** is formed, which retains the square pyramidal, monomeric structure of the original complex i.e . $MoO(mnt)_2^{1-}$. Species **B** is easily reduced to **A**, such that the redox couple **A⇌B** is completely electrochemically reversible.

Under the conditions necessary for standard spectroelectrochemistry (higher concentrations), however, the reaction appears to proceed via at least one intermediate on oxidation:-

$$\mathbf{A} \rightarrow \mathbf{D} \rightarrow \mathbf{E}$$

The inability to regenerate the starting material during standard spectroelectrochemistry, even over prolonged periods of time, is consistent with suspicions that the species observed is not the first product of the oxidation, but the second or third. The well-behaved nature of the redox couple requires that the complex suffers minimal structural and chemical alterations on oxidation in the electrochemical experiment. This should manifest itself in a spectroelectrochemical experiment by the facile and complete regeneration of $MoO(mnt)_2^{2-}$ on a comparable timescale to that required for the prior oxidation. It is evident that the experimental results do not conform to these expectations.

Species **B** is, therefore, assumed to undergo decomposition to species **D**, which is no longer easily converted back to **B**. Species **B** is sufficiently short-lived not to develop a significant concentration and does not appear in the spectra, so that the bands observed at 957.6, 2210.0 and 2220.4 cm^{-1} correspond to species, **D**, which accounts for the apparent chemical irreversibility of the reaction.

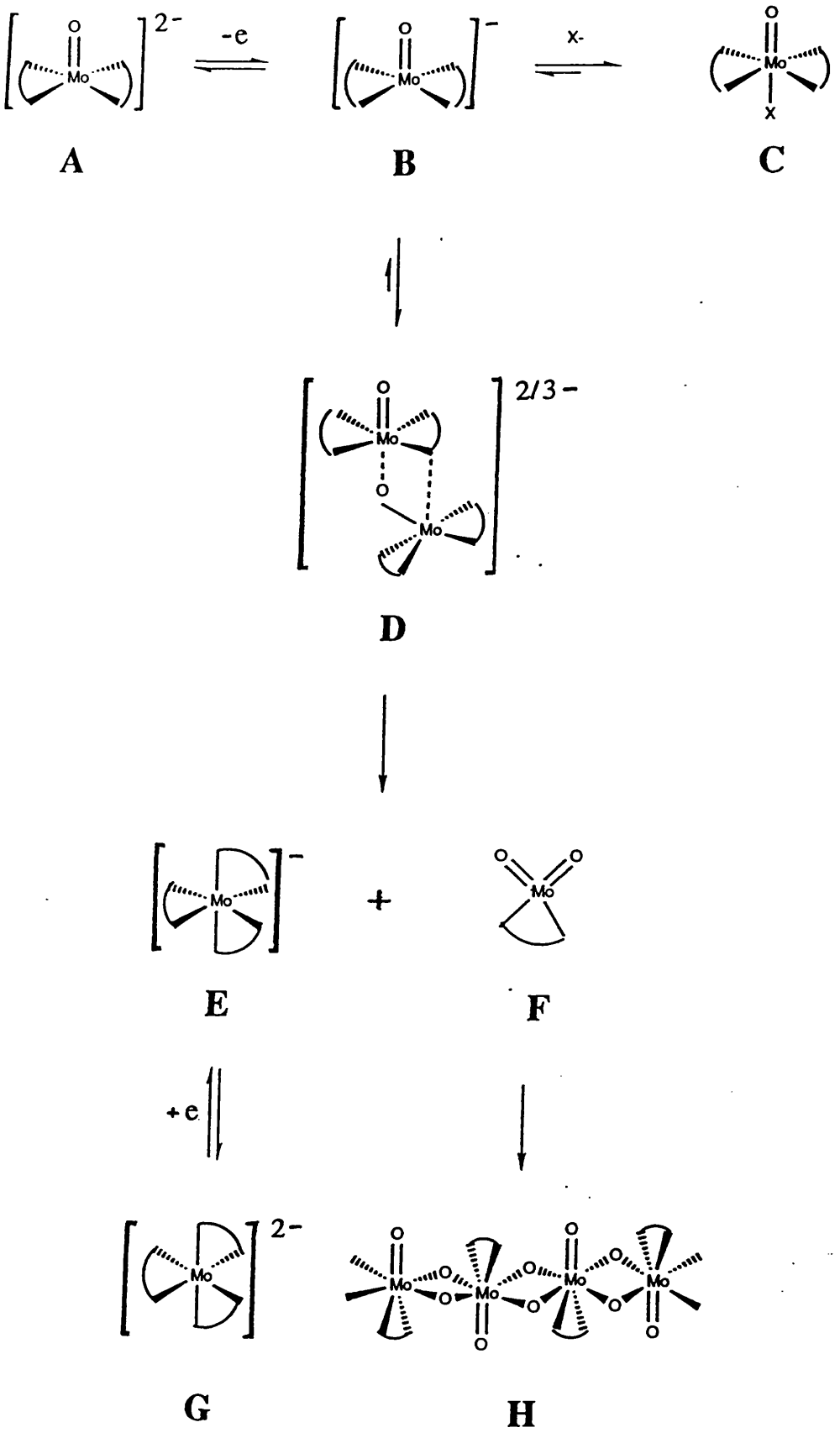

Fig. 3.16 Scheme for the electron transfer and following reactions of $MoO(mnt)_2^{2-}$

Results from modulation experiments serve to further substantiate this proposition. Chemically reversible behaviour can only be achieved using the small, 2 mm diameter, working electrode at -5 °C. Even then, it was necessary to allow thirty times as long for the reduction process as for the oxidation (60 s compared to 2 s). This suggests that the rate of the reduction process is no longer a function of mass transport and is kinetically controlled by the slow rate of electron transfer to the oxidised species or the slow chemical change following electron transfer.

The first species seen to form when the potential is switched to V_f has an intense band at 957.6 cm^{-1}, indicating the presence of a terminal oxo ligand in the complex. Cyanide stretching bands at 2210.0 and 2220.4 cm^{-1} suggest that the mnt ligands remain intact on the metal centre. The shift by both modes of vibration to a higher frequency on oxidation accords with predictions derived from the molecular orbital scheme described earlier. The loss of an electron from the b_2 non-bonding orbital would enhance the extent of π and σ donation by the oxo group and the σ-bonding by the mnt ligands to the metal atom centre. The HOMO remains b_2, no antibonding orbitals being occupied, so that the bond multiplicity of Mo=O is not lost. Hence, both the cyanide and oxomolybenum bonds would be shorter and stronger.

On the basis of these experiments, it is not possible to elaborate upon the nature of **D**, or even conjecture as to the total number of intermediate species. This required further work to clarify the oxidation process or identify the final products.

There is little evidence for a single (di)oxomolybdenum species in the final product(s). Instead, the cluster of weak, indistinct peaks in the 900-1000 cm^{-1} region is characteristic of a mixture of compounds, possibly with a combination of terminal and bridging oxo moieties. Clearer interpretation can be made on the basis of electronic spectra and the ν(CN) region in the infrared. The cyanide bands (2215.6 and 2223.8 cm^{-1}) occur at almost identical frequencies to those observed for the monoanionic tris-mnt species, $Mo(mnt)_3^{1-}$ (2215.6 and 2224.0 cm^{-1}). This is corroborated by ultra-violet/visible spectroelectrochemical data - the bands of the oxidised product were observed at 696 and 495 nm, which compared well with the 690 and 493 nm values obtained for $Mo(mnt)_3^{1-}$. The inference from this is that one of the reaction products **E** is the monoanionic tris-mnt complex.

The reduction process seems to comprise one step only, resulting in the

formation of yet another species **G**. From comparison of the spectra with the available data for the tris-mnt complexes, it is clear that species **E** - $MoO(mnt)_2^{1-}$ - undergoes facile reduction to the dianion - $Mo(mnt)_3^{2-}$. The dianionic tris-mnt complex is known to have cyanide stretching bands at 2202.6 and 2213.0 cm^{-1}, and electronic transitions occurring at 667 and 495 nm. Species **G** has bands at 2202.6 and 2213.0 cm^{-1} in the infrared region, and electronic transitions at 672 and 495 nm. Species **G** is, therefore, concluded to be $Mo(mnt)_3^{2-}$.

The conversion from an oxobis-mnt complex to a non-oxo tris-mnt species must involve the loss of a terminal oxo group and the gain of an extra mnt ligand. Since the sole source of mnt ligands in solution is the complex itself, it follows that the third mnt could only be acquired by transfer from another $MoO(mnt)_2^{2-}$ molecule. The oxidation reaction must, therefore, include an oligomerisation process. The oligomerisation may involve the combination of two molecules of **B** to give a dimer of overall double-negative charge or the combination of one molecule of **B** with one molecule of unreacted **A**, yielding a trianionic, mixed-valence dimer. A possible formulation for **D** is $[OMo(mnt)_2\text{-}(mnt)_2MoO]^{2-/3-}$, although it is not possible to distinguish between the dimers from the results of spectroelectrochemical experiments.

Electrochemical oxidation of $MoO(mnt)_2^{2-}$, species **A**, leads to the formation of a complex, $MoO(mnt)_2^{1-}$, species **B**, which is coordinatively unsaturated. The tendency for the sixth, vacant coordination site, trans to the oxo group, to be filled is greater in the oxidised species, **B**, than in the parent compound, **A**. Therefore, in the absence of other ligands, or a coordinating solvent, the probability of dimer/oligomer formation is significantly enhanced.

The resulting dimeric structure, species **D**, is strongly inferred to involve the terminal oxos of one molecule adopting a bridging mode by coordinating to the vacant sixth position of another molecule. The close proximity of the two molecules would then enable one of the mnt ligands from the six-coordinate member to bond weakly to the metal centre of the other member via one sulphur atom. It seems more likely that "oxo-donor" molecule is the monoanionic species, **B**, given the propensity of Mo^V to form μ-oxo species, whilst the "oxo-acceptor" exists in oxidation state IV as species **A**. The dimer can then adopt a configuration suitable for simultaneous transfer of oxo and mnt ligands between the metal centres.

The exact mechanism for the cleavage of the dimer is unknown. However, it is likely that, as the reaction proceeds, the new Mo-O bond, to the sixth coordination site of monomer **A**, shortens and strengthens, at the expense of the old Mo-O linkage to the oxo-donor species, **B**. The "donor" mnt ligand, from monomer **A**, takes up an entirely bridging mode, each sulphur atom being bonded to a molybdenum atom. Ultimately, the old Mo-O bond breaks, effectively transferring an oxo group to the other metal, and the second sulphur atom of the mnt ligand coordinates to the the non-oxo molybdenum, completing the transfer of the oxo and mnt ligands.

The other product of the dimerisation process, species **F**, is probably a dioxomolybdenum (V) species, with one mnt ligand. The coordinatively unsaturated nature of the unstable monomer, **F**, would favour the formation of relatively robust polymeric species, **H**, possessing a mixture of terminal and bridging oxo groups. Both species would give rise to a large collection of oxomolybdenum vibrational modes, contributing to the complexity of the infrared spectrum. The set of indistinct bands observed in the 900-1000 cm^{-1} region are assumed to arise from these species.

A test of the validity of the proposed dimer formation, is to compare the relative concentrations in solution of the starting material and the final product. According to the proposition, the ratio of $Mo(mnt)_3^{1-}$, species **E**, to $MoO_2(mnt)$/polymeric material, species **F** and **H**, should be 1:1 and the concentration of either component no more than half the initial concentration of $MoO(mnt)_2^{2-}$. This is accomplished by working with solutions of known concentration of $MoO(mnt)_2^{2-}$ and calculating the concentration of $Mo(mnt)_3^{1-}$, using the published values for the molar decadic extinction coefficient. In this way, the concentration of $Mo(mnt)_3^{1-}$ is consistently found to be 50(±5)% of the concentration of $MoO(mnt)_2^{2-}$. Furthermore, this is observed to be the case for a range of starting concentrations (from 2.34×10^{-3} to 29.52×10^{-3} $moldm^{-3}$).

To summarise, during cyclic voltammetry, the starting compound **A** undergoes oxidation to **B** (**Fig. 3.14**). The reaction timescale and dilution are such that the product **B** is simply related to **A** and interconversion between the two is diffusion controlled. When the reaction is examined by spectroelectrochemical techniques, higher concentrations of the reactive species **B** are produced, favouring dimerisation to species **D**. Species **D** is responsible for the intermediate bands noted in spectra. The

electrochemically irreversible redox reaction between **A** and **D** is monitored using the modulation technique. In standard spectroelectrochemistry, the potential is maintained at V_f long enough for the break up of dimer **D** into an oxo complex **F** and a tris-mnt species **E**. Following the breakup of the dimer, there is no indication that the reaction products can be converted back to **A** (i.e. **E** to **D** to **B** to **A**). Final reduction results in the formation of the dianionic tris-mnt species **G**.

According to the above explanation, the first product of the oxidation reaction is a square pyramidal species. If the sixth coordination position were to be occupied, then it could be possible to prevent dimerisation occurring and introduce some degree of chemical reversibility into the reaction. In order to examine this proposal, a coordinating ligand, the bromide ion, was added to the reaction solution.

The infrared and ultra-violet/visible spectra of $MoO(mnt)_2^{2-}$ do not alter with the addition of bromide, indicating that little coordination occurs to the starting material. The new set of spectral bands observed upon oxidation and its partial chemical reversibility (approximately 50% of the starting material, **A**, is regenerated) imply that the reaction pathway had not been followed to its ultimate product of the tris-mnt species. This signifies that the $MoO(mnt)_2^{1-}$ complex, **B**, has been successfully trapped by Br^- and dimer formation has been prevented. The band due to ν(Mo=O) is observed at a different frequency (976.0 rather than 931.1 cm^{-1}) for species **C**, $[MoO(mnt)_2Br]^{2-}$, due to the sensitivity of the oxo-molybdenum group to trans ligation.

Trans ligation decreases the π-acceptor capacity of the metal atom towards the terminal oxo, and decreases the strength of the Mo-O π- and σ-bonding. This is illustrated by a decrease in the molybdenum-oxygen stretching frequency. Therefore, although ν(Mo=O) for $[MoO(mnt)_2Br]^{2-}$ occurs at 976.0 cm^{-1}, the corresponding mode for the unsubstituted species would be expected to occur at a significantly higher wavenumber. The vanadyl complex $VO(acac)_2$ (acac=acetylacetonate), which also has the electronic configuration d^1, is known to exhibit a shift of almost 50 cm^{-1} in its vanadium-oxygen stretching frequency on trans ligation by pyridine (from 1004 to 956 cm^{-1} in dichloromethane).[8] Therefore, ν(MoO) for $MoO(mnt)_2^-$ would be expected at between 1000 and 1020 cm^{-1}.

A large proportion (approximately 50%) of the starting material, **A**, is regenerated when the experiment is carried out in the presence of bromide ions. The

improvement in chemical reversibility is a direct result of the trans ligation of the halide, which prevents dimerisation. The incomplete recovery of $MoO(mnt)_2^{2-}$, however, suggests that a significant fraction of the compound still undergoes side-reactions, yielding a variety of products. These may be responsible for the unassigned bands in the electronic spectra, although their vibrational modes are either too weak to be observed, or do not occur, in the regions of the spectrum under scrutiny.

3.7 Conclusions

Whereas this work was intended to be a study of a simple molecule, exhibiting very well-behaved electrochemical reactions, it transpired that the electrochemically reversible oxidation gives rise to a series of complex, chemically irreversible steps in spectroelectrochemical experiments. Although the chemistry could be examined at certain points along the pathway, using various techniques, once the dimer had been formed, it was difficult to prevent the occurrence of following reactions involving the transfer of both the oxo group and the mnt ligand.

The presence of a sixth ligand trans to the oxo group is presumed to trap the $MoO(mnt)_2^{1-}$ species, preventing attack from the terminal oxo of another molecule as a prelude to dimer formation. The use of other strongly-binding ligands in sufficiently high concentrations to combine with all molecules of $MoO(mnt)_2^{2-}$ on oxidation prevents dimerisation, but would also cause problems with respect to the reduction of the electrogenerated species. The reaction would no longer be electrochemically reversible. An alternative would be to replace the mnt groups with bulky ligands to sterically hinder the sixth coordination position and prevent attack by other molecules of the complex.

This problem is especially pertinant where five-coordinate Mo^V species are formed. In this oxidation state, there is a strong tendency for molybdenum to adopt six-coordination by forming oxo-bridged compounds. Once the dimer is formed, the subsequent modes of reaction depend upon the oxidation state of the complex and the other ligands present, either coordinated to the complex or readily available in solution. There can be no guarantee of the dimer splitting up to give precisely the

same monomers as were initially present in the solution.

The majority of this work was carried out on a strictly time-controlled basis with rapid data acquisition. The use of only one technique would have been insufficient to permit adequate monitoring of the reaction. However, by analysing electrochemical data in conjunction with information obtained from standard and modulated spectroelectrochemical experiments, it was possible to identify intermediates and suggest a feasible pathway for the redox reaction.

These results serve to highlight the diverse nature of the chemistry of molybdenum. This is particularly apparent in the distinct behaviour and properties exhibited by complexes of the metal in the individual oxidation states. The chemistry of the higher oxidation states is especially applicable to the study of biological systems, and a deeper insight into the behaviour of molybdoenzymes can be gained when oxo groups are present in the compound or oxo-transfer is a constituent stage of the reaction.

References

1. J. A. McCleverty, J. Locke, B. Ratcliff, E. J. Wharton, *Inorg. Chim. Acta*, (1969), **3**, 283

2. J. Selbin, *Angew. Chem. (Int. Ed.)*, (1966), **5**, 712

3. J. Selbin, *J. Chem. Ed.*, (1964), **41**, 86

4. F. A. Cotton, R. M. Wing, *Inorg. Chem.*, (1965), **4**, 867

5. P. C. H. Mitchell, *Quart. Rev.*, (1966), **20**, 103

6. C. R. Hare, I. Bernal, H. B. Gray, *Inorg. Chem.*, (1962), **1**, 831

7. J. Selbin, *Chem. Rev.*, (1965), **65**, 153

8. J. Selbin, L. H. Holmes, Jr., S. P. Glynn, *J. Inorg. Nucl. Chem.*, (1963), **25**, 1359

9. H. B. Gray, C. R. Hare, *Inorg. Chem.*, (1962), **1**, 363

10. C. J. Ballhausen, H. B. Gray, *Inorg. Chem.*, (1962), **1**, 111

11. Nugent, Mayer, "Metal-ligand Multiple Bonds", Wiley, New York, (1988)

Chapter 4

Spectroelectrochemical Studies of $Fe_4S_4(NO)_4$

Of all the transition metals present in biological systems, iron is the most profligate.[1-3] Trace amounts are essential to all organisms if two crucial functions - electron transfer and oxygen transport/storage - are to be performed. For example, higher animals are dependent on *haemoglobin*, probably the best-known iron protein, to transport oxygen from the lungs to muscle tissue, at which point it is transferred to *myoglobin* for use in respiration. The latter consists of a single haem group containing one iron atom, whilst *haemoglobin* can be described as a tetramer of *myoglobin*, comprising four haem groups bound to four protein chains. The process of transporting iron to the site of synthesis of iron-containing compounds, such as *haemoglobin* or a *cytochrome*, is carried out by *transferrins* (in higher animals) and *siderophores* (in lower organisms).

In many systems, electron transfer is performed very efficiently by a variety of iron proteins. These are generally classified as to whether or not they contain haem groups. *Cytochrome c* was one of the earliest biologically significant chemicals to be evolved and is important to the processes of photosynthesis and respiration. It is an example of a haem protein in which the iron atom is held in a porphyrin ring and varies between oxidation states +2 and +3 during the active cycle of the *cytochrome*.[1,4]

There are also several important categories of non-haem electron transfer agents, known as *rubredoxins* and *ferredoxins*, which are also characterised by relatively low molecular masses (**Fig. 4.1**). *Rubredoxins* (R.M.M.≈6000)[1,2] contain only one iron atom (**Fig. 4.1a**), tetrahedrally coordinated to four sulphur atoms from cysteine residues.[5] *Ferredoxins* contain two, four or eight iron atoms with an equivalent number of sulphur atoms and have slightly higher relative molecular masses (6-12 000).[1,2]

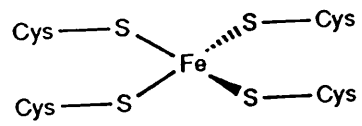

a) [Fe-S] Rubredoxin

b) [2Fe-2S] Ferredoxin

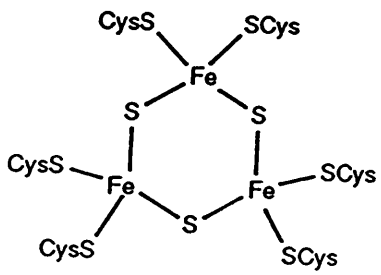

c) [3Fe-3S] Ferredoxin

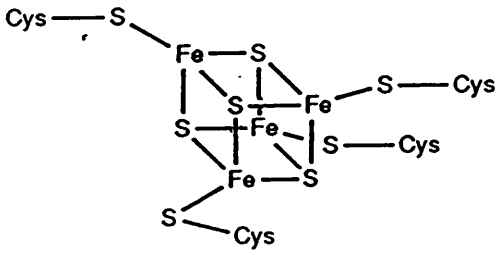

d) [4Fe-4S] Ferredoxin

Fig. 4.1 Iron sulphur proteins

[2Fe-2S] plant *ferredoxins* (Fig. 4.1b) have the general formula $Fe_2S^*_2(S\text{-cys})_4$, where S^* is known as an "inorganic" or "labile" sulphur atom, as opposed to the sulphur donor atom of a coordinating cysteine residue.[2] S^* sulphurs can bridge two or three iron atoms, whilst the S-cys sulphurs are linked terminally to one iron atom only. [4Fe-4S] bacterial *ferredoxins* (Fig. 4.1d) consist of two interpenetrating tetrahedra, one of iron atoms, the other of "labile" sulphur atoms, giving molecules with a cubane-type structure and general formula $Fe_4(\mu_3\text{-}S^*)_4(S\text{-cys})_4$.[1-3]

The [8Fe-8S] bacterial *ferredoxins* contain two Fe_4S_4 clusters. A very rarely-occurring form of Fe-S structure, recently detected in *Azobacter vinelandii Fd I*,[6] is the [3Fe-3S] site.[2] This was characterised crystallographically[7] and found to consist of an approximately six-membered $Fe_3S^*_3$ ring, the iron atoms of which achieved four-coordination by having two additional terminal ligands each (Fig. 4.1c).

[4Fe-4S] *ferredoxins* are further sub-divided into two categories - those which operate between oxidation states 2+/1+ with $E_{½} \approx -0.420$ V, and those which cycle between oxidation states 3+/2+ with $E_{½} \approx +0.350$ V.[2,3,5] The latter type are less common and, because they undergo redox reactions at very positive potentials, are designated "*HiPIP*'s (high-potential iron proteins). The normally-occurring state of *ferredoxins* is $\mathbf{Fd_{ox}}$ and the reduced is $\mathbf{Fd_{red}}$. These correspond to the reduced state $\mathbf{HP_{red}}$ and the super-reduced $\mathbf{HP_{s\text{-}red}}$ states respectively of a *HiPIP*, the latter of which is not biologically active. The oxidised state of a *HiPIP* is comparable to the inactive super-oxidised *ferredoxin* $\mathbf{Fd_{s\text{-}ox}}$ state.

All the non-haem iron proteins mentioned above are members of a large group of biologically-active chemicals - the iron-sulphur proteins. As well as being instrumental in electron transfer, these iron-sulphur proteins also form important constituent parts of the enzymes controlling hydrogen uptake, nitrogen fixation, the reduction of nitrates, nitrites and sulphites, and the oxidation of xanthine and aldehydes.[2,3] The presence of [4Fe-4S] clusters in *azoferredoxin* and the P-type clusters of *molybdoferredoxin* in nitrogenase has been well documented (see **Introduction**).

The importance of iron to biological systems, and the large variety of iron proteins present in them, has attracted the interest of numerous research groups. Extensive studies have been carried out to determine the electronic structure and bonding[6-13] at the metal atom centre of the active site. One consequence of this has been the preparation of many synthetic analogues modelling the active site of the protein.[2,14-21]

The initial work on iron-sulphur compounds was carried out in the 1850's by the French chemist, Z. Roussin, resulting in the production of two salts, which now take his name.[22] However, it was not until 1882 that "Roussin's Red" salt was correctly formulated by Pavel[23] as a dimeric iron complex with two bridging sulphur atoms and two terminal nitrosyl groups - $K_2[Fe_2(NO)_2(\mu_3\text{-}S^*)_2]$. The structure of "Roussin's Black" salt remained a mystery for a century until solved by Johansson and Lipscombe.[24] It was shown to be an iron tetramer, with three face-capping sulphurs and seven terminal nitrosyls - $K[Fe_4(NO)_7(\mu_3\text{-}S^*)_3]$. The red salt reacts with thiols to give a series of red diamagnetic complexes of the type $Fe_2(NO)_2(SR)_2$ (R=Me, Et, ^{i}Pr, ^{t}Bu, Ph, CH_2Ph), known as Roussin's Red esters.[1,2] A large area of research has also

opened up with the preparation of analogous compounds based upon the black salt - e.g. $Fe_4(\mu_3\text{-}S^*)_4(SR)_4^{n-}$,[25] $Fe_4(\mu_3\text{-}X^*)_4(\eta^5\text{-}C_5H_5)_2^{n+}$ (X^*=S, Se, Te),[11,26] $Fe_4(\mu_3\text{-}S^*)_4(NO)_4$.[27]

Of the many iron clusters studied, $Fe_4(\mu_3\text{-}S^*)_4(NO)_4$ is relatively well-characterised.[8,27] The structure of the $Fe_4S^*_4$ core closely resembles that of the [4Fe-4S] proteins, but the features of particular interest to the spectroscopist are the terminal nitrosyl groups on each iron atom (**Fig. 4.2**). Nitrosyl substituents give rise to very intense, easily-monitored bands in the infrared spectrum between 1950 and 1300 cm^{-1}, depending upon their mode of coordination. For $Fe_4(\mu_3\text{-}S^*)_4(NO)_4$, any significant alteration in the charge distribution is likely to be reflected by a shift in the wavenumber of ν(NO).

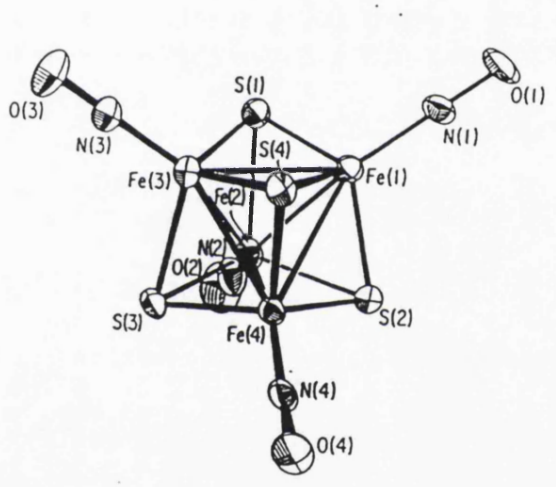

Fig. 4.2 Structure of $[Fe_4(\mu_3\text{-}S^*)_4(NO)_4]$

Chu, Lo and Dahl[27] showed that $Fe_4(\mu_3\text{-}S^*)_4(NO)_4$ undergoes two reversible reductions, and were able to isolate and characterise the monoanionic species. In this work, a third electrochemically-reversible reduction has been identified and spectroelectrochemical experiments have enabled the first characterisation of both the dianionic and trianionic species. The newly-developed spectroelectrochemical cell and modulation technique proved to be ideally suited for handling this air-sensitive compound and the reactive electrochemically-generated products.

4.1 Electronic Structure

$Fe_4(\mu_3\text{-}S^*)_4(NO)_4$ possesses a cubane-like structure of approximately cubic T_d symmetry, the iron and sulphur atoms occupying alternate corners of a distorted cube (**Fig. 4.2**).[27] Crystallographic studies of the complex indicate that all six Fe-Fe distances have approximately the same length (2.651 Å), an observation in keeping with the electron count, which gives a completely bonding Fe_4 tetrahedron. The twelve chemically-equivalent Fe-S bonds are found to have bond lengths between 2.208(1) and 2.224(2) Å, whilst the four Fe-N bondlengths have values ranging from 1.661(5) to 1.666(5) Å. The distribution of atoms is such as to give a localised symmetry of C_{3v} around each iron atom. All the nitrosyl groups are linear - $\angle$FeNO=176.9(5)-178.8(5)°.

One of the first molecular orbital analyses of metal clusters was carried out by Lauher,[28] who explained the bonding in terms of cluster valence electrons and molecular orbitals. This scheme was used as the basis of the appraisal of $Fe_4(\mu_3\text{-}S^*)_4(NO)_4$ by Dahl et al.[27] until Glidewell and Hoffmann[13] carried out extended Hückel calculations on several nitrosylated iron-sulphur clusters. Their quantitative description of the electronic structure of $Fe_4(\mu\text{-}S^*)_4(NO)_4$ will be used here.

Each iron atom in the neutral tetramer adopts a $3d^7$ (formally oxidation state I) electronic configuration, if coordination by NO^+ and S^{2-} is assumed.[13] As a result 60 electrons, 28 of them from the four iron atoms, are available for cluster bonding. The low-lying molecular orbitals (**Fig. 4.3**) possess only nitrosyl and sulphide character and are not directly involved in the Fe_4S_4 cage bonding. These are, in order of increasing energy:- 4 nitrosyl 3σ-based orbitals with a large oxygen 2s component (a_1+t_2), 4 nitrosyl 4σ-based orbitals with large nitrogen 2s component, (a_1+t_2), 4 non-bonding sulphur 3s orbitals, (a_1+t_2) and 8 π-bonding nitrosyl-based orbitals ,($e+t_1+t_2$).

All subsequent higher-energy molecular orbitals are responsible for the cluster bonding and are occupied by the 60 cluster valence electrons. The first set of these, (a_1+t_2), accounts for Fe-N bonding and has 5σ nitrosyl character, with a large component from oxygen 2p atomic orbitals. 12 Fe-S bonds are formed from the interaction between sulphur 3p atomic orbitals and metal atomic orbitals. They are represented by 12 molecular orbitals ($a_1+e+t_1+2t_2$), which are delocalised over the

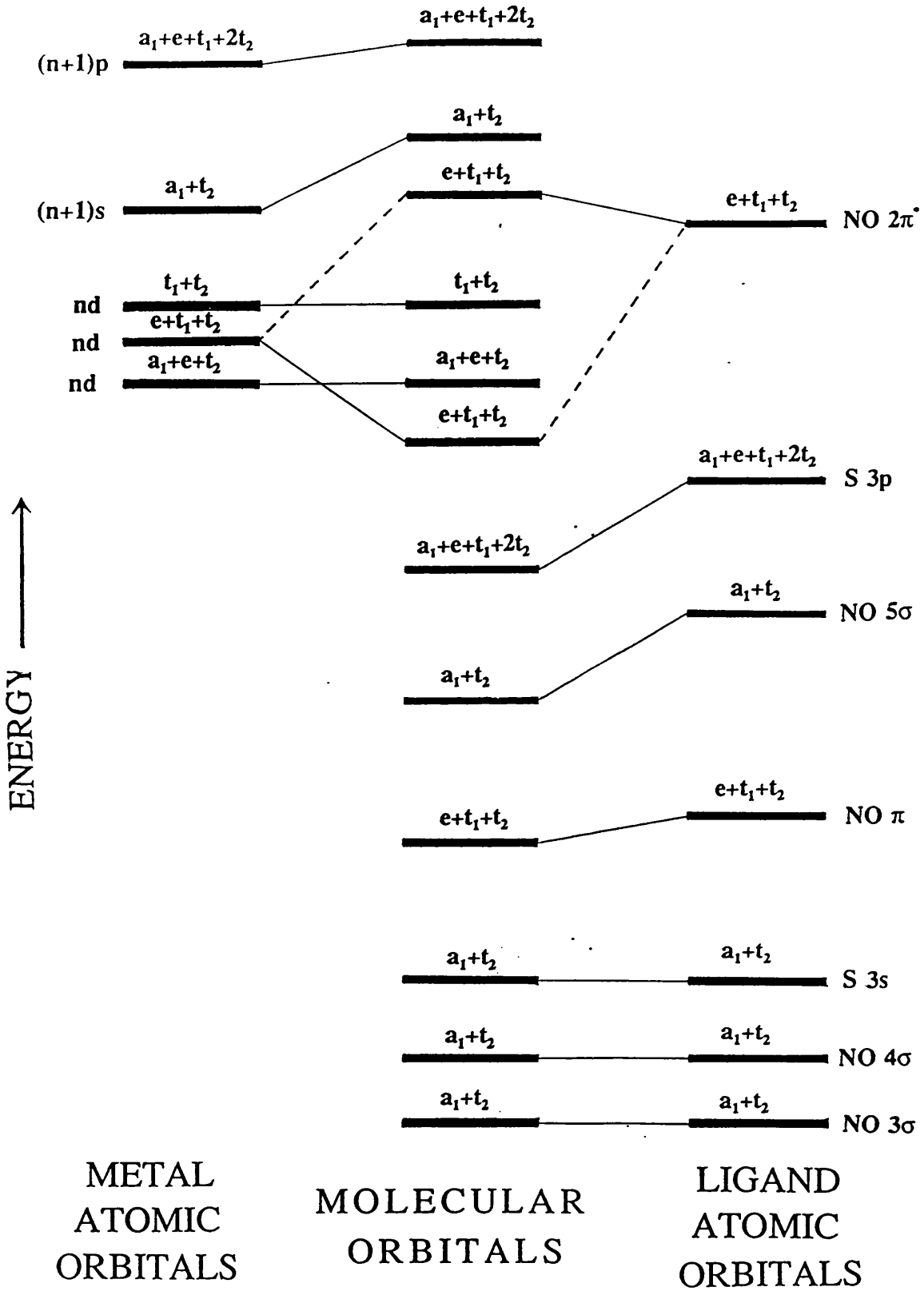

Fig. 4.3 Molecular orbital scheme for $[Fe_4(\mu_3\text{-}S^*)_4(NO)_4]$

entire cluster.

The iron atomic orbitals of symmetry ($e+t_1+t_2$) are not directly involved in Fe-Fe interactions and combine with 2π nitrosyl antibonding orbitals to give a degenerate set of 8 essentially non-bonding molecular orbitals ($e+t_1+t_2$). Metal d orbitals of symmetry (a_1+e+t_2) give rise to a set of 6 degenerate bonding molecular orbitals of unchanged symmetry. These are the Fe_4 cluster bonding orbitals, leading to a nett bond order of 6 for Fe-Fe bonds, and form the HOMO of the system. The LUMO (t_1+t_2) is antibonding with respect to the Fe_4 cage and consists of the remaining iron d orbitals.

In its ground state, $Fe_4(\mu_3\text{-}S^*)_4(NO)_4$ has the electronic configuration $(e+t_1+t_2)^{16}$ $(a_1+e+t_2)^{12}$. Glidewell and Hoffmann[13] propose that, because these two sets of orbitals are of comparable energy, they overlap and interact to a large extent. As a result, it is claimed that the HOMO is, in fact, a non-bonding molecular orbital and that the cluster would suffer minimal changes on the removal of an electron. Reduction of the complex would entail the addition of an electron to antibonding cluster orbitals (t_1+t_2) and, hence, a lowering of the Fe-Fe bond-order.

Crystallographic investigations carried out by Dahl et al.[27] have shown that all four nitrosyl groups are linear and coordinated terminally, acting as 3 electron donors via σ and π orbitals. The N=O linkage is, therefore, nominally a triple bond, although it is significantly weakened by metal $d\pi$ to ligand π^* backbonding. As the complex is reduced, more electrons are fed into the system, raising the energies of the metal d orbitals and causing them to approach that of the nitrosyl 2π orbitals. While the HOMO is formally Fe-Fe antibonding, it is likely to involve π back-bonding into the NO^* antibonding orbitals, weakening and lengthening the N-O bond. Consequently, the frequency of the nitrosyl stretching vibration is expected to shift to a lower wavenumber on reduction.

4.2 Electrochemistry

The electrochemistry of $Fe_4(\mu_3\text{-}S^*)_4(NO)_4$ has been studied in dichloromethane by Dahl et al.,[27] who observed two reversible redox couples with $E_{½}$=0.13 and -0.65

V (versus S.C.E.). It was claimed that, these electrochemical reactions represented two one electron reductions to the mono- and dianion respectively.

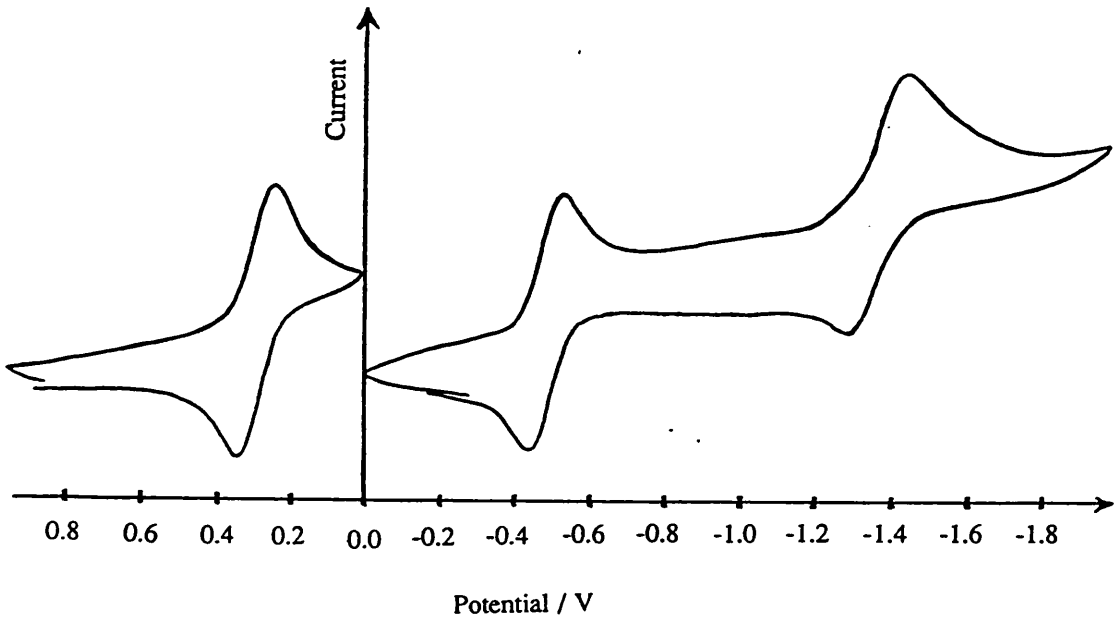

Fig. 4.4 Cyclic voltammogram of $[Fe_4(\mu_3\text{-}S^*)_4(NO)_4]$ in CH_2Cl_2

Our findings also indicate two reversible redox couples in dichloromethane (**Fig. 4.4**) with $E_{1/2}$ values of +0.27 and -0.51 V versus ferrocene. However, an additional reduction was noted with a half-wave redox potential of -1.40 V. Although $i_{Pa}=i_{Pc}$, and both were of the same magnitude as those of the first two redox couples, the difference between E_{Pa} and E_{Pc} was over 100 mV, suggesting that the reaction is not electrochemically reversible.

4.3 Synthesis

$Fe_4(\mu_3\text{-}S^*)_4(NO)_4$ was prepared according to the method of Dahl et al.[27] The entire reaction was carried out under an inert atmosphere to prevent decomposition of the product.

$$2Hg[Fe(CO)_3(NO)]_2 + \tfrac{3}{4}S_8 \rightarrow Fe_4S^*_4(NO)_4 + 2HgS + 3CO$$

Mercury bis(iron tricarbonyl nitrosyl)* (3.03 g; $5.6x10^{-3}$ mol) and elemental sulphur (0.54 g; 0.0168 mol) were added to toluene (88.5 cm^3) and the reddish-brown solution refluxed under a constant stream of nitrogen for 20 hours. After cooling to room temperature, a black solid, containing mainly mercury sulphide, elemental mercury and $HgFe(CO)_4$, was removed by filtration and washed with toluene until the washings were colourless. The washings were added to the remainder of the solution, which contained the dissolved product. The solvent was removed to give black crystals of $Fe_4(\mu_3\text{-}S^*)_4(NO)_4$.

* $Hg[Fe(CO)_3(NO)]_2$ was prepared in 52% yield according to King's method,[29] from mercury (II) cyanide and iron pentacarbonyl.

$$Fe(CO)_5 + KNO_2 \rightarrow KFe(CO)_3(NO) + CO\uparrow + CO_2\uparrow$$
$$2KFe(CO)_3(NO) + Hg(CN)_2 \rightarrow Hg[Fe(CO)_3(NO)]_2 + 2KCN$$

4.4 Infrared Spectro electrochemistry

The nitrosyl stretching mode, $\nu(NO)$ for $Fe_4(\mu_3\text{-}S^*)_4(NO)_4$ gives rise to a very intense, sharp band occurring at 1788.9 cm^{-1}.[27] The smaller diameter (2 mm) working electrode was used throughout this study, since the reaction rates obtained using the larger electrode were insufficiently rapid to allow stabilisation of the more highly-reduced product. It was found to be necessary to constantly monitor the reference electrode for any bleeding of the solute into the salt bridge. This was found to cause drifting of the potential of the working electrode, leading to the undesired formation of the monoanionic species.

Great care had to be taken to exclude all oxygen from the system, since this often contributed to the decomposition of the reduction products to Roussin's black salt and the possible subsequent disintegration of the cluster. Although there were no indications of the presence of Roussin's red salt ($\nu(NO)$=1716 cm^{-1}), several experiments were discovered, on closer examination, to have been contaminated with the black salt ($\nu(NO)$=1745, 1800, 1708 cm^{-1}).[12]

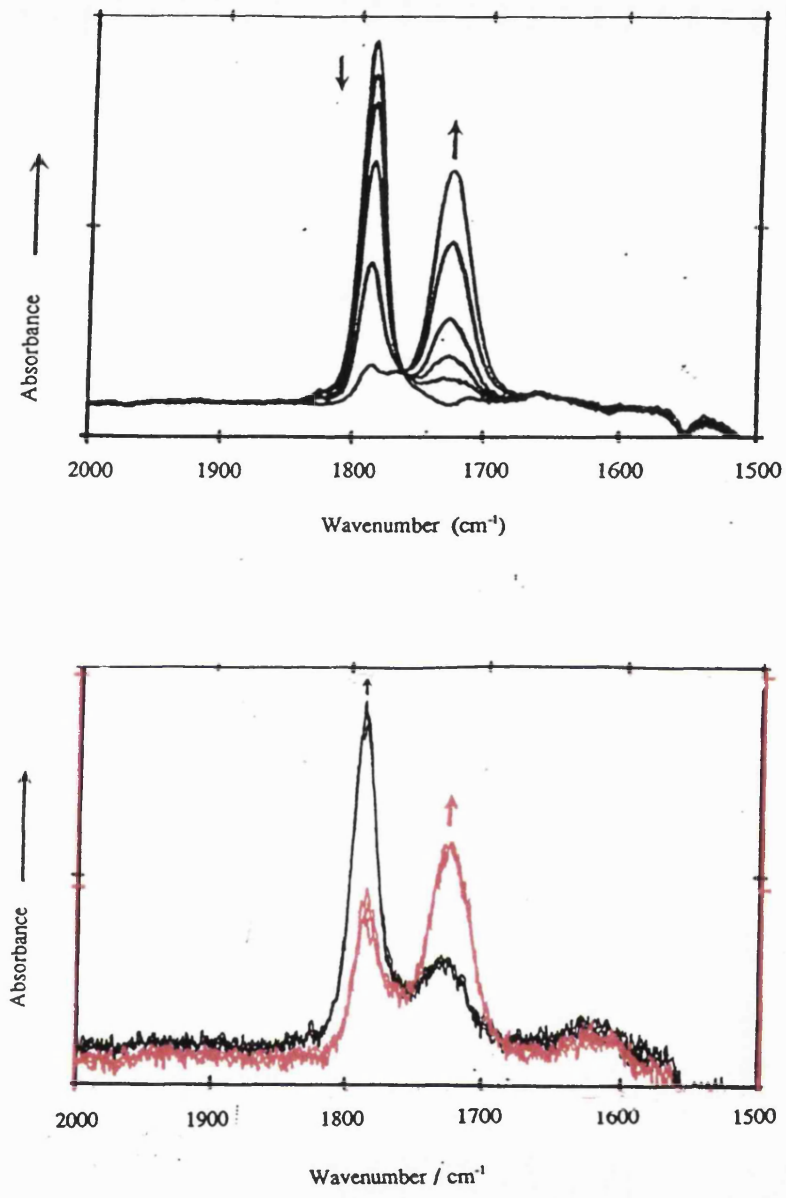

Fig. 4.5 Changes observed in ν(NO) for the spectroelectrochemistry reduction of [4Fe-4S] using **a)** normal **b)** modulated techniques

The peak at 1788.9 cm^{-1} collapsed and a new band, approximately three-quarters the intensity of the original, appeared at 1727.6 cm^{-1} (**Fig. 4.5a**) on switching

the potential from V_i to V_f[4Fe-4S]$^{1-}$ [a]. The monoanion was sufficiently stable at -10 °C for virtually all the starting material to be regenerated on switching the potential back to V_i. Modulation experiments, allowing equal times for the reduction and re-oxidation, demonstrated complete chemical, as well as electrochemical, reversibility. All spectra collected at V_i were superimposable, as were those collected at V_f[4Fe-4S]$^{1-}$ (**Fig. 4.5b**). Reversibility was confirmed by the regular and repetitive behaviour of the charging and reaction current during the experiment (**Fig. 4.6**).

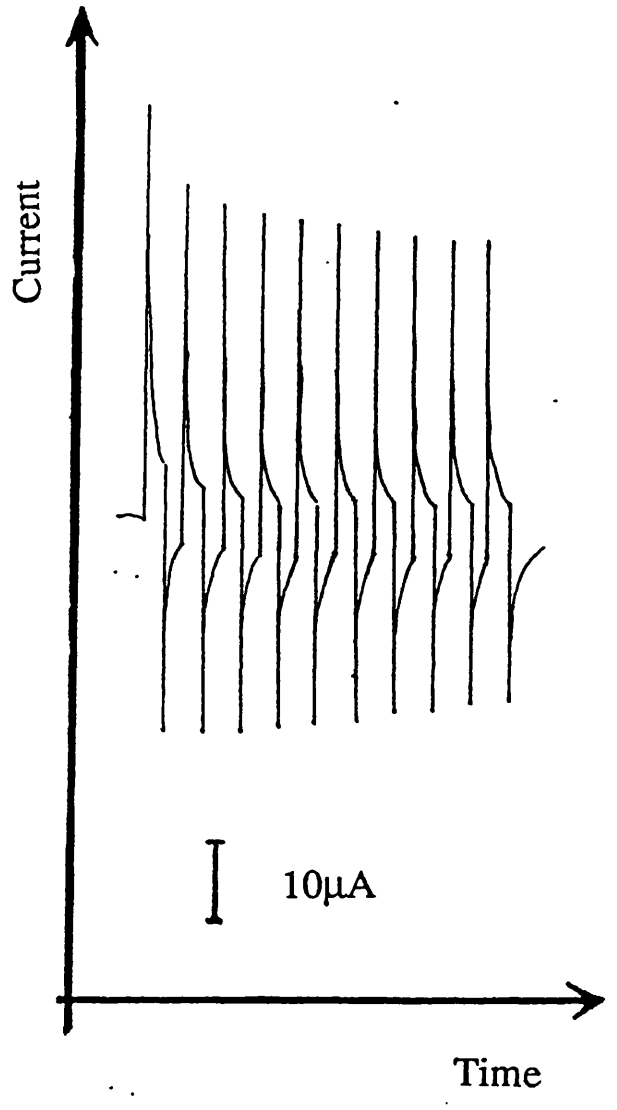

Fig. 4.6 Current response for the modulated spectroelectrochemical reduction of [4Fe-4S]

[a] V_i is potential at which only the neutral species exists in solution - V_i = +1.0V
V_f for the one electron reduction to the monoanionic species (i.e. potential at which the monoanion predominates in solution) in the reaction:-

$$[4Fe\text{-}4S]^0 + e^- \rightleftharpoons [4Fe\text{-}4S]^{1-}$$

where [4Fe-4S] = $Fe_4(\mu_3\text{-}S^*)_4(NO)_4$.
V_f[4Fe-4S]$^{2-}$ = 0.0V

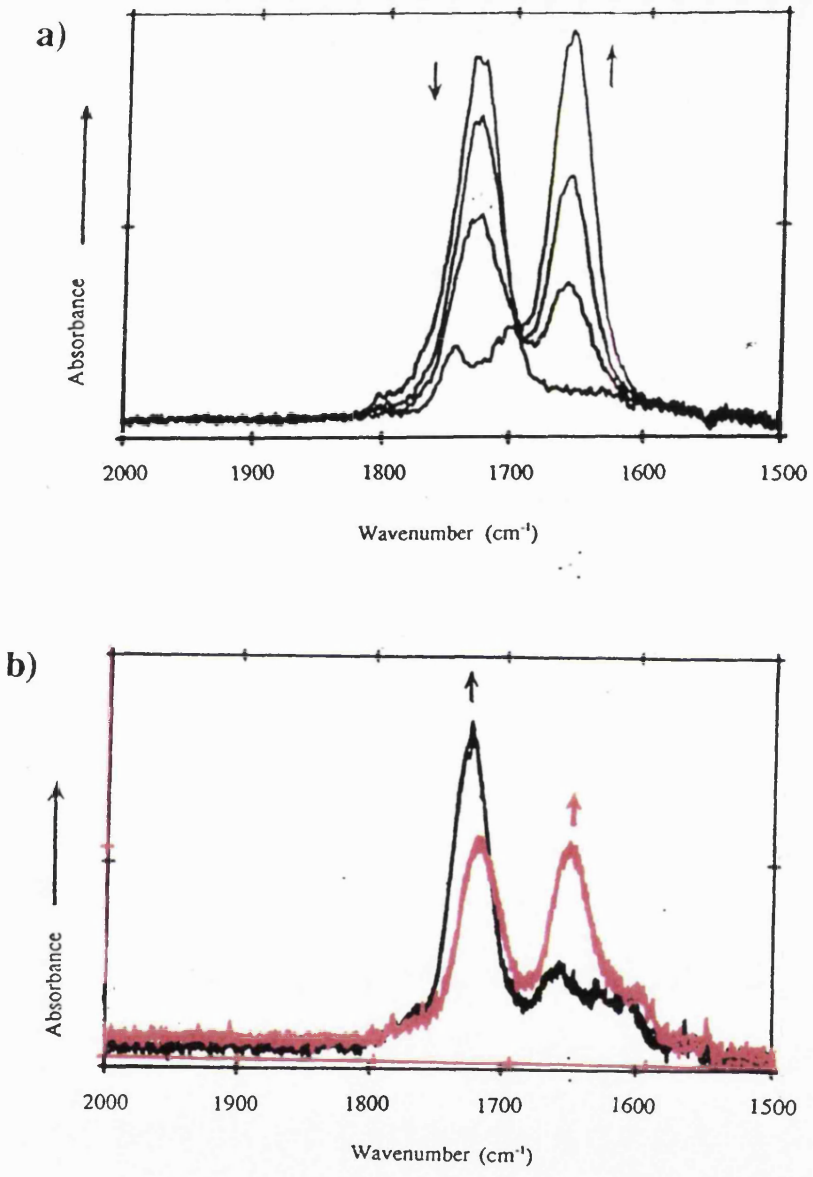

Fig. 4.7 Changes observed in ν(NO) for the spectroelectrochemical reduction of [4Fe-4S]$^{1-}$ using
a) normal **b)** modulated techniques

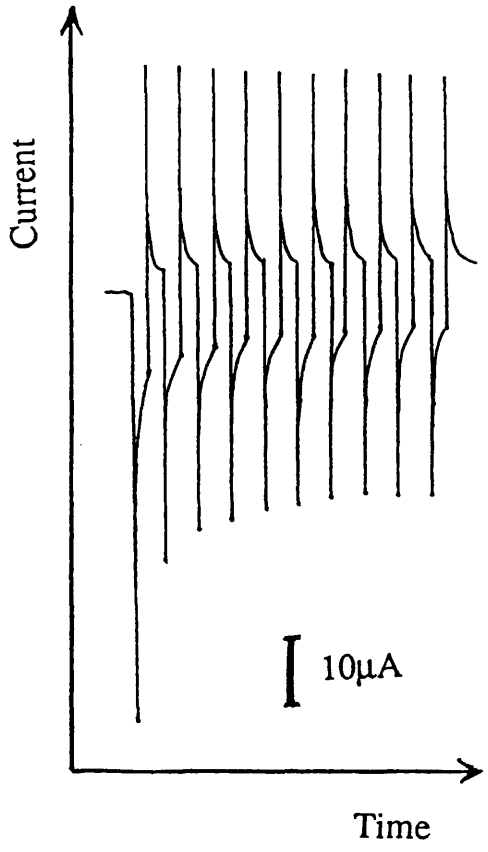

Fig. 4.8 Current response for the modulated spectroelectrochemical reduction of [4Fe-4S]$^{1-}$

The peak at 1727.6 cm^{-1} observed for the monoanion in the above reaction, disappeared when the potential was changed to V_f**[4Fe-4S]$^{2-}$** [b]. A new band could be seen at 1658.7 cm^{-1}, of similar intensity to ν(NO) for the neutral species and comparable in width to both the previous peaks (**Fig. 4.7a**). The results obtained from experiments carried out using the modulation technique emphasised the chemical reversibility of this particular couple - a cycle could be set up to give a repetitive and identical pattern of behaviour, with the potential being kept at V_f**[4Fe-4S]$^{1-}$** and V_f**[4Fe-4S]$^{2-}$** for equal lengths of time (**Fig. 4.7b**). This was further confirmed by analysing the current response at each change of potential (**Fig. 4.8**). These experiments were carried out at reduced temperature to prevent decomposition of the reactive reduced species.

The product of the third reduction could not be adequately stabilised using normal spectroelectrochemical techniques. However, modulation experiments made possible the repeated generation of small quantities of the trianionic species (**Fig. 4.9**). Although spectra obtained using "asymmetric" timescales (e.g. maintaining the

---

[b] V_f for the one electron reduction to the dianionic species (i.e. potential at which the dominant species in solution is the dianionic complex) for the reaction:-

$$[4Fe\text{-}4S]^{1-} + e^- \rightleftharpoons [4Fe\text{-}4S]^{2-}$$

For this couple, V_i = V_f**[4Fe-4S]$^{1-}$** V_f**[4Fe-4S]$^{2-}$** = -1.0V

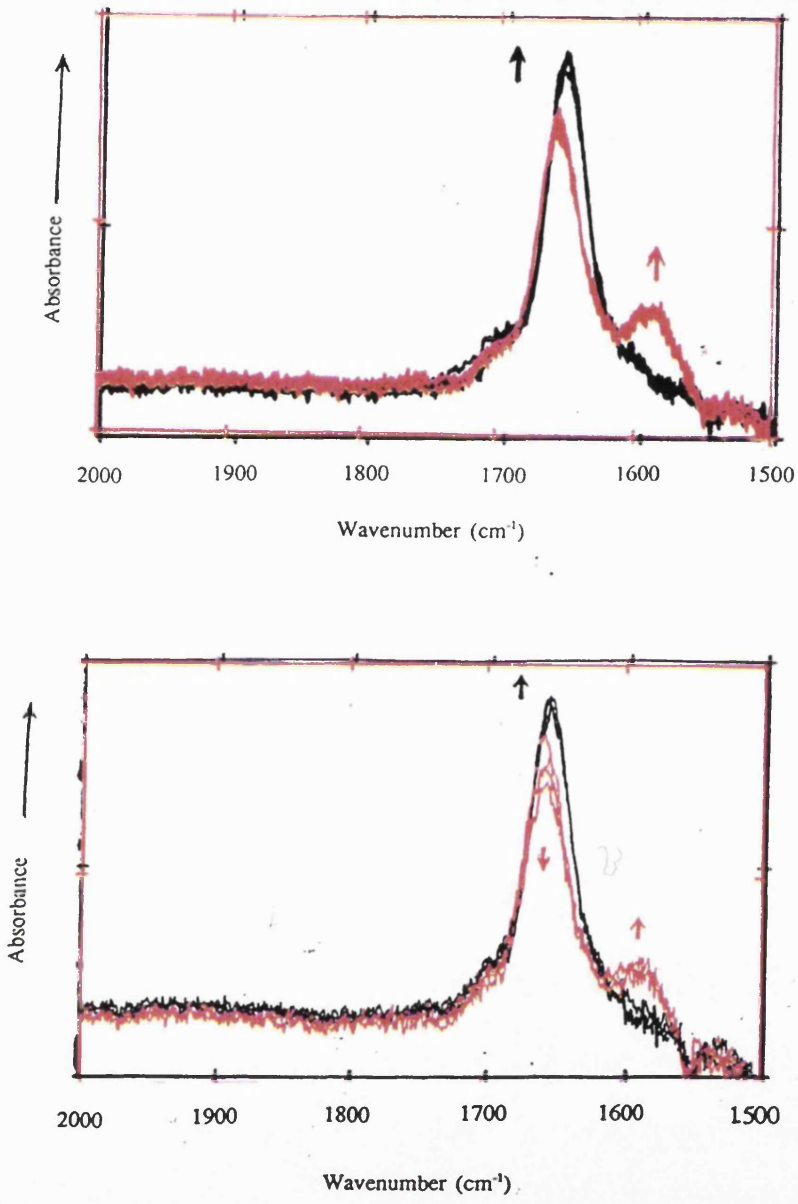

Fig. 4.9 Changes observed in ν(NO) for the modulated spectroelectrochemical reduction of $[4Fe\text{-}4S]^{2-}$ at
a) -3.0 °C **b)** -25.8 °C

potential at $V_f[4Fe\text{-}4S]^{2-}$ for 10.0 s and at $V_f[4Fe\text{-}4S]^{3-}$ [c] for 4.0 s) at -3.0° C conformed to reversibility requirements, the results from experiments, carried out at -3.0° C using "symmetric" timescales (e.g. 4.0 s at $V_f[4Fe\text{-}4S]^{2-}$; 4.0 s at $V_f[4Fe\text{-}4S]^{3-}$), proved to be equally reliable (**Fig. 4.9a**). Also, both the charging and reaction currents in current-time graphs demonstrated behaviour typical of chemically-reversible reactions (**Fig. 4.10**).

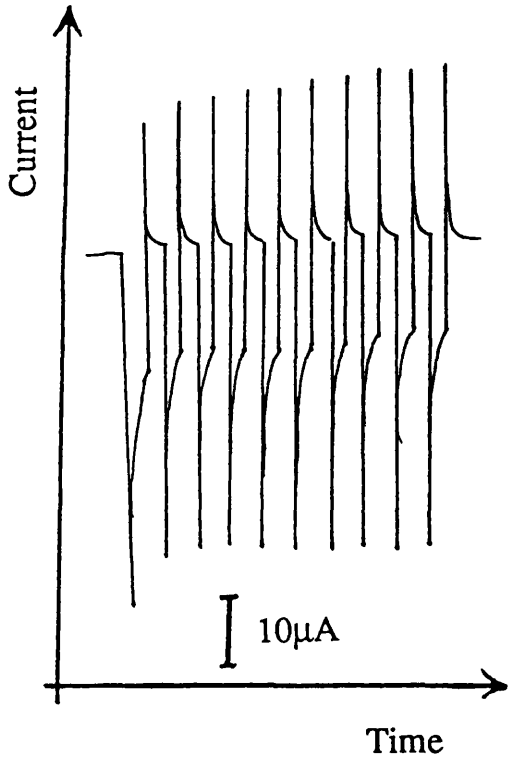

Fig. 4.10 Current response for the modulated spectroelectrochemical reduction of $[4Fe\text{-}4S]^{2-}$

Studies at -25.8 °C served to further improve the stability of the trianionic species in solution. As a result, the peak noted in the above experiments appeared with increased intensity (**Fig. 4.9b**). This band was observed at 1590.2 cm^{-1}, and was broader and somewhat less intense then the ν(NO) of the neutral, mono- and dianionic complexes.

---

[c] V_f for the one electron reduction to the trianionic species, according to the reaction:-

$$[4Fe\text{-}4S]^{2-} + e^- \rightleftharpoons [4Fe\text{-}4S]^{3-}$$

For this couple, $V_i = V_f[4Fe\text{-}4S]_{2-}$

$V_f[4Fe\text{-}4S]^{3-} = -2.0V$

4.5 Discussion

The observation of two redox couples with $E_{½}$ values of +0.26 and -0.51 V was in agreement with the findings of Dahl et al.[27] However, a third couple ($E_{½}$=-1.40 V) was noted, possessing identical i_{Pa} and i_{Pc} values to those observed for the other two redox couples. This redox reaction is, therefore, attributed to a further one-electron reduction of $Fe_4(\mu_3\text{-}S^*)_4(NO)_4$, rather than to any impurities or contaminants in the system. Data from spectroelectrochemical experiments, combined with observations of the current response behaviour, proved all the redox reactions to be chemically reversible, including the final reduction, for which E_{Pa}-E_{Pc} was significantly greater (100 mV) than the 59 mV stipulated for electrochemical reversibility.

Although the claim by Dahl et al.[27] that the first couple ($E_{½}$=+0.26 V) was a one electron reduction, and not an oxidation, initially seemed suspect, our experimental evidence appeared to confirm this statement. Infrared spectra of the neutral compound (as KBr discs) revealed a nitrosyl band at 1789 cm^{-1}, which remained unaltered during spectroelectrochemical experiments where V_f=+2.0 V. Instead, three new species were observed with ν(NO) at lower frequencies and more negative potentials. Therefore, the spectral bands noted correspond to neutral and anionic forms of the complex $[Fe_4(\mu_3\text{-}S^*)_4(NO)_4]^n$, where n=0, 1-, 2- and 3-, but not cationic.

The chemical reversibility of all three reductions is an indication of the lack of major structural differences between the neutral, mono-, di- and trianionic forms of the complex. There is no evidence, either in the spectral or electrochemical data, of the molecule breaking up. The Fe_4 cluster is remarkably stable and the retention of the intact $Fe_4(\mu_3\text{-}S^*)_4$ core in solution in a wide variety of oxidation states has been reported for several complexes. Notable amongst these is $Fe_4(\mu_3\text{-}S^*)_4(\eta^5\text{-}C_5H_5)_4$,[10] which has been identified in five oxidation states, the neutral, mono-,[11] and di-cationic[30] forms of which have been isolated and studied using X-ray crystallography. Several *ferredoxins* have also been monitored during the various stages of their active cycle of behaviour and were found to preserve the Fe_4 cluster throughout without any disintegration.[2,3]

The observed frequency of 1727.6 cm^{-1} for the nitrosyl stretching band of the monoanion was in good agreement with the ν(NO) of 1730 cm^{-1} reported by Dahl,[27] whose group had succeeded, after many attempts, in preparing $[Fe_4(\mu_3\text{-}S^*)_4(NO)_4]^{1-}$, as the $[K(2,2,2\text{-crypt})]^+$ salt, and determining its crystal structure. The addition of one electron to the complex had resulted in a slight structural distortion, changing from an idealised T_d to a tetragonal D_{2d} symmetry. The close agreement of the two ν(NO) frequencies suggests that the molecule adopts virtually identical structures in the solid state and in solution.

On reduction, the Fe-Fe bonds were observed to divide into two sets of four short and two long bonds, all with significantly increased bondlengths compared to the neutral species. Fe-S bonds were also longer than in the starting material, and were split into two groups (of four and eight distances). All four Fe-N bonds were shorter in the monoanion, whilst the four N-O bonds were found to increase in length on reduction.

As the metal d orbital occupancy increases on the formation of the monoanion, the energies of the orbitals will be raised, giving rise to more extensive metal dπ to ligand π backbonding. Since the back donation occurs to the nitrosyl antibonding π^* orbitals, the N-O bond order is reduced. This is consistent with the observed shift to lower frequency of the nitrosyl stretching vibration on reduction, indicating a lengthening and weakening of the N-O bond.

The shifts observed in ν(NO) on the first, second and third reductions - 61.3, 68.9 and 68.5 cm^{-1} respectively - are of almost equal magnitude. Since the frequency of the nitrosyl stretching vibration is a measure of the extent of back-bonding into the ligand π^* orbitals, this indicates that the extent of back-donation has increased by approximately an equal amount in each reduction step. This can only occur if all the electrons are sequentially entering metal-based orbitals of similar character and energy.

It should theoretically be possible to deduce the structure of the molecule in all its reduced forms by analysis of the nitrosyl stretching vibrations. Tetrahedral geometries have $\Gamma_{NO}=a_1+t_2$, of which only t_2 is infrared active, whilst the lower-symmetry D_{2d} geometry has $\Gamma_{NO}=a_1+b_2+e$, of which two modes - b_2 and e - are predicted to be infrared active. However, this proved to be of little use, since the spectrum of the monoanion closely resembled that of the neutral species in exhibiting

only one nitrosyl band in the 2000 to 1500 cm^{-1} region, despite the lowering of its symmetry to D_{2d}. It is possible that the second predicted nitrosyl band occurs at low frequencies and is, therefore, subject to camouflage by solvent bands or other skeletal vibrational modes of the complex. If the band were relatively weak, then it would prove equally difficult to identify and monitor through two reductions, even if it was to be found in the region expected for ν(NO).

A lowering of the molecular symmetry results in the loss of structural equivalence of the nitrosyl groups - this would serve to further increase the number of observable ν(NO) bands. The appearance of a single intense ν(NO) band in the monoanionic species, with no apparent splitting, suggests the retention of high molecular symmetry. the four nitrosyl groups remaining equivalent. This could only occur if the electrons were added to orbitals which were delocalised over the entire Fe_4 cluster and the filling of which would affect each iron atom equally.

To create the "61 electron species", the electron is added to the LUMO (t_1+t_2) set of orbitals (**Fig. 4.3**), which are antibonding with respect to the Fe_4 cluster - the t_1 component, lying lower in energy than the t_2, is occupied preferentially. This decreases the net Fe-Fe bond order to 5.5, causing the observed increase in size of the Fe_4 tetrahedron. As the complex is further reduced, more electrons are fed into the antibonding orbitals of the system, weakening the cluster bonding. The Fe-Fe bond order decreases progressively from 6.0 (for $[4Fe\text{-}4S]^0$) to 5.5 (for $[4Fe\text{-}4s]^{1-}$) to 5.0 (for $[4Fe\text{-}4S]^{2-}$) to 4.5 (for $[4Fe\text{-}4s]^{3-}$). The Fe_4 core of the cluster is, therefore, expected to continue to expand with the escalating negative charge of the complex. Glidewell and Hoffmann[13] predicted a 27% decrease in the Fe-Fe overlap as a result of the filling of one of the pair of the degenerate LUMO's.

The increase in the d electron occupancy from 7 in the neutral species to 8 in the monoanion has an additional effect, in that it gives a Jahn-Teller active configuration. The resultant distortions elongate the Fe_4 cluster, removing the structural equivalency of the iron atoms and increasing the length of two of the Fe-Fe bonds relative to the others, such that the molecule no longer conforms to T_d symmetry. Dahl et al.[27] postulate that the degeneracy of the t_1 level is removed, splitting it into two levels (a_2+e), with the unpaired electron residing in the lower-energy a_2 orbital. A

comparable structural feature, similarly attributable to the Jahn-Teller effect, has also been noted for several iron proteins.

When the degeneracy of the t_1 level splits in the monoanion, as a result of the Jahn-Teller effect, the a_2 non-degenerate orbital is stabilised, whilst the e component is raised in energy. The centre of gravity is maintained. Although the HOMO is known (a_2), the LUMO is less easily identifiable, because of the redistribution of the energy levels. If the distortion was sufficient to raise the e molecular orbital above one of the components of the t_2 orbital, then the latter would become the LUMO of the system. However, it is more probable that the LUMO is the e orbital, since the modifications in the energy levels due to the Jahn-Teller effect are relatively small for tetrahedral complexes.

The energy differences between the a_2, e and t_2 orbitals necessarily play an important role in determining the electronic configurations of the complex after the second reduction. Two alternative configurations are possible - a low-spin one, in which the electron is added to the a_2 level, or a high-spin one, where the electron is added to the LUMO. If the energy difference between the HOMO and LUMO were greater than that required to pair electrons in the a_2 level, then the a_2 level would be doubly-filled, stabilising the D_{2d} geometry. The energy difference is likely to be small, causing the complex to conform to Hund's rules and adopt a high-spin $(a_2)^1$ $(e)^1$ or, less probably, a $(a_2)^1$ $(t_2)^1$ configuration, containing a maximum number of unpaired electrons. Both the latter configurations are Jahn-Teller active, so D_{2d} geometry would be retained.

Following a similar argument, the third electron added could occupy the e orbital singly (if the previous configuration had been $(a_2)^2$) or doubly in a high-spin configuration $(a_2)^1$ $(e)^2$ - both would significantly increase the size of the Fe_4 cluster. The former electronic configurations would maintain the Jahn-Teller distortion and stabilise the D_{2d} geometry with respect to the T_d. The double filling of the e orbital in the latter would remove the need for Jahn-Teller distortion, such that the cluster could revert to T_d geometry. A third feasible option is the lowering of the t_2 level to an energy below that of the e orbital, with a possible removal of the degeneracy of the t_2 orbital and its splitting into a and e levels.

The small energy differences involved may cause "scrambling" of the four orbitals and it is difficult to determine the precise orbital occupancy from this work alone. Additional techniques, such as EPR spectroscopy, would be of use in identifying the number of unpaired electrons in each form of the complex. However, even the results from such experiments would be insufficient to enable the various permutations of orbital occupancies possible for a given number of unpaired electrons to be distinguished.

It is widely accepted that an empirical correlation exists between the frequency of the nitrosyl stretching mode and the nature of the bonding between the ligand and the metal.[1,4,5] Although the effect is difficult to quantify, it is recognised that the lower the ν(NO), the greater the likelihood that the ligand has changed from three electron to one electron donation (i.e. linear to bent configuration). The frequency is reduced further still with the adoption of doubly and triply bridging modes of coordination.

X-ray crystal studies[27] have shown that the nitrosyl groups in both the neutral and monoanionic species all adopt a linear coordination mode (average ∠FeNO=177.6° and 177.5° respectively). The infrared bands of these complexes occurs in a region of the spectrum (ca. 1950-1650 cm^{-1}) generally recognised to be characteristic of the stretching vibrations of terminally-coordinated **linear** nitrosyl groups. The bands observed in the trianionic species appear to fall within the range quoted (ca.1690-1525 cm^{-1}) for complexes containing terminally-coordinated **bent** nitrosyl groups, whereas that of the dianion occur at the point of overlap between the two ranges and cannot be assigned with confidence to either geometry on this basis.

A likely consequence of the build-up of electron density on the iron atoms is the destabilisation of the three-electron donating mode of nitrosyl coordination relative to the one-electron mode. The electron pair used in π donation is less readily accepted by the metal and the possibility that it resides in a non-bonding orbital of the nitrogen atom increases, thus reducing the FeNO angle. However, some compounds have been reported, in which the nitrosyl is coordinated in a linear fashion, but exhibits a ν(NO) of ca.1500 cm^{-1}. This tends to occur only in complexes with very high negative charges e.g. $[Cr(CN)_5(NO)]^{4-}$ which has a ν(NO) of 1515 cm^{-1}.

Although the $Fe_4(\mu_3\text{-}S^*)_4(NO)_4^{n-}$ (n=0, 1, 2, 3) cluster is highly negatively-charged overall, the charge is delocalised over the entire complex. As a result, there

is a nett increase of only ¾ of an electron per iron atom even after the the third reduction. When viewed in this light, it seems less likely that the build-up of electron density on the metal atoms is sufficiently large to force such a dramatic change in the coordination mode of the nitrosyl ligands.

4.6 Conclusions

The work described above further illustrates our ability to handle and study reactive and air-sensitive species efficiently. Dahl's work[27] on the electrochemistry of $Fe_4(\mu_3\text{-}S^*)_4(NO)_4$ and the characterisation of the monoanionic species was corroborated and extended. More detailed study revealed the presence of a third redox step, which led to the identification of the dianionic and trianionic forms of the complex.

The cluster structure was remarkably robust and remained intact throughout the experiments. This is a particularly important point, because of the presence of the Fe_4S_4 unit in a vast number of biological systems. Apart from the relatively small alterations in geometry caused by the Jahn-Teller effect, and a small expansion of the cluster on each reduction, the molecule retained the same general structure, with no sign of severe distortion, in its mono-, di- and trianionic forms.

Significantly, all the redox steps observed were chemically reversible. The results of the spectroelectrochemical experiments indicated the filling of a series of cluster-based molecular orbitals delocalised over the entire Fe_4 core, such that all nitrosyl groups remained effectively equivalent throughout the reductions. The increased electron density on the Fe_4 tetrahedron caused an escalation of metal to ligand back-bonding into nitrosyl π^* orbitals. The effect of this was to decrease the nitrogen-oxygen bond order and reduce the N-O force constant, such that a significant shift to lower wavenumbers was observed for ν(NO).

The wavenumbers of the ν(NO) bands for the mono-, di- and trianionic species occurred in a region of the spectrum usually associated with nitrosyl ligands in a bent mode of coordination. The spectral evidence has to be carefully weighed against the considerations of electronic configuration and molecular orbital occupancy. It was concluded that although the frequency of the ν(NO) band cannot be used to determine

the mode of ccordination of the nitrosyl, it is a useful measure of the extent of π back-bonding into the ligand antibonding orbitals and the delocalisation of charge over the entire complex.

References

1. N. N. Greenwood, A. Earnshaw, "*Chemistry of the Elements*", (1985), Pergamon Press, New York

2. T. G. Spiro (ed.), "*Iron-Sulphur Proteins*", (1982), Wiley-Interscience, New York

3. C. D. Garner, Chapter 4, "*Transition-metal Clusters*", B. F. G. Johnson (ed.)

4. J. E. Huheey, "*Inorganic Chemistry*", 3rd ed., (1983), Harper International, Cambridge

5. F. A. Cotton, G. Wilkinson, "*Advanced Inorganic Chemistry*", (1980), Wiley-Interscience, New York

6. M. H. Emptage, T. A. Kent, B. H. Huynh, J. Rawlings, W. H. Orme-Johnson, E. Münck, *J. Biol. Chem.*, (1980), **255**, 1793

7. C. D. Stout, D. Ghosh, V. Pattabhi, A. H. Robbins *J. Biol. Chem.*, (1980), **255**, 1797

8. R. S. Gall, C. T-W. Chu, L. F. Dahl, *J. Am. Chem. Soc.*, (1974), **96**, 4019

9. I. Bertini, F. Briganti, C. Luchinat, A. Scozzafava *Inorg. Chem.*, (1990), **29**, 1874

10. J. A. Ferguson, T. J. Meyer, *Chem. Comm.*, (1971), 623

11. Trinh-toan, W. P. Fehlhammer, L. F. Dahl, *J. Am. Chem. Soc.*, (1977), **99**, 402

12. C. T-W. Chu, L. F. Dahl, *Inorg. Chem.*, (1977), **16**, 3245

13. S-S. Sung, C. Glidewell, A. R. Butler, R. Hoffmann, *Inorg. Chem.*, (1985), **24**, 3856

14. C. Chen, J. Cai, Q. Liu, D. Wu, X. Lei, K. Zhao, B. Kang, J. Lu, *Inorg. Chem.*, (1990), **29**, 4878

15. R. W. Johnson, R. H. Holm, *J. Am. Chem. Soc.*, (1978), **100**, 5338

16. E. J. Laskowski, R. B. Frankel, W. O. Gillum, G. C. Papaefthymiou, J. Renaud, J. A. Ibers, R. H. Holm, *J. Am. Chem. Soc.*, (1978), **100**, 5322

17. J. G. Reynolds, E. J. Laskowski, R. H. Holm, *J. Am. Chem. Soc.*, (1978), **100**, 5215

18. T. D. P. Stack, J. A. Wengel, R. H. Holm, *Inorg. Chem.*, (1990), **29**, 3745

19. J. Jordanov, E. K. H. Roth, P. H. Freiss, L. Noodleman, *Inorg. Chem.*, (1990), **29**, 4288

20. S. Ciurli, M. Carrié, J. A. Weigel, M. J. Carney, T. D. P. Stack, G. C. Papaefthymiou, R. H. Holm, *J. Am. Chem. Soc.*, (1990), **112**, 2654

21. L. L. Nelson, F. Y-K. Lo, A. D. Rae, L. F. Dahl, *J. Organomet. Chem.*, (1982), **225**, 309

22. Z. Roussin, *Ann. Chim. Phys.*, (1858), **3**, 52, 258

23. O. Pavel, *Ber.*, (1882), **15**, 2600

24. G. Johansson, W. N. Lipscombe, *Acta Crystallogr.*, (1958), **11**, 594; *J. Chem. Phys.*, (1957), **27**, 1417

25. B. A. Averill, T. Herskovitz, R. H. Holm, J. A. Ibers, *J. Am. Chem. Soc.*, (1973), **95**, 3523

26. C. H. Wei, G. R. Wilkes, P. M. Treichel, L. F. Dahl, *Inorg. Chem.*, (1966), **5**, 900; R. A Schunn, C. J. Fritchie Jr., C. T. Prewitt, *Inorg. Chem.*, (1966), **5**, 892; Trinh-Toan, B. K. Teo, J. A. Ferguson, T. J. Meyer, L. F. Dahl, *J. Am. Chem. Soc.*, (1977), **99**, 408

27. C. T-W. Chu, F. Y-K. Lo, L. F. Dahl, *J. Am. Chem. Soc.*, (1982), **104**, 3409

28. J. W. Lauher, *J. Am. Chem. Soc.*, (1978), **100**, 5305

29. R. B. King, *Organomet. Synth.*, (1965), **1**, 165

30. Trinh-Toan, B. K. Teo, J. A. Ferguson, T. J. Meyer, L F. Dahl, *J. Am. Chem. Soc.*, (1977), **99**, 408

Chapter 5

Spectroelectrochemical Studies of $cpMo(CO)_2(NO)$

Numerous transition metal complexes have been prepared containing nitric oxide as a coordinated ligand. They are of particular interest because, NO^+ is part of an isoelectronic series of ligands together with carbon monoxide, CO, and cyanide, CN^-.[1-4] Many studies have been conducted to investigate the similarities between the behaviour of these groups as ligands and the nature of their bonding to the metal atom centre. Attempts have also been made to formulate criteria for differentiating between the various modes of coordination adopted by the ligands.

A terminal linkage (**Fig. 5.1a**), involving a linear metal-ligand M-X-Y bond, is the preferred mode of coordination for all three ligands.[2,4] Whilst this form of coordination predominates for carbonyls and cyanides, the nitrosyl ligand is noted for its ability to adopt alternative modes of coordination. In 1968, Hodgson et al.[5] reported a compound containing a distinctly bent terminal M-N-O linkage (**Fig. 5.1b**) - the Ir-N-O bond angle in $[IrCl(CO)(NO)(PPh_3)_2]^+$was crystallographically determined to be 124 (1)°.

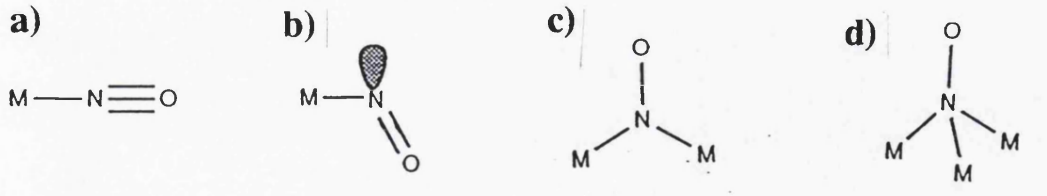

Linear terminal Bent terminal Doubly-bridging Triply-bridging

Fig. 5.1 Different modes of coordination for the nitrosyl ligand

Two years later, Eisenberg et al.[6] reported the synthesis of a ruthenium dinitrosyl complex, which exhibited both modes of coordination. $[RuCl(NO)_2(PPh_3)_2]^+$ was shown to have both bent (∠RuNO=136 (2)°) and linear (∠RuNO=179 (2)°)

nitrosyl linkages. Eisenberg's group were also responsible for the subsequent studies of linear-bent nitrosyl equilibria in complexes undergoing η^3-η^1 allyl interconversion.[7]

Nitrosyl ligands can also adopt bridging modes of coordination (**Fig. 5.1c,d**).[1,2,4] Although this mode of coordination is less common, significantly more examples of bridging nitrosyls are known than bridging carbonyl or cyanide ligands. Compounds such as $[Cr(\eta^5\text{-}C_5H_5)(NO)_2]_2$ contain two terminally-linked linear nitrosyls and two doubly-bridging nitrosyl groups spanning the chromium atoms.[2] Instances of triply-bridging nitrosyl species are rarer. An example of this type of coordination is found in $(\eta^5\text{-}C_5H_5)_3Mn_3(NO)_4$,[8] which comprises an equilateral triangle of manganese atoms with a doubly-bridging nitrosyl group along each side and a triply-bridging nitrosyl ligand directly below.

Several descriptions have been proposed for the coordination of the ligands to the metal atom in the various coordination modes.[1,2,4,9-11] It is generally accepted that the nature of the metal-ligand bond in complexes with linear terminally-coordinated groups is broadly similar. Cyanide, carbonyl and nitrosyl ligands all act both as σ donors and π acceptors. Although carbonyl and nitrosyl groups are the better π acceptors and tend to stabilise complexes of transition metals in low oxidation states, the negative charge of the cyanide ligand decreases its effectiveness as a π acceptor. Cyanide ligands are better σ donors and are, therefore, generally to be found in complexes where the metal is in a higher oxidation state.

As the mode of coordination of the ligand deviates from linear terminal, the overlap between the metal and ligand orbitals decreases, reducing the extent of π back-bonding. Ultimately, when the group adopts bent terminal or bridging linkages, the metal-ligand bond comprises only the σ component, with the lone pair residing on the nitrogen atom. The extent of π back-bonding is a particularly important consideration, since it reflects the metal d orbital occupancy. A consequence of any alteration in the amount of back-donation is a modification of the ligand bond strength and its force constant, which manifests itself as a variation in the frequency of the ligand stretching vibration.[4]

All three ligands have infrared-active ligand stretching vibrational mode giving rise to very intense bands. The positions and intensities of these bands are very sensitive to the d electron occupancy of the metal and the extent of π back-bonding

to the ligand. As a result, both can be used to probe the electronic structure of complexes. This effect has been demonstrated in the case of ν(CN), in **Chapter 2** and **3**, and ν(NO), in **Chapter 4**, and is known, from a broad range of studies, to hold true for ν(CO).

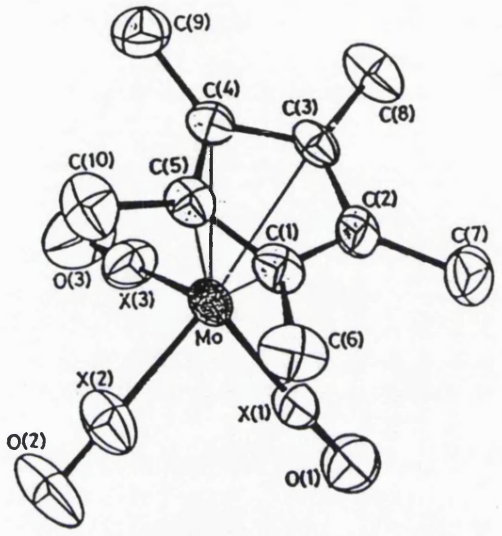

Fig. 5.2 Structure of $(\eta^5\text{-}C_5Me_5)Mo(CO)_2(NO)$

The compound $(\eta^5\text{–}C_5Me_5)Mo(CO)_2(NO)$ (**Fig. 5.2**) is one of a series described as having a "piano-stool" structure and contains two of the ligands discussed above. Both the nitrosyl and carbonyl groups give rise to easily-monitored bands in the infrared spectrum between 2100 and 1300 cm^{-1}. The nitrosyl group is linear and, in fact, cannot be distinguished from the carbonyl ligands in X-ray crystallographic studies.[12] This compound exhibits at least one reversible one-electron reduction, the product of which was studied by Geiger et al. using EPR spectroscopy.[13] The results of this study were interpreted in terms of the radical anion having a bent terminal nitrosyl linkage.

5.1 Electronic Structure

The bonding of cyanide, carbonyl and nitrosyl groups can be broadly described in terms of σ and π components.[2] The σ ligand-to-metal bond arises from the combination of sp_σ orbitals on the carbon atoms of CO and CN^- with suitable d_σ orbitals on the metal. The metal-to-ligand π bond is formed by the overlap of filled metal d_π orbitals with empty $2p_\pi^*$ antibonding orbitals based on the carbon atom. The withdrawal of electron density from the metal allows for increased σ-donation of

electrons from the ligand to the metal, thereby strengthening the σ bond. This is known as the synergic effect.

Nitrosyl ligands differ slightly from cyanides and carbonyls, in that they are formally three, rather than two, electron donors. The bonding model involves electron-pair donation from the ligand to the metal to form a σ bond, preceded by preliminary transfer of an electron from the NO to the metal. σ bond formation occurs only when the ligand is in the NO^+ form. Similarly to the effect noted for carbonyls and cyanides, σ donation is made easier by the back-donation of d_π electrons from the metal into nitrosyl π^* antibonding molecular orbitals.[14]

As a result, both the metal-nitrogen and the nitrogen-oxygen bonds are short. The nitrogen-oxygen linkage is formally a triple bond, although this tends to be slightly weakened by the π back-bonding. In coordinated nitrosyls, the nett positive charge resides on the nitrogen atom. The oxygen atom, which has a formal positive charge in free NO^+, gradually acquires more negative charge as the extent of back-bonding increases.[14]

The linear terminal form of coordination is found to be less common in complexes of the later transition metals and in complexes of metals in low oxidation states, where low-lying metal orbitals are filled. In these situations, the metal centre is less able to accept three electrons from the ligand and the nitrosyl, of necessity, behaves as a one-electron donor. The remaining pair of electrons resides in a non-bonding orbital on the nitrogen atom, which is formally described as sp^2 hybridised.[11]

The bond order of the N=O linkage is reduced from a formal triple bond in linear terminal coordinations to a double bond in systems containing the bent configuration. The metal nitrogen bond increases by as much as 12 pm as the ligand changes from linear to bent terminal coordination. The metal-nitrogen-oxygen bond angle also decreases significantly, the usual range for bent nitrosyls being 120-140°.[9] This mode of coordination is not observed for either carbonyl or cyanide ligands.

Examples of double bridging are known for carbonyl and nitrosyl ligands.[2,4,9-11] The former donates one electron to each metal via σ bonds from an sp^2 hybridised carbon atom and remains a two-electron donor overall. The latter transfers one electron to one metal atom to form a σ bond similar to that in the bent form of coordination. The lone pair of electrons on the nitrogen atom are then involved in a

dative bond to the other metal atom; accordingly the nitrosyl formally remains a three-electron donor. Carbonyls and nitrosyls can bridge three metal atoms, but this occurs very rarely.[2]

There have been several attempts[2,4] to categorise the various modes of coordination according to the frequency of the nitrosyl, carbonyl or cyanide stretching vibration. Authors of many standard texts[9-11] quote frequency ranges for ν(NO) for the linear, bent and bridging forms of the ligand. However, the classifications vary significantly from author to author and overlap to a great extent, thereby lessening their diagnostic utility. The frequencies of the vibrational modes are especially sensitive to the coordination number of the complex, the oxidation state of the metal and the nature of the other ligands present. For this reason, numerous compounds have been found whose nitrosyl stretching vibrations appear to fall outside the range allotted for their particular mode of coordination.

The frequencies of carbonyl stretching vibrations can be categorised more easily. A generally accepted range for ν(CO) for a terminally coordinated ligand is 2125-1850 cm^{-1}. Bridging ligands can be identified by the presence of ν(CO) bands at lower wavenumbers i.e. 1875-1725 cm^{-1}.[2,10] Care has to be exercised with the assignment, as with the nitrosyl ligands, as several examples are known of terminally-coordinated carbonyl groups giving rise to stretching bands below 1800 cm^{-1}.

The nitrosyl and carbonyl groups in $cpMo(CO)_2(NO)$ have all been determined to be linear, using X-ray crystallographic data.[12] The molecule adopts a "piano-stool" type of structure (**Fig. 5.2**) with point group C_S. Although no molecular orbital schemes have been devised for this molecule, some correlations can be drawn from work carried out by Fenske and Lichtenberger[15] to determine the frontier molecular orbitals of $cpMn(CO)_3$ and $cpFe(CO)_2Cl$.

Lichtenberger and Fenske's calculations[15] on the $cpMn(CO)_3$ molecule indicate a set of low-lying filled energy levels derived from carbonyl (a_1 and e) and cyclopentadienyl σ (a_2'') interactions with the metal centre. Orbitals of a symmetry were found to interact with the metal d_{z^2} atomic orbitals, whilst the e levels combined with d_{xz} and d_{yz} orbitals. The e_1'' cyclopentadienyl p_π orbital interacts with metal d_{xz} and d_{yz} orbitals to give a strongly bonding molecular orbital. The empty e_2'' level of $C_5H_5^-$, with δ symmetry, overlaps with d_{xy} and $d_{x^2-y^2}$ metal orbitals, giving an unfilled

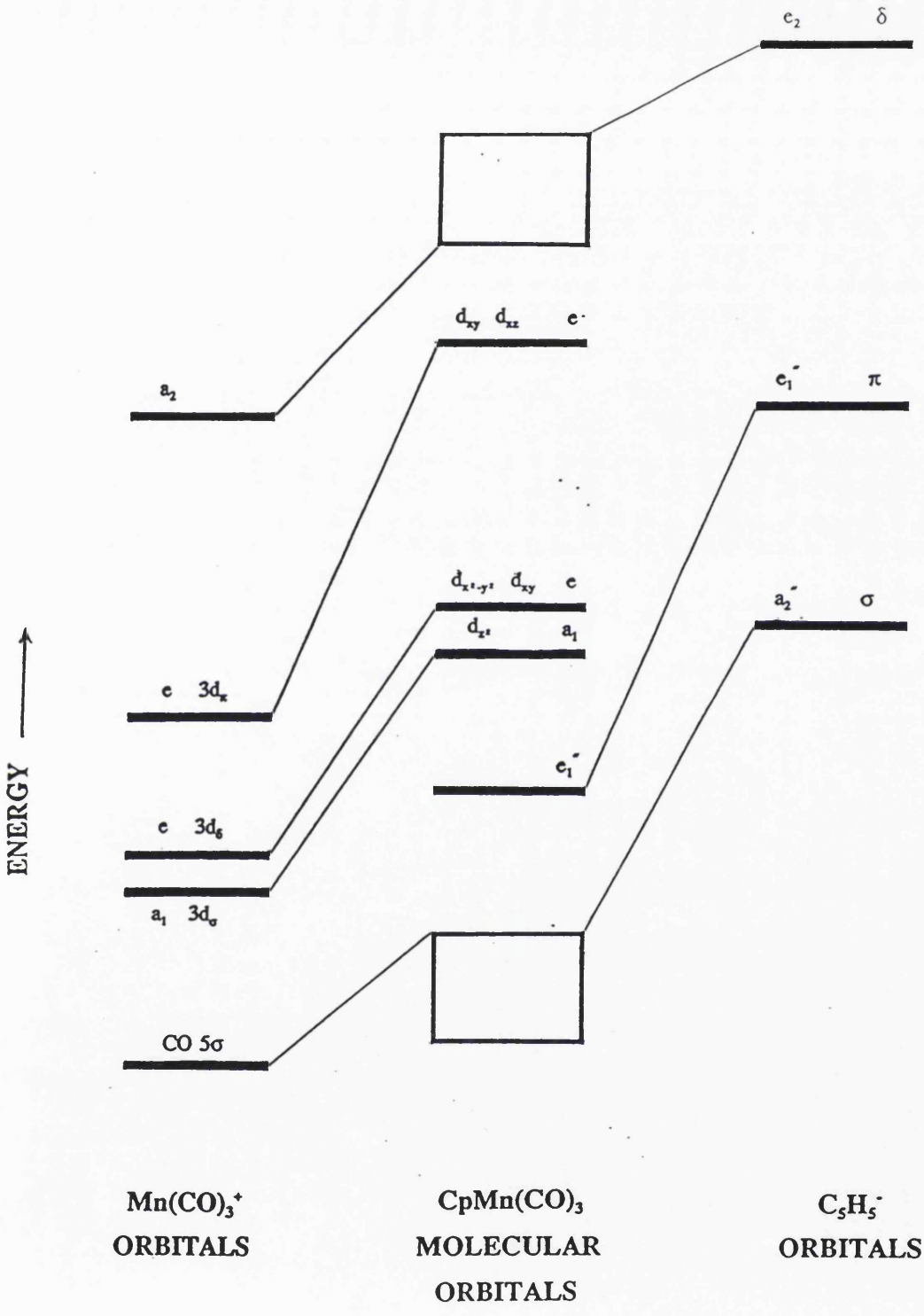

Fig. 5.3 Molecular orbital scheme for $CpMn(CO)_3$

molecular orbital of very high energy.

The frontier molecular orbitals of the system are formed from the interaction of metal d orbitals with the 2π orbitals of the carbonyl ligands. The latter transform as a_1, 2e and a_2. The lowest-lying is the a_1 level, arising from the strong interaction with the metal d_{z^2} orbital. The lower-lying e orbital, resulting from an overlap with the $d_{x^2-y^2}$ and d_{xz} metal energy levels, forms the HOMO of the system. The LUMO, also of e symmetry, has significant d_{yz} and d_{xz} character.

The substitution of a nitrosyl group for one of the carbonyl ligands would result in the removal of the degeneracy of the metal d orbitals as the symmetry of the molecule is lowered. However, the effects may not be as significant as those noted[15] for the substitution of a halide for a carbonyl group in $cpFe(CO)_2X$ (X=Cl, Br, I), since the nitrosyl ligand bears a much closer resemblance to carbonyl groups, with respect to the nature of its bonding to the metal atom, than halide ions.

5.2 Electrochemistry

Geiger et al.[13] studied the redox chemistry of $cpMo(CO)_2(NO)$ in non-aqueous solvents, using alternating and direct current polarography, cyclic voltammetry and bulk coulometry. They observed a one-electron reduction ($\mathbf{E_{½}}$=-1.73 V versus S.C.E. in THF), which was not fully reversible, in a chemical or eletrochemical sense, until the temperature was lowered to -40 °C. At room temperature, Geiger postulated that the one-electron reduced product underwent a chemical transformation, followed by another electrochemical reduction (ECE mechanism). He[13] also suggested that the decomposition product was responsible for both the anodic waves observed at -0.58 and -0.28 V and the further irreversible reduction with an $\mathbf{E_{½}}$ value of -2.20 V.

Cyclic voltammetry experiments were carried out to confirm Geiger's results.[13] In tetrahydrofuran, a one-electron reduction with $\mathbf{E_{½}}$=-1.83 V versus ferrocene (**Fig. 5.4a**) was observed. The heights of the anodic and cathodic peaks were equal, even for experiments conducted at room temperature. The separation between the anodic and cathodic peaks ($\mathbf{E_{Pa}}$-$\mathbf{E_{Pc}}$) increases with increasing scan rate (**Fig. 5.4b**) e.g. at 200 mVs^{-1} ($\mathbf{E_{Pa}}$-$\mathbf{E_{Pc}}$)=310 mV; at 600 mVs^{-1} ($\mathbf{E_{Pa}}$-$\mathbf{E_{Pc}}$)=420 mV. Although these values are

a)

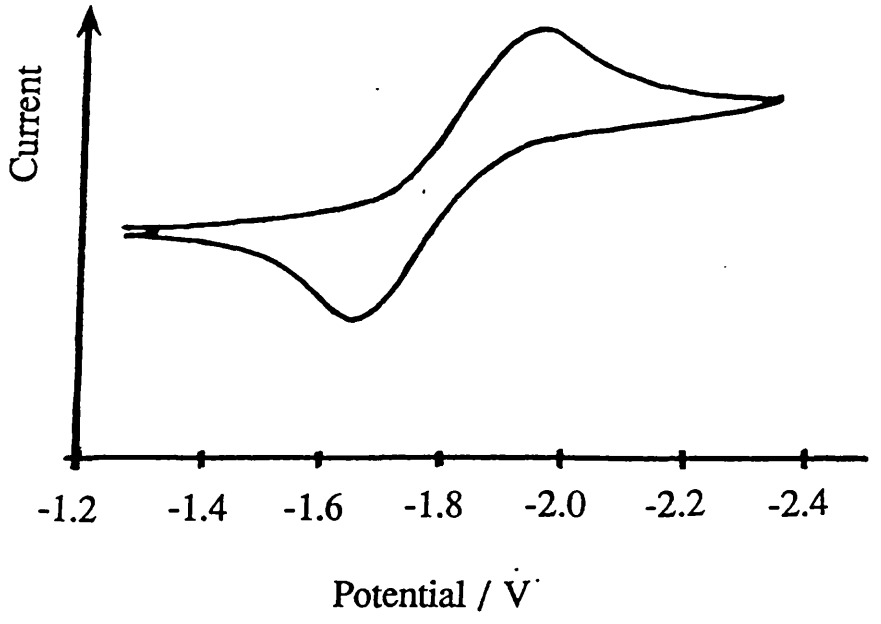

b)

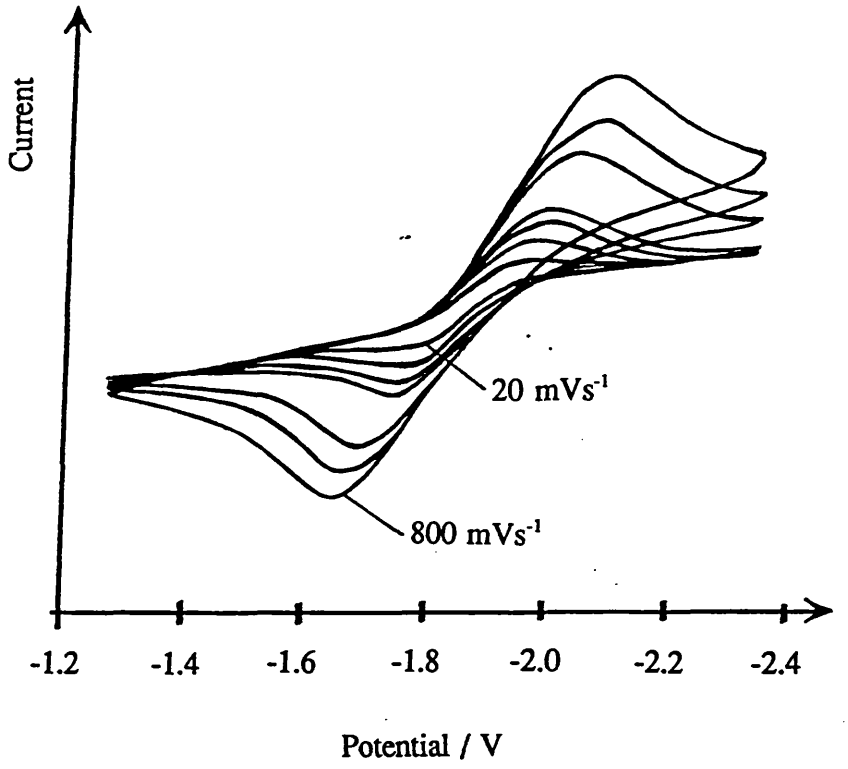

Fig. 5.4 Cyclic voltammtery of $CpMo(CO)_2(NO)$ recorded at
a) 200 mVs^{-1}
b) various scan rates (20 - 800 mVs^{-1})

significantly greater than the 59 mV expected for reversible one-electron processes, (E_{pa}-E_{pc}) for ferrocene was found to be 310 mV at 100 mVs^{-1}.

Contrary to the observations made by Geiger's group,[13] there was no indication that any oxidation processes were occurring. There was also little evidence of either the decomposition noted by Geiger during slow scan rate experiments or the oxidation waves arising from the decomposition product, even at room temperatures.

5.3 Synthesis

All reactions and manipulations were carried out under a nitrogen atmosphere in a fume hood. All solvents were distilled and degassed prior to use.

$$[cpMo(CO)_3]_2 + Na^* \rightarrow 2Na[cpMo(CO)_3]$$

$$Na[cpMo(CO)_3] + p\text{-}CH_3C_6H_4SO_2N(NO)CH_3^{**} \rightarrow cpMo(CO)_2(NO) + CO + p\text{-}CH_3C_6H_4SO_2N(CH_3)Na$$

* sodium amalgam

** N-methyl-N-nitrosyl-paratoluenesulphonamide (Diazald)

Commercially available dimeric cyclopentadienyl molybdenum tricarbonyl (4.20 g; $8.57x10^{-3}$ mol) was dissolved, with stirring, in tetrahydrofuran (ca. 150 cm^3). The resulting deep purple solution was transferred using a canula to a Schlenk tube containing 0.39% sodium amalgam (prepared from triply-distilled mercury (1.36 g; $6.8x10^{-3}$ mol) and sodium metal (0.53 g; 0.023 mol) under nitrogen). The mixture was stirred vigorously for 1 hour, during which time the solution had become green. After removal of the solid by filtration, N-methyl-N-nitrosyl-paratoluenesulphonamide (4.48 g; 0.021 mol), commonly known as Diazald, was dissolved in a minimum volume of tetrahydrofuran and added dropwise, over 20 minutes, to the stirred green molybdenum cyclopentadienyl tricarbonyl solution. After the effervescence had ceased, the mixture was left, with stirring, overnight. An off-white precipitate was removed by filtration

and washed twice with tetrahydrofuran before being discarded - the washings were added to the filtrate. The solvent was then removed to give a brown solid, which was extracted with several portions of petroleum ether (b.p. 40-60° C). Storage at -30° C overnight yielded a crop of bright orange crystals, which were removed from solution and stored under nitrogen.

Elemental analysis:-

Calculated:-	C=34.03%	H=2.04%	N=5.69%
Found:-	C=35.21%	H=2.55%	N=6.60

5.4 Infrared Spectroelectrochemistry

$cpMo(CO)_2(NO)$ has two distinct, easily-monitored sets of bands in the infrared spectrum - those arising from carbonyl stretching vibrations, and those due to the vibrations of the nitrosyl group. For this compound, ν(CO) occur at 2014.1 and 1936.3 cm^{-1} in tetrahydrofuran solution. Under the same conditions, ν(NO) is observed at 1669.3 cm^{-1}. All three bands are very intense and sharp.

In all spectroelectrochemical experiments, $\mathbf{V_i}$ was taken to be -1.1 V, whilst a value of -2.1 V was always used for $\mathbf{V_f}$. The small (2 mm) diameter working electrode was used throughout.

As the potential is switched from $\mathbf{V_i}$ to $\mathbf{V_f}$, the carbonyl bands at 2014.1 and 1936.3 cm^{-1} gradually collapse and new peaks appear at 1876.7 and 1763.9 cm^{-1} (**Fig. 5.5**). Both the new bands are reduced in intensity by approximately one third and are noticeably broader than the original peaks. The nitrosyl stretching band at 1669.3 cm^{-1} is replaced by a very broad, weak peak at a lower wavenumber. This band is extremely ill-defined, without an easily identifiable maximum. As a result, it is estimated to be 1559(±5) cm^{-1}.

Some decomposition of the reduced species is observed under the conditions of normal spectroelectrochemistry. However, the rate of decomposition appears to be quite slow and sufficient quantities of the monoanion remain, even after 30-60 s, to undergo oxidation to the neutral species. At room temperature, after maintaining the

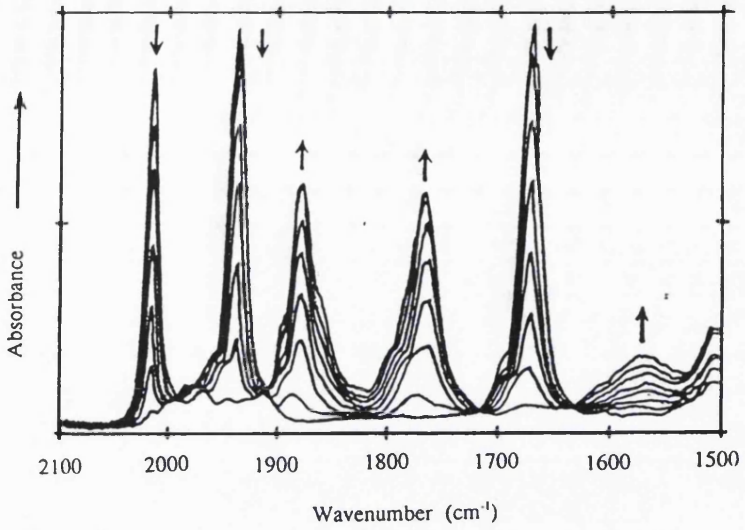

Fig. 5.5 Changes observed in ν(CO) and ν(NO) during the normal spectroelectrochemical reduction of $CpMo(CO)_2(CO)$

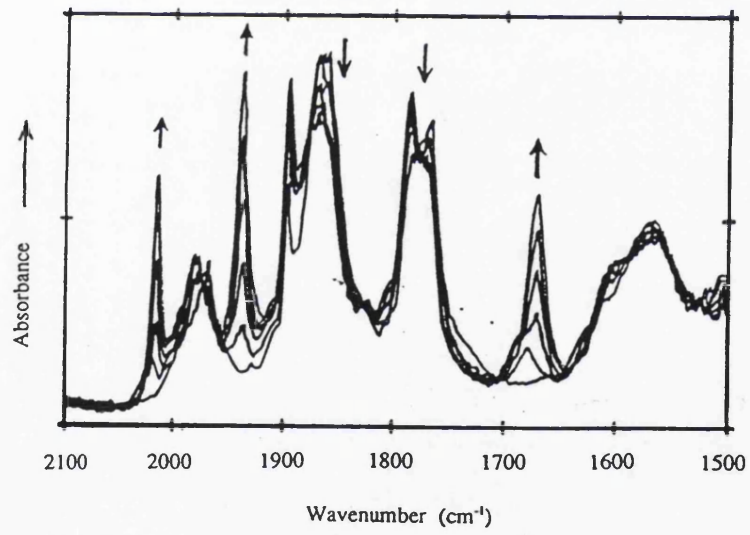

Fig. 5.6 Changes observed in ν(CO) and ν(NO) during normal spectroelectrochemical re-oxidation of $CpMo(CO)_2(NO)$

potential at V_f for 60 s, approximately 35% of the starting material is regenerated on switching the potential to V_i (**Fig. 5.6**). Lowering the temperature increases the lifetime of the electrogenerated monoanion, such that at -12.0 °C the amount of

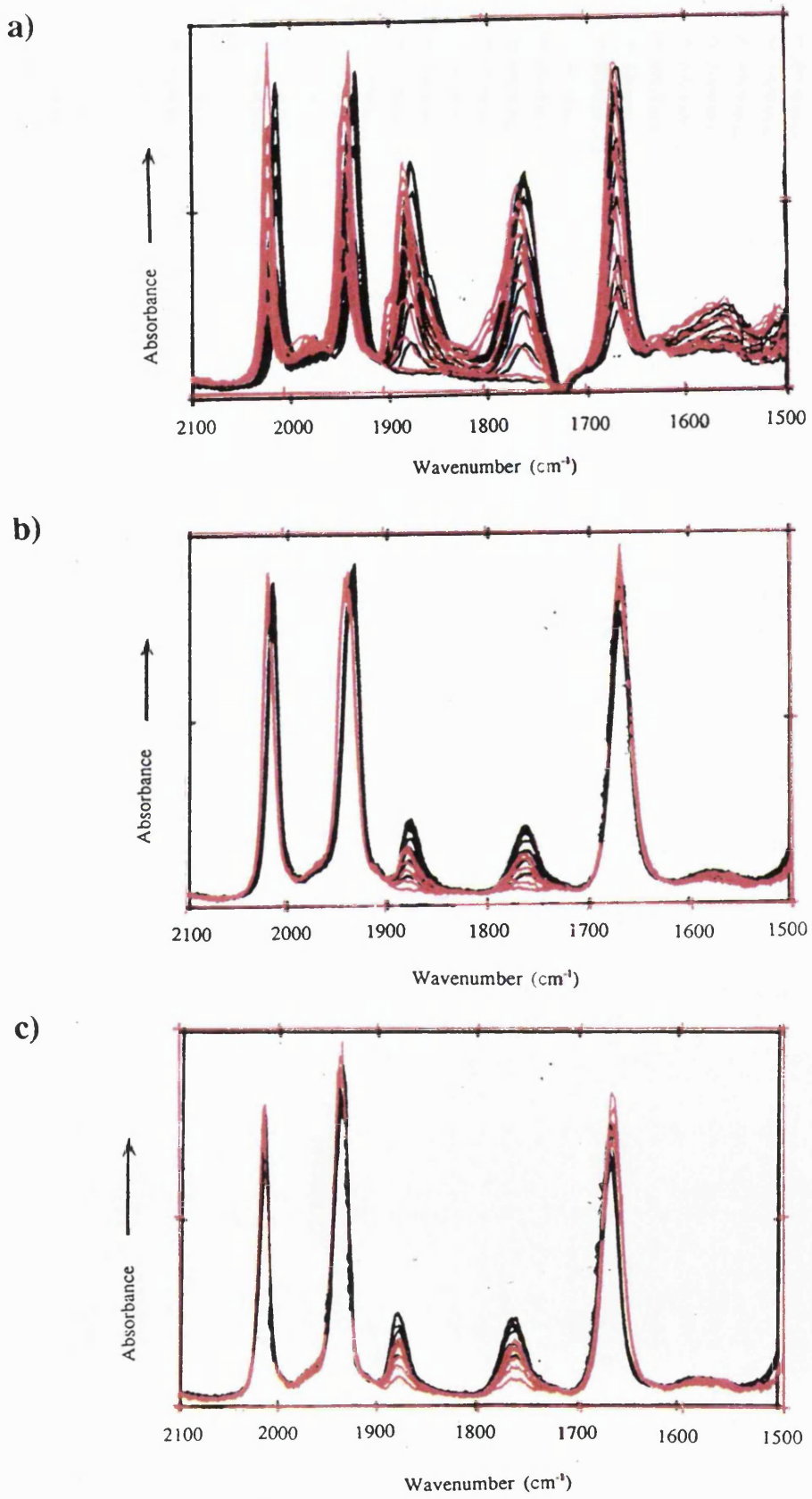

Fig. 5.7 Changes observed in ν(CO) and ν(NO) during 5.0 s/5.0 s modulated spectroelectrochemical reduction
a) 20 °C **b)** -22 °C **c)** -45 °C

$cpMo(CO)_2NO$ recovered rises to 60-65%. At -21.0 °C, 75% regeneration is observed.

The lack of chemical reversibility is emphasised by the results of modulation experiments. When equal times are allowed for both the oxidation and reduction processes (e.g. 3.0 s or 5.0 s), the bands of the starting material are gradually depleted at successive cycles and no regeneration is observed (**Fig. 5.7a**). Ultimately, a situation is reached where complete interconversion to the reduced complex has occurred. Identical behaviour is observed at reduced temperatures of -22.0 and -45.5 °C (**Fig. 5.7b,c**). Examination of the current versus time graphs obtained for all the above experiments showed a change in both the charging and reaction currents at V_i

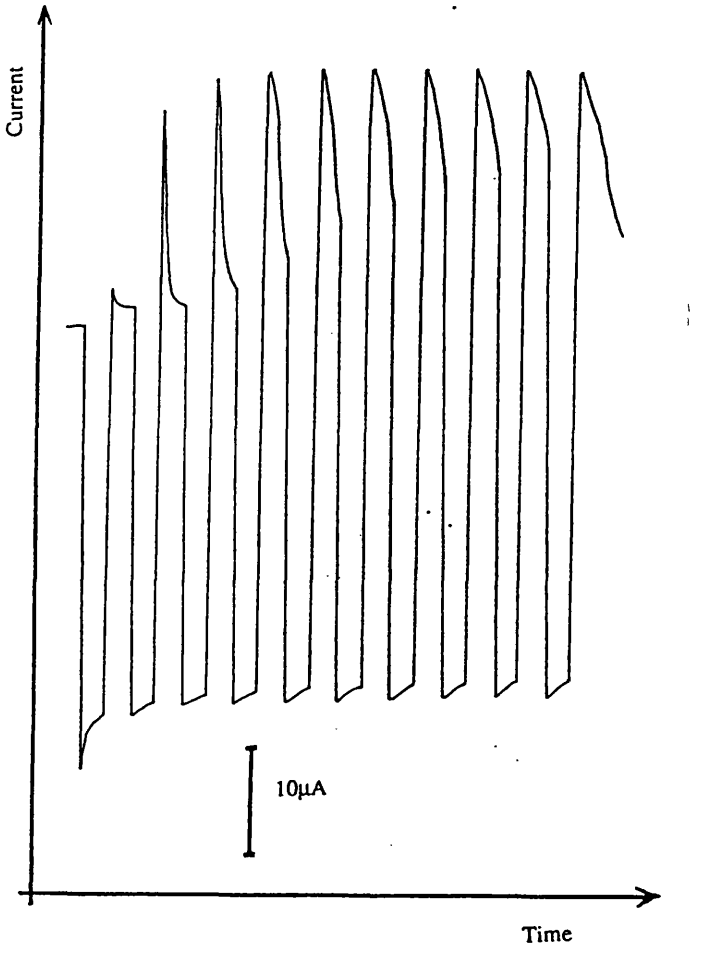

Fig. 5.8 Current response for the 3.0 s/ 10.0 s modulated spectroelectrochemical reduction of $cpMo(CO)_2(NO)$

and V_f at consecutive cycles (**Fig. 5.8**). This is another indication of the chemical irreproducibility of the reaction under these conditions. A very large difference is noted between the current behaviour at the two potentials in all modulation experiments.

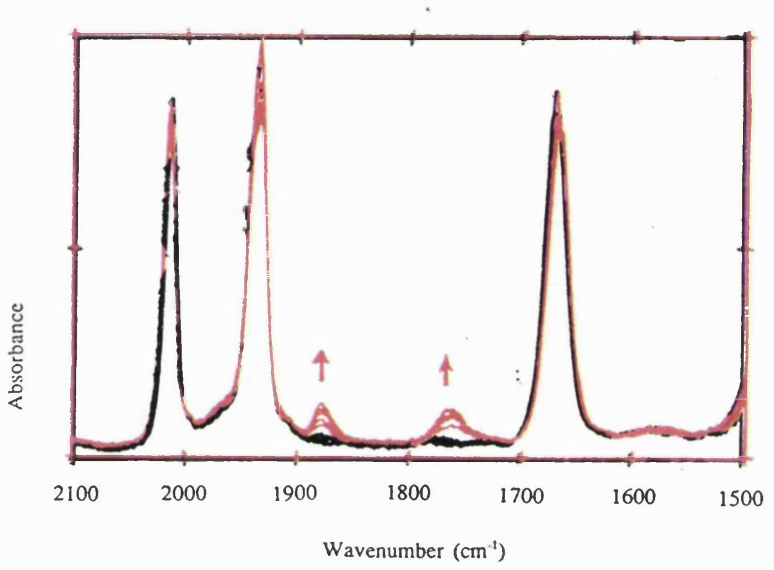

Fig. 5.9 Changes observed in ν(CO) and ν(NO) during 3.0 s/10.0 s modulated spectroelectrochemical reduction of $cpMo(CO)_2(NO)$ at -23 °C

Significant improvements are observed, even at room temperature, when the potential is kept at V_i for a longer time than at V_f. At -23.4 °C (allowing 3.0 s for reduction and 10.0 s for oxidation) all spectra collected at V_i are almost superimposable (**Fig. 5.9**), and only small variations are noted between the spectra collected at V_f. Although all the bands due to the starting complex are easily observed, only the carbonyl stretching modes of the reduced species can be monitored, since the changes occurring in the new nitrosyl band are very small and indistinct. Chemically reversible behaviour is observed only when the temperature is lowered to -43.4 °C (**Fig. 5.10**). This is borne out by the improved current behaviour observed in the current-time graphs for this experiment (**Fig. 5.11**).

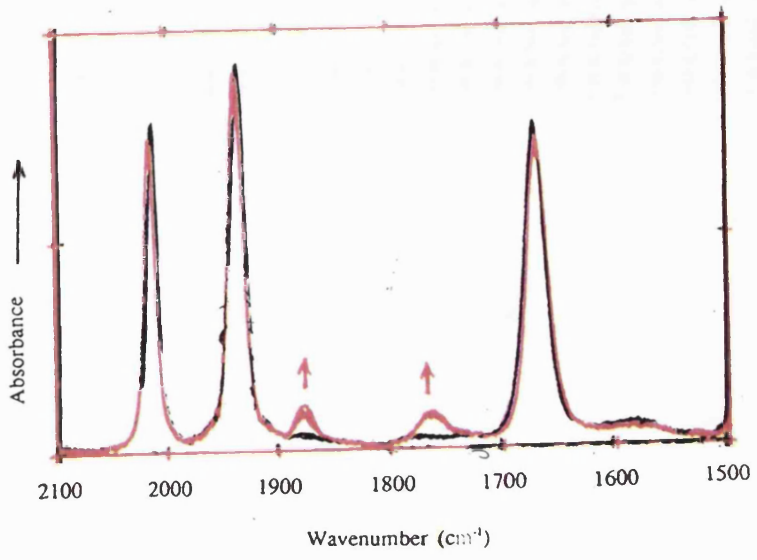

Fig. 5.10 Changes observed in ν(CO) and ν(NO) during 3.0 s/10.0 s modulated spectroelectrochemical reduction of $cpMo(CO)_2(NO)$ at -45 °C

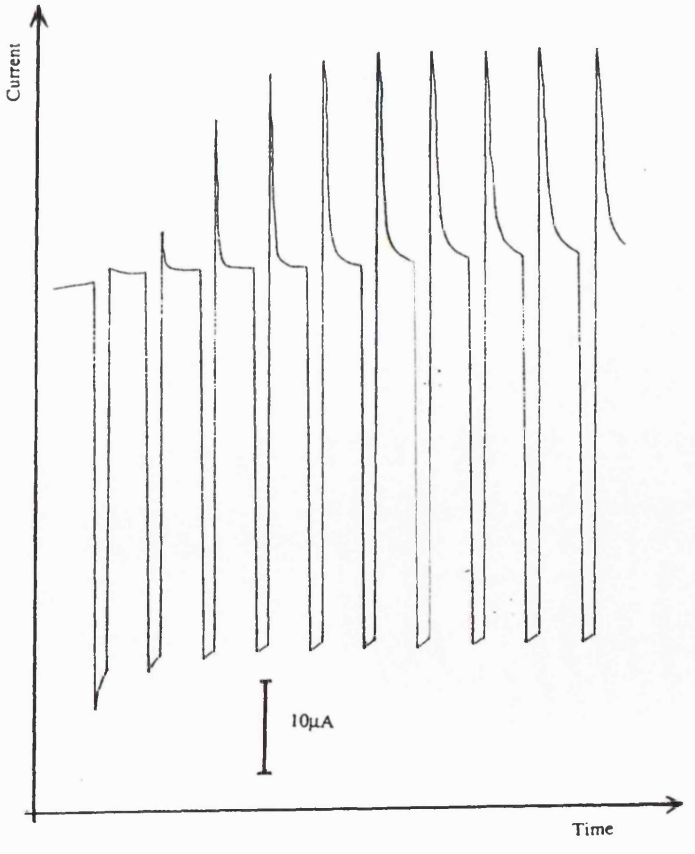

Fig. 5.11 Current response for the 3.0 s/10.0 s modulated spectroelectrochemical reduction of $cpMo(CO)_2(NO)$ at -23 °C

5.5 Discussion

The complicated set of electrochemical reactions observed for this compound by Geiger et al.[13] were not reproduced in our experiments. The cyclic voltammetry (**Fig. 5.4**) showed only one redox couple - a quasi-reversible one-electron reduction with an $E_{½}$ value of -1.83 V versus ferrocene. This compares well with the $E_{½}$ value of -1.73 V (versus SCE) reported by Geiger.[13] Apart from this reduction, no other oxidation or reduction waves were seen.

There is no evidence of impurities in the prepared sample either from the elemental analysis or the infrared spectrum, which showed no spectral bands other than those previously reported for the complex.[13,16,17] This suggests that the additional oxidation and reduction waves reported by Geiger et al.[13] may be due to the presence of contaminants.

Although the anodic i_{Pa} and cathodic i_{Pc} currents are identical for the -1.83 V reduction, the redox reaction is not strictly reversible in an electrochemical sense, since the separation between the anodic and cathodic peaks is larger than the 59 mV per electron transferred criterion. Geiger[13] reported an increased E_{Pa}-E_{Pc} value for the first reduction, which is slightly smaller than that observed in our experiments. Even at reduced temperatures, the couple is not reversible, showing a shift in the peak separation as the scan rate was changed (**Fig. 5.4b**). This is an indication that the redox reaction is not simple and involves chemical reaction or structural rearrangement.

The results from spectroelectrochemical experiments corroborate the findings of cyclic voltammetry. There was little evidence of chemical reversibility for the reduction to the monoanion under the experimental conditions required for normal or modulated spectroelectrochemistry. Under modulated spectroelectrochemical conditions, it was only possible to maintain the concentration of the starting material at a constant level throughout the experiment by preventing large scale decomposition of the radical anion. This was achieved by holding the potential at V_i for three times as long as at V_f.

In the course of normal, non-modulated spectroelectrochemistry, at room temperature, almost 70% of the monoanion was found to undergo decomposition in

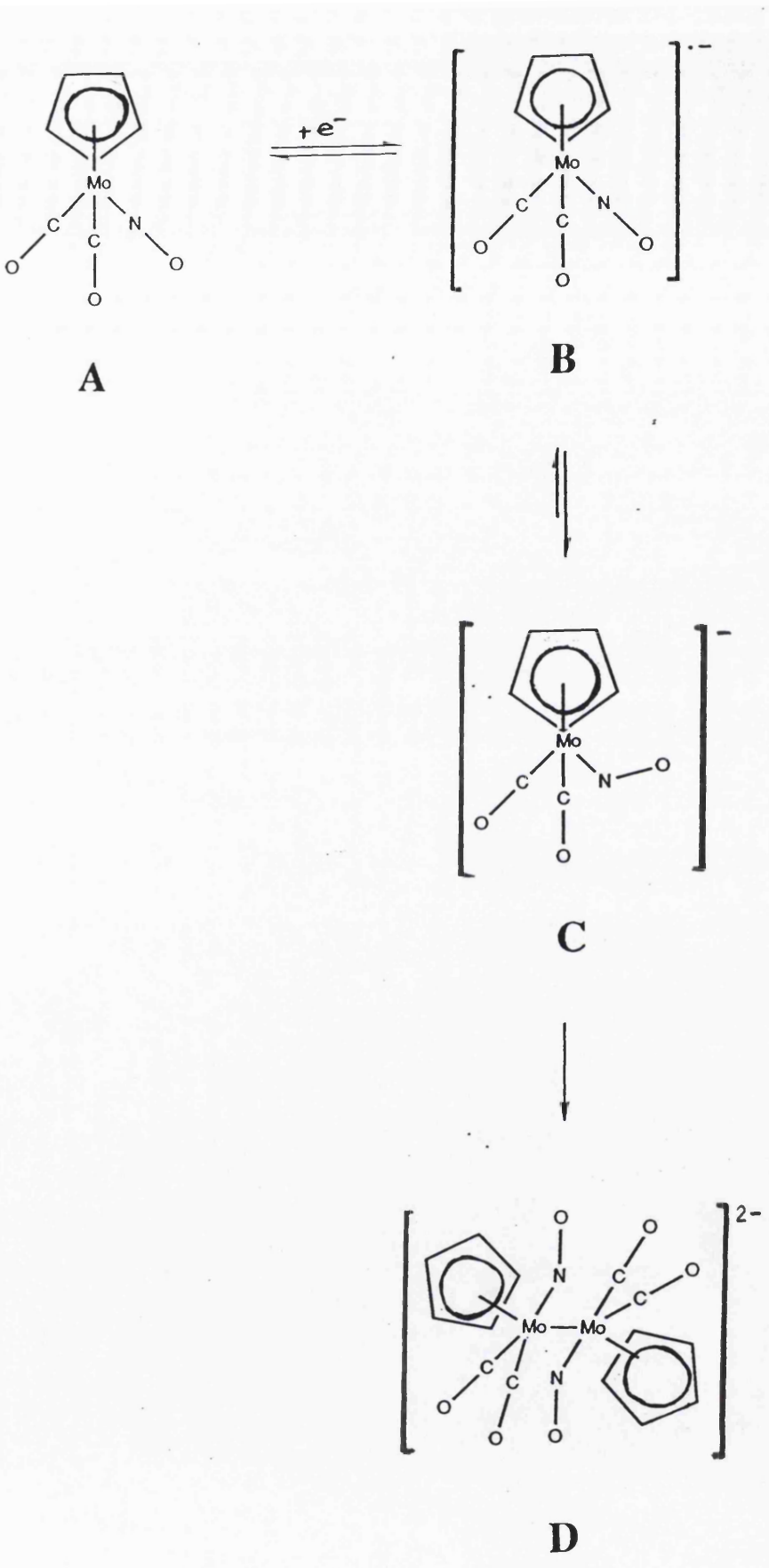

Fig. 5.12 Proposed reaction scheme for the electron transfer and following reactions of $cpMo(CO)_2(NO)$

approximately 60s. Therefore, only 30-40% of the original complex could be regenerated on switching the potential back to V_i. Although significant stabilisation of the electrogenerated species could be achieved by lowering the temperature, complete regeneration of $cpMo(CO)_2(NO)$ was not observed, even at -45 °C.

Despite its reactivity even at reduced temperatures, the species electrogenerated in these experiments appears to be significantly more long-lived than that described by Geiger.[13] The reported half-life for the monoanion at 298 K was 0.9 s, increasing to 7.0 s at 263 K. If this had been the case, then it would have been impossible to monitor the monoanion over such a prolonged period of time as 60-90 s at room temperature. A likely explanation for this could be that the observed infrared bands arise from the decomposition product of the monoanion (**Fig. 5.12 product C, D etc.**), rather than the monoanion itself (**Fig. 5.12 product B**). However, precisely the same bands, and no others, are seen at low temperatures, when the species is expected to be more stable. This suggests that the same species is electrogenerated at both temperatures.

The shifts observed in all the spectral bands are very large. Most stretching vibrations are expected to shift by up to 50 cm^{-1} in frequency on undergoing a reduction or oxidation, which does not involve chemical or structural rearrangement. However, the symmetric carbonyl stretching mode, the band seen at the higher frequency, moves by 137.4 cm^{-1} on reduction, whilst the antisymmetric mode shifts by 172.4 cm^{-1}. Both bands in the reduced species are broader than those in the starting material. If the metal-ligand bonding in carbonyl compounds is assumed to be analogous to that in cyanide complexes, then the increase in band width could be attributed to increased π back-donation into the ligand antibonding orbitals.

Closer inspection of the $\nu(CO)$ bands revealed a change in their relative intensities as the experiment progressed. This is an important observation, because the ratio of the intensities of the two bands may be related to the angle between the carbonyl ligands, according to the following equation:-[10]

$$\frac{R_{asym}}{R_{sym}} = \tan^2\theta$$

$R_{sym/asym}$ = intensity of symmetric/antisymmetric bands

2θ = bond angle between the two carbonyl ligands

The bond angle can be determined by analysing the relative intensities of the bands. All the parameters required for the calculation, such as heights, full widths at half-height and Gaussian/Lorentzian ratios, of both the bands (for the initial complex and the reduced species) were determined using the "Bandshape" program described in **Appendix IV**. Results are given for two separate experiments in **Tables 5.1** and **5.2**. The first set of data is obtained from a spectroelectrochemical experiment carried out at room temperature, whilst the second is derived from a reduction at low temperature (-20.8 °C).

The average calculated CMoC bond angle for the starting complex is 92.04°. This is almost within the experimental error of the crystallographically determined average XMoX (X=C, N) bond angle of 91.6°. The nitrosyl and carbonyl groups are crystallographically indistinguishable.

The data indicates a gradual increase in the CMoC bond angle of $cpMo(CO)_2(NO)$ as the reduction progresses, from approximately 92° to 106(±2)°, irrespective of the temperature (**Fig. 5.13**). Alternatively, the possibility cannot be excluded that a weak underlying band, due to another species, is causing the change in the ratio of the relative intensities of the ν(CO) bands. However, the same bond angle in the monoanionic species remains constant throughout all experiments at 89(±1)°.

The behaviour of the nitrosyl stretching band is less easily monitored. The new band is very broad (the full width at half-height is approximately 70 cm^{-1}) and very weak in comparison with the original band and both pairs of carbonyl peaks. It is also very much more indistinct than all the other spectral bands observed and, as a result, the maximum is difficult to determine.

The band shifts by almost 100 cm^{-1} to approximately 1559 cm^{-1}. It is possible that the shape of the band is due to the presence of several weak bands in close proximity to one another. According to standard texts,[9-11] the new ν(NO) band occurs at the lower end of the range designated for the bent mode of coordination and

Table 5.1 Change of CMoC bond angle in $cpMo(CO)_2(NO)$ during spectroelectrochemical reduction

SPECTRUM NO.	R(symm)	R(asymm)	2θ/°
1	88.5	97.0	92.9
2	93.5	99.0	91.6
3	96.0	99.0	90.9
4	94.0	98.0	91.2
5	90.0	99.0	92.7
6	88.0	99.0	93.4
7	82.0	95.0	94.2
8	90.0	103.0	93.9
9	85.0	101.0	94.9
10	74.0	97.0	97.7
11	72.0	95.0	97.9
12	71.0	94.0	98.0
13	56.0	73.0	97.6
14	37.0	51.0	99.2
15	22.5	31.0	99.1
16	12.0	17.0	99.9
17	4.5	8.0	106.3
18	4.0	4.5	92.7
19	2.0	4.0	109.5
20	1.5	3.0	109.5

Table 5.2 Change of CMOC bond angle in $cpMo(CO)_2(NO)$ during spectroelectrochemical reduction at -20.8 °C

SPECTRUM NO	R_{symm}	R_{asymm}	2θ/°
1	93.0	98.0	91.5
2	95.0	102.0	92.0
3	88.0	97.0	92.8
4	86.0	95.0	92.9
5	92.0	98.0	91.8
6	97.0	105.0	92.3
7	98.0	106.0	92.3
8	94.0	105.0	93.2
9	88.0	99.0	93.4
10	81.0	98.0	95.5
11	79.0	98.0	96.2
12	79.0	98.0	96.2
13	61.0	76.0	96.3
14	43.0	60.0	99.5
15	30.0	45.0	101.5
16	20.0	29.0	100.6
17	10.5	17.0	103.7
18	7.5	11.5	102.2
19	5.5	9.0	104.0
20	5.5	8.5	102.4

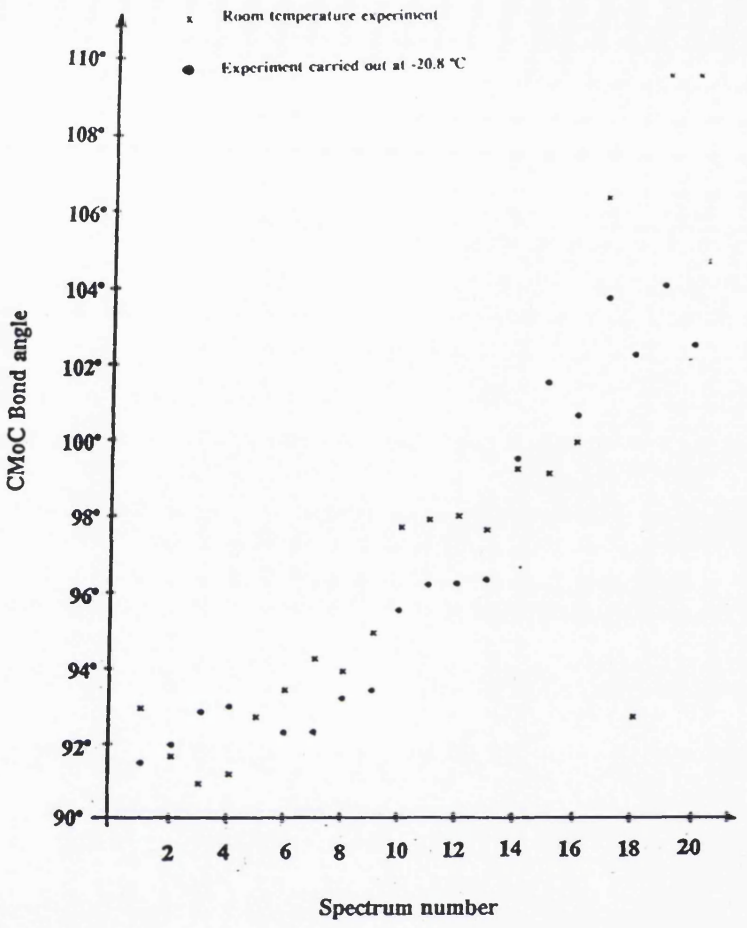

Fig. 5.13 Variation in CMoC bond angle with time on spectroelectrochemical reduction

approaching that for the doubly-bridging. It is difficult, therefore, to assign a mode of coordination to the nitrosyl group from the vibrational bands alone.

According to the proposed reaction scheme (**Fig. 5.12**), on one electron reduction, the complex (**product A**) becomes a reactive nineteen electron system (**product B**). This acts as an impetus for chemical or structural rearrangement to produce a molecule complying with the "eighteen electron rule". Using the results of EPR experiments, Geiger[13] suggests that the added electron enters a molecular orbital, which has significant nitrosyl antibonding character. This causes a structural rearrangement to accommodate the increase in electron density, in which the nitrosyl

ligand is forced to change to the bent mode of coordination (**product C**). The transformation of the nitrosyl ligand from three to one electron donation, however, yields an similarly unstable seventeen electron system. A likely explanation for the stability of the observed product could be a subsequent dimerisation process, involving the formation of ligand bridges or metal-metal bonds to create a species complying with the "eighteen electron rule".

Bridging carbonyls remain two electron donors and, as such, do not affect the "electron count" of the molecule. A dimeric 36 electron complex can be envisaged, involving one bridging nitrosyl group. However, one molybdenum atom of the dimer would effectively be a seventeen electron unit, containing one bent nitrosyl, whilst the other would formally be a nineteen electron unit, due to the donation of a lone pair of electrons from the bridging nitrosyl. The two bands due to carbonyl stretching vibrations observed in the spectrum of the final product are further evidence that this is not a likely structure for the dimer, since this conformation would result in an increased number of ν(CO) bands, the carbonyl groups on each of the constituent monomeric units no longer being equivalent.

The desired "electron count" could also be achieved by the formation of a single metal-metal bond, if the nitrosyl groups of both monomeric units were assumed to retain their bent terminal mode of coordination. The tendency to form metal-metal bonds is greater for the heavier transition elements, such as molybdenum, in low oxidation states. The resulting dimer would then be a 36 electron system overall, with each metal atom contributing eighteen electrons.

Although the ν(CO) bands occur in a spectral region generally accepted to be characteristic of bridging ligand vibrations, no assumptions as to the mode of coordination of the carbonyl groups can be made on this basis alone. Of the two isomers - *syn* and *anti* - possible, it is likely that the less sterically-hindered *anti* conformation would be favoured. The presence of only two ν(CO) bands in the infrared spectrum precludes the possibility of both isomers being present in solution.

To summarise, the addition of an electron to the molecule (**A**), therefore, produces a short-lived nineteen electron species (**B**) which interconverts, via a change from linear to bent coordination of the nitrosyl group, to a seventeen electron species (**C**). The latter undergoes a dimerisation, probably involving metal-metal bond

formation (**D**). For the reasons explained above, the spectral bands observed are assumed to arise from the dimeric structure (**D**).

The reduction to the nineteen electron species (**B**) is probably electrochemically reversible, although it initiates the rapid transformation of the nitrosyl group from the linear terminal into the linear bent conformation. Although the **B**⇌**C** rearrangement process may be chemically reversible, the ensuing dimerisation step is likely to be more complicated and chemically irreversible. The reverse oxidation reaction, involving the cleavage of the dimer (**D**) and the subsequent rearrangement of the monomer into the seventeen electron species (**C**) is much slower and neither chemically or electrochemically reversible.

The species observed by Geiger[13] was reported to have a half-life of 7.0 s at 263 K. Rapid modulation spectroelectrochemical techniques should have been sufficiently powerful to allow the detection of this complex. Instead, the same bands were observed, irrespective of the temperature. The probable explanation for this is that Geiger, too, was studying the dimer (**D**), rather than either of the preceding monomers. The experimental conditions of spectroelectrochemistry may be more efficient at excluding oxygen and contaminants from the system than other apparatus. This could have inhibited the rate of decomposition of the dimer, such that it appeared to be more long-lived and stable than in ESR experiments.

The increase in the CMoC bond angle of the starting material suggests a deformation of the carbonyl and nitrosyl "legs" of the "piano-stool" structure towards the plane of the cyclopentadienyl ring. The effect of this would be to decrease the electrostatic repulsion experienced by a molecule approaching trans to the delocalised ring system. The carbonyl groups of the final, possible dimeric, species would then assume positions with an average bond angle of 89°, closely resembling that of the initial complex.

The change of coordination of the nitrosyl group from linear to bent decreases the number of electrons it can donate to the metal centre. However, in the bent mode of coordination, the nitrosyl π^* orbitals lie higher in energy than in the linear form, and the ligand is no longer able to act as an acceptor for $d\pi$ electrons from the metal. The resultant increase in electron density on the metal centre is eased by increased back-donation to the antibonding orbitals of the carbonyl ligands. This causes a

weakening of the C=O bond and a large decrease in the frequency of the carbonyl stretching mode. The presence of the nitrosyl ligand in a bent mode of coordination accounts for the shift in the frequency of ν(NO) to a lower wavenumber.

5.6 Conclusions

The work described above emphasises our ability to conduct studies under anaerobic conditions, enabling the spectroscopic detection of previously unobserved air-sensitive species. Electrochemical investigation of $cpMo(CO)_2(NO)$ corroborated the work of Geiger et al.[13] by indicating a quasi-reversible one-electron reduction, although none of the additional oxidation and reduction waves reported by Geiger were observed. Although experiments conducted at low temperatures exhibited 75% regeneration of the initial complex, significantly reduced temperatures and further modifications to the apparatus utilised would be required to achieve complete chemical reversibility.

The infrared spectroelectrochemical results indicated a significant increase in electron density on the metal atom centre on reduction, manifested as a large shift to lower wavenumbers by the carbonyl and nitrosyl stretching vibrations. The characteristics of the ν(CO) spectral bands could be used as a basis for an assessment of the nature of their bonding to the metal atom and their displacement relative to one another, i.e. the CMoC bond angle. Inferences could be made as to the extent of π back-bonding into ligand antibonding orbitals from the wavenumber of the nitrosyl stretching vibration. However, it was also concluded that ν(NO) could not be used as a diagnostic of the mode of coordination of the ligand.

The addition of an electron to $cpMo(CO)_2(NO)$ initiated a series of chemically irreversible rearrangements, involving a change in the mode of coordination of the nitrosyl ligand. The resultant seventeen electron species is likely to achieve greater stability by undergoing a dimerisation process via metal-metal bond formation. A scheme can be proposed for the sequence of reactions, based upon electrochemical, EPR[13] and infrared spectroelectrochemical data. The accuracy of the scheme could be verified by carrying out further EPR and spectroelectrochemical studies on dilute

solutions of the complex, in an attempt to monitor the dimerisation process and detect intermediate species.

References

1. B. F. G. Johnson, J. A. McCleverty, *Prog. Inorg. Chem.*, (1966), **7**, 277
2. W. P. Griffith, *Comp. Inorg. Chem.*, **4**, 105
3. G. B. Richter-Addo, P. Legzdins, *Chem. Rev.*, (1988), **88**, 991
4. W. P. Griffith, *Adv. Organomet. Chem.*, (1968), **7**, 211
5. D. J. Hodgson, N. C. Payne, J. A. McCleverty, R. G. Pearson, J. A. Ibers, *J. Am. Chem. Soc.*, (1968), **90**, 4486
6. C. G. Pierpoint, D. G. Van Derveer, W. Durand, R. Eisenberg, *J. Am. Chem. Soc.*, (1970), **92**, 4760
7. M. W. Schoonover, E. C. Baker, R. Eisenberg, *J. Am. Chem. Soc.*, (1979), **101**, 1880
8. R. C. Elder, F. A. Cotton, R. A. Schunn, *J. Am. Chem. Soc.*, (1967), **89**, 3645
9. N. N. Greenwood, A. Earnshaw, *Chemistry of the Elements*, Pergamon Press, New York, (1984)
10. F. A. Cotton, G. Wilkinson, *Advanced Inorganic Chemistry*, 4th ed., Wiley-Interscience, New York, (1980)
11. J. E. Huheey, *Inorganic Chemistry*, 3rd ed., Harper & Row, New York, (1983)
12. J. T. Malito, R. Shakir, J. L. Atwood, *J. Chem. Soc., Dalton Trans.*, (1980), 1253
13. W. E. Geiger, P. H. Rieger, B. Tulyathan, M. D. Rausch, *J. Am. Chem. Soc.*, (1984), **106**, 7000
14. S. C. Avanzino, A. A. Bakke, H-W. Chen, C. J. Donahue, W. K. Jolly, T. H. Lee, A. J. Ricco, *Inorg. Chem.*, (1980), **19**, 1931
15. D. L. Lichtenberger, R. F. Fenske, *J. Am. Chem. Soc.*, (1976), **98**, 50
16. A. E. Crease, P. Legzdins, *J. Chem. Soc., Dalton Trans.*, (1973), 1501
17. D. Seddon, W. G. Kita, J. Bray, J. A. McCleverty, *Inorg. Synth.*, (1976), **16**, 24

Conclusions

The most significant contribution to this work was the development of the "Modulation Technique". Although some electrogenerated products are easily monitored using standard spectroelectrochemical techniques, involving bulk electrosynthesis, many have an insufficiently long lifetime to be detected in this way. The ability to generate reactive products, with the option of working at reduced temperatures, for short periods of time enabled the detection of most of the species described above. Computer control and synchronisation of spectral data acquisition and potential switching has significantly increased the flexibility and applicability of the technique, whilst improvements in the apparatus and sample-handling procedures enhanced the quality and reliability of the data obtained.

The "Modulation Technique" has been demonstrated to be suitable for the study of a wide range of complexes, by monitoring a large number of vibrational modes. The latter provide valuable information about the structural or chemical changes occurring in the molecule, from which deductions can be made about the frontier molecular orbitals of the system. The technique has also been shown to be useful in studying reactions which, although being electrochemically reversible, exhibited chemical irreversibility under the conditions of spectroelectrochemistry.

Infrared spectra were obtained, using modulated spectroelectrochemical techniques, of short-lived tetra-anionic tris-mnt complexes. The combination of modulated infrared spectroelectrochemical studies with ultra-violet/visible spectroelectrochemistry proved invaluable in the identification of the intermediates and final products of the one-electron oxidation reaction of $MoO(mnt)_2^{2-}$. A series of cubane structures, $Fe_4(\mu_3\text{-}S)_4(NO)_4^{n-}$ (n=0, 1, 2, 3), have also been detected and shown to retain an intact Fe_4S_4 cage throughout, whilst the products of the reduction of $cpMo(CO)_2(NO)$ could not have been studied without the rigorously anaerobic conditions of the "Modulation Technique".

The flexibility of the "Modulation Technique" is such that the possibility exists of further modification to enable the investigation of increasingly short-lived species in ever-lower concentrations. The development of experimental procedures to allow the simultaneous collection of ultra-violet/visible and infrared spectral data would provide one of the most powerful techniques for studying electrogenerated species.

Appendix 1

Potentiostat Control Program

This computer program, written in BASIC, monitors the white light interferometer of the FTIR spectrometer for the 5 V pulse produced at the commencement of each forward motion of the scanning mirror. Once this is detected, the microcomputer initiates a change of potential to the working electrode of the IRRAS cell by sending a signal, via a digital-to-analogue converter and amplifier, to the potentiostat. The user is able to specify the required potential values before the experiment begins.

```
10 REM "METROHM CONTROL PROGRAM"
20 REM "======================"
30 MODE 4
40 INITIAL=0:FINAL=1:REST=0
50 V=0:Z=0
60 NSS=0:DELAY=0
70 @%=&2020A
80 IF V=1 THEN PROCsetup
90 IF V=1 THEN GOTO 190
100 PROCmenu
110 COLOUR 0:COLOUR 129
120 PRINT TAB(9,8);"MENU"
130 COLOUR 3;COLOUR 128
140 PRINT TAB(2,25);"PRESS <RETURN> TO ENTER COMMAND MODE"
150 PRINT TAB(2,27);"PRESS <ESCAPE> TO EXIT PROGRAM"
160 G%=GET
170 REPEAT UNTIL G%=13
180 PROCsetup
190 T=3:TIME=0
200 REPEAT UNTIL TIME>=100*T
210 @%=10
220 PROCcheck
230 T=3:TIME=0
240 REPEAT UNTIL TIME>=100*T
250 PROCrun
260 T=3:TIME=0
270 REPEAT UNTIL TIME>=100*T
280 PROCend
```

```
290 END
300REM~~~~~~~~~~~~~~~~~~~~~~~~~~~~~~~~~~~~~~~~~~~~~~~~~~~~~~~~~~~~~~~~~~~~
310 DEF PROCmenu
320 COLOUR 0:COLOUR 131
330 PRINT TAB(3,3);"********************************"
340 PRINT TAB(3,4);"* METROHM CONTROL PROGRAM DELAY*"
350 PRINT TAB(3,5);"********************************"
360 COLOUR 3:COLOUR 128
370 MOVE 20,20
380 DRAW 1260,20
390 DRAW 1260,1004
400 DRAW 20,1004
410 DRAW 20,20
420 MOVE 40,40
430 DRAW 1240,40
440 DRAW 1240,984
450 DRAW 40,984
460 DRAW 40,40
470 PRINT TAB(4,8);"MODE"
480 IF Z=1 THEN GOTO 540
490 IF REST<0 THEN PRINT TAB(3,12);"Rest potential ..............";REST;"V" ELSE PRINT TAB(3,12);"Rest potential ...............";REST;"V"
500 IF INITAL<0 THEN PRINT TAB(3,15);"Initial potential ...........";INITIAL;"V" ELSE PRINT TAB(3,15);"Initial potential ............";INITIAL;"V"
510 IF FIANL<0 THEN PRINT TAB(3,18);"Final potential .............";FINAL;"V" ELSE PRINT TAB(3,18);"Final potential ..............";FINAL;"V"
520 PRINT TAB(3,21);"Number of scans .............";NSS
530 PRINT TAB(3,27);"                              "
540 ENDPROC
550 REM ~~~~~~~~~~~~~~~~~~~~~~~~~~~~~~~~~~~~~~~~~~~~~~~~~~~~~~~~~~~~~~~~~~~
560 REM ~~~~~~~~~~~~~~~~~~~~~~~~~~~~~~~~~~~~~~~~~~~~~~~~~~~~~~~~~~~~~~~~~~~
570 DEF PROCsetup
580 Z=0
590 CLS
600 PROCmenu
610 COLOUR 0:COLOUR 129
620 PRINT TAB(9,8);"SETUP"
630 COLOUR 3:COLOUR 128
640 REPEAT
650 PRINT TAB(23,25);"          "
660 INPUT TAB(3,25);"ENTER REST POTENTIAL";REST$
670 IF LEN(REST$)=0 THEN GOTO 700 ELSE REST=VAL(REST$)
680 IF REST<-2 OR REST>2 THEN PRINT TAB(3,27);"POTENTIAL OUT OF RANGE"
690 UNTIL REST>=-2 AND REST<=2
700 PROCmenu
710 REPEAT
720 PRINT TAB(25,25);"          "
730 INPUT TAB(3,25);"ENTER INITAL POTENTIAL";INITIAL$
740 IF LEN(INITAL$)=0 THEN GOTO 770 ELSE INITAL=VAL(INITIAL$)
750 IF INITIAL<-2 OR INITAL>2 THEN PRINT TAB(3,27);"POTENTIAL OUT OF RANGE"
760 UNTIL INITAL>=-2 OR INITAL<=2
770 PROCmenu
780 REPEAT
790 PRINT TAB(23,25);"          "
800 INPUT TAB(3,25);"ENTER FINAL POTENTIAL";FINAL$
810 IF LEN(FINAL$)=0 THEN GOTO 840 ELSE FINAL=VAL(FINAL$)
820 IF FINAL<-2 OR FINAL>2 THEN PRINT TAB(3,27);"POTENTIAL OUT OF RANGE"
830 UNTIL FINAL<=2 AND FINAL>=-2
```

```
840 PROCmenu
850 @%=10
860 PRINT TAB(3,25);"ENTER NUMBER OF SCANS REQUIRED";NSS
870 IF LEN(NSS$)=0 THEN GOTO 900 ELSE NSS=VAL(NSS$)
880 PRINT TAB(33,25);NSS;"    "
890 PRINT TAB(3,25);"                                   "
900 @%=&2020A

910 Z=1
920 ENDPROC
930 REM ~~~~~~~~~~~~~~~~~~~~~~~~~~~~~~~~~~~~~~~~~~~~~~~~~~~~~~~~~~~~~~~~~~~~~~~~~~~~~
940 REM ~~~~~~~~~~~~~~~~~~~~~~~~~~~~~~~~~~~~~~~~~~~~~~~~~~~~~~~~~~~~~~~~~~~~~~~~~~~~~
950 DEF PROCcheck
960 CLS
970 PROCmenu
980 COLOUR 0:COLOUR 129
990 PRINT TAB(9,8);"CHECKLIST"
1000 COLOUR 3:COLOUR 128
1010 PRINT TAB(3,11);"This program will record ";NSS;
1020 @%=&2020A
1030 PRINT TAB(3,13);"spectra, alternating between an"
1040 PRINT TAB(3,15);"inital potential of ";INITAL;"V and a"
1050 PRINT TAB(3,17);"final potential of ";FINAL;"V"
1060 PRINT TAB(3,19);"The rest potential is ";REST;"V"
1070 PRINT TAB(3,21);"The time delay is ";DELAY;"s"
1080 @%=10
1090 PRINT TAB(3,25);"DO YOU WISH TO ALTER ANYTHING"
1100 INPUT TAB(3,27);"BEFORE YOU CONTINUE (Y/N)"Q$
1110 IF Q$="N" THEN GOTO 1130
1120 IF Q$="Y" THEN V=1:GOTO 70
1130 CLS
1140 PROCmenu
1150 COLOUR 0:COLOUR 129
1160 PRINT TAB(9,8);"CHECKLIST"
1170 COLOUR 3:COLOUR 128
1180 PRINT TAB(3,29);"Press <RETURN> when ready"
1190 PRINT TAB(3,11);"IS THE CELL READY ............?"
1200 REPEAT
1210 G%=GET
1220 UNTIL G%=13
1230 PRINT TAB(34,11);"YES"
1240 PRINT TAB(3,13);"IS THE METROHM READY .........?"
1250 REPEAT
1260 G%=GET
1270 UNTIL G%=13
1280 PRINT TAB(34,13);"YES"
1290 PRINT TAB(3,15);"ARE BRUKER PARAMETERS SET ....?"
1300 REPEAT
1310 G%=GET
1320 UNTIL G%=13
1330 PRINT TAB(34,15);"YES"
1340 PRINT TAB(3,17);"ARE FLS AND OFL CORRECTLY SET.?"
1350 REPEAT
1360 G%=GET
1370 UNTIL G%=13
1380 PRINT TAB(34,19);"YES"
1390 PRINT TAB(3,19);"IS PSC CORRECTLY SET .........?"
1400 REPEAT
```

```
1410 G%=GET
1420 UNTIL G%=13
1430 PRINT TAB(34,19);"YES"
1440 PRINT TAB(3,21);"DOES NSS ON BRUKER EQUAL 1 ...?"
1450 REPEAT
1460 G%=GET
1470 UNTL G%=13
1480 PRINT TAB(34,21);"YES"
1490 ENDPROC
1500 REM ~~~~~~~~~~~~~~~~~~~~~~~~~~~~~~~~~~~~~~~~~~~~~~~~~~~~~~~~~~~~~~~~~~~~~~~~
1510 REM ~~~~~~~~~~~~~~~~~~~~~~~~~~~~~~~~~~~~~~~~~~~~~~~~~~~~~~~~~~~~~~~~~~~~~~~~
1520 DEF PROCrun
1530 Z=1
1540 CLS
1550 PROCmenu
1560 COLOUR 0:COLOUR 129
1570 PRINT TAB(9,8);"RUN"
1580 COLOUR 3:COLOUR 128
1590 PRINT TAB(3,11);"This program records ";NSS;" spectra"
1600 @%=&2020A
1610 PRINT TAB(3,13);"alternating between an initial"
1620 PRINT TAB(3,15);"potential of ";INITIAL;"V and a final"
1630 PRINT TAB(3,17);"potential of ";FINAL;"V"
1640 PRINT TAB(3,19);"The rest potential is ";REST;"V"
1650 @%=10
1660 Y=(REST*10+20.078)*6.375
1670 PROCvolt
1680 PRINT TAB(3,25);"TYPE 'TRS#' ON THE BRUKER    "
1690 PRINT TAB(3,27);"                              "
1700 PRINT TAB(3,28);"PRESS <RETURN> TO CONTINUE"
1710 G%=GET
1720 REPEAT UNTIL G%=13
1730 PRINT TAB(3,25);"PRESS <RETURN> TO START EXPERIMENT"
1740 PRINT TAB(3,28);"                            "
1750 G%=GET
1760 REPEAT UNTIL G%=13
1770 REM scanning
1780 S=0
1790 PRINT TAB(3,24);"Sample scan no ...............";S
1800 PRINT TAB(3,25);"                                    "
1810 PRINT TAB(3,28);"Reference scan no ............";S
1820 Y=(INITIAL*10+20.078)*6.375
1830 PROCvolt
1840 REPEAT
1850 Y=(FINAL*10+20.078)*6.375
1860 PROCtrigger2
1870 PROCvolt
1880 S=S+1:PRINT TAB(33,24);S
1890 SOUND 1,-15,148,2
1900 Y=(INITIAL*10+20.078)*6.375
1910 PROCtrigger2
1920 PROCvolt
1930 PRINT TAB(33,28);S
1940 SOUND 1,-15,148,2
1950 UNTIL S=NSS/2
1960 Y=(REST*10+20.078)*6.375
1970 T=3:TIME=0:REPEAT UNTIL TIME>=100*T
1980 PROCvolt
```

```
1990 ENDPROC
2000 REM ----------
2010 DEF PROCvolt
2020 Y%=Y
2030 A%=&93
2040 X%=&FC
2050 CALL &FFF4
2060 ENDPROC
2070 REM ----------
2080 REM ~~~~~~~~~~
2090 REM ~~~~~~~~~~
2100 DEF PROCend
2110 Z=1
2120 CLS
2130 PROCmenu
2140 COLOUR 0:COLOUR 129
2150 PRINT TAB(9,8);"END"
2160 COLOUR 3:COLOUR 128
2170 PRINT TAB(3,11);"You have recorded ";NSS;" spectra"
2180 PRINT TAB(3,13);"alternating between an initial"
2190 @%=&2020A
2200 PRINT TAB(3,15);"potential of ";INITIAL;"V and a final"
2210 PRINT TAB(3,17);"potential of ";FINAL;"V, from a rest"
2220 PRINT TAB(3,19);"potential of ";REST;"V"
2230 @%=10
2240 INPUT TAB(3,24);"DO YOU WANT ANOTHER RUN (Y/N)";Q$
2250 V=0
2260 CLS
2270 IF Q$="Y" THEN GOTO 40
2280 ENDPROC
2290 REM ~~~~~~~~~~
2300 DEF PROCtrigger2
2310 TIME=0
2320 A%=&97
2330 X%=&6C
2340 Y%=0
2350 CALL &FFF4
2360 REPEAT
2370 A%=&96
2380 X%=&6D
2390 N%=USR(&FFF4)
2400 UNTIL (N% AND &20000)=&20000
2410 IF TIME>=80 THEN GOTO 2480
2420 TIME=0
2430 A%=&97
2440 X%=&61
2450 Y%=0
2460 CALL &FFF4
2470 GOTO 2360
2480 ENDPROC
```

Appendix II

Normal Spectroelectrochemistry

This BASIC program is designed to detect the 5 V pulse produced by the white light interferometer of the FTIR spectrometer at the beginning of each forward motion of the scanning mirror. It allows the collection of one spectrum at the $\mathbf{V_i}$ potential before initiating a change of potential to $\mathbf{V_f}$, at which value it is held during the acquisition of the remaining spectra. The values of $\mathbf{V_i}$ and $\mathbf{V_f}$, as well as the number of spectra required, are specified by the user at the beginning of the program.

```
10 REM "NORMAL SPECTROELECTROCHEMISTRY"
20 MODE 4
30 INITIAL=0:FINAL=0:NSS=0:S=0:Z=0
40 @%=&2020A
50 COLOUR 0:COLOUR 129
60 PROCmenu
70 COLOUR 3:COLOUR 128
80 PRINT TAB(2,27);"PRESS <RETURN> TO ENTER COMMAND MODE"
90 G%=GET
100 REPEAT UNTIL G%=13
110 PROCsetup
120 T=3:TIME=0
130 REPEAT UNTIL TIME>=100*T
140 PROCcheck
150 @%=10
160 T=3:TIME=0
170 REPEAT UNTIL TIME>=100*T
180 PROCrun
190 T=3:TIME=0
200 REPEAT UNTIL TIME>=100*T
210 PROCend
220 END
230 REM ~~~~~~~~~~~~~~~~~~~~~~~~~~~~~~~~~~~~~~~~~~~~~~~~~~~~~~~~~~~~~~~~~~~~~~~~~~~~
240 DEF PROCmenu
250 COLOUR 1:COLOUR 131
260 PRINT TAB(3,3);"*******************************"
270 PRINT TAB(3,4);"*      MCP - STRAIGHT SEC     *"
280 PRINT TAB(3,5);"*******************************"
290 COLOUR 3:COLOUR 128
300 MOVE 20,20
```

```
310 DRAW 1260,20
320 DRAW 1260,1004
330 DRAW 20,1004
340 DRAW 20,20
350 MOVE 40,40
360 DRAW 1240,40
370 DRAW 1240,984
380 DRAW 40,984
390 DRAW 40,40
400 PRINT TAB(4,8);"MODE"
410 IF Z=1 THEN GOTO 450
420 IF INITIAL<0 THEN PRINT TAB(3,12);"Initial potential .........";INITIAL;"V" ELSE PRINT
TAB(3,12);"Initial potential ..........";INITIAL;"V"
430 IF FINAL<0 THEN PRINT TAB(3,15);"Final potential ...........";FINAL;"V" ELSE PRINT
TAB(3,15);"Final potential ............";FINAL;"V"
440 PRINT TAB(3,18);"Number of scans ............";NSS
450 ENDPROC
460 REM ~~~~~~~~~~~~~~~~~~~~~~~~~~~~~~~~~~~~~~~~~~~~~~~~~~~~~~~~~~~~~~~~~~~~~~~~~~~
470 DEF PROCsetup
480 CLS
490 PROCmenu
500 COLOUR 0:COLOUR 129
510 PRINT TAB(9,8);"SETUP"
520 COLOUR 3:COLOUR 128
530 INPUT TAB(3,25);"ENTER INITIAL POTENTIAL";INITIAL$
540 IF LEN(INITIAL$)=0 THEN GOTO 550 ELSE INITIAL=VAL(INITIAL$)
550 PROCmenu
560 PRINT TAB(3,25);"                              "
570 INPUT TAB(3,25);"ENTER FINAL POTENTIAL";FINAL$
580 IF LEN(FINAL$)=0 THEN GOTO 590 ELSE FINAL=VAL(FINAL$)
590 PROCmenu
600 PRINT TAB(3,25);"                              "
610 REPEAT
620 INPUT TAB(3,25);"ENTER NUMBER OF SCANS";NSS$
630 IF LEN(NSS$)=0 THEN GOTO 640 ELSE NSS=VAL(NSS$)
640 IF NSS=0 THEN PRINT TAB(3,25);"ZERO SCANS IMPOSSIBLE-TRY AGAIN" ELSE GOTO 680
650 TIME=0:T=1
660 REPEAT UNTIL TIME>=T*100
670 GOTO 600
680 PROCmenu
690 UNTIL NSS>1
700 @%=&2020A
710 Z=1
720 ENDPROC
730 REM ~~~~~~~~~~~~~~~~~~~~~~~~~~~~~~~~~~~~~~~~~~~~~~~~~~~~~~~~~~~~~~~~~~~~~~~~~~~
740 DEF PROCcheck
750 CLS
760 PROCmenu
770 COLOUR 0:COLOUR 129
780 PRINT TAB(9,8);"CHECK"
790 COLOUR 3:COLOUR 128
800 PRINT TAB(3,12);"The potential will be switched from"
810 PRINT TAB(3,15);INITIAL;"V to ";FINAL;"V after the first"
820 PRINT TAB(3,18);"scan. It will be kept at this value"
830 PRINT TAB(3,21);"for the remaining ";(NSS-1);" scans."
840 PRINT TAB(3,25);"DO YOU WISH TO CHANGE ANYTHING"
850 PRINT TAB(3,27);"BEFORE YOU CONTINUE (Y/N) ";Q$
860 Z=0
```

```
870 IF Q$="N" THEN GOTO 880 ELSE GOTO 110
880 ENDPROC
890 REM ~~~~~~~~~~~~~~~~~~~~~~~~~~~~~~~~~~~~~~~~~~~~~~~~~~~~~~~~~~~~~~~~
900 DEF PROCrun
910 CLS
920 Z=1
930 PROCmenu
940 COLOUR 0:COLOUR 129
950 PRINT TAB(9,8);"RUN"
960 COLOUR 3:COLOUR 128
970 Y=(INITIAL*10+20.078)*6.375
980 PROCvolt
990 SOUND 1,-15,148,2
1000 PRINT TAB(3,12);"POTENTIAL CURRENTLY AT ...";INITIAL;"V"
1010 PRINT TAB(3,23);"TYPE 'TRS#' ON BRUKER"
1020 PRINT TAB(3,26);"PRESS <RETURN> TO BEGIN"
1030 G%=GET
1040 REPEAT UNTIL G%=13
1050 PRINT TAB(3,23);"                    "
1060 PRINT TAB(3,26);"                         "
1070 Y=(FINAL*10+20.078)*6.375
1080 PROCtrigger
1090 PROCtrigger
1100 PROCvolt
1110 SOUND 1,-15,148,2
1120 PRINT TAB(3,12);"POTENTIAL CURRENTLY AT ...";FINAL;"V"
1130 FOR S=2 TO NSS
1140 PROCtrigger
1150 PRINT TAB(7,18);"Scan number.......";S
1160 NEXT S
1170 TIME=0:T=3
1180 REPEAT UNTIL TIME>=T*100
1190 Y=(INITIAL*10+20.078)*6.375
1200 PROCcolt
1210 PRINT TAB93,12);"POTENTIAL CURRENTLY AT ...";INITIAL;"V"
1220 ENDPROC
1230 REM ~~~~~~~~~~~~~~~~~~~~~~~~~~~~~~~~~~~~~~~~~~~~~~~~~~~~~~~~~~~~~~~~
1240 DEF PROCend
1250 Z=1
1260 CLS
1270 PROCmenu
1280 COLOUR 0:COLOUR 129
1290 PRINT TAB(8,9);"END"
1300 COLOUR 3:COLOUR 128
1310 INPUT TAB(3,25);"DO YOU WANT ANOTHER RUN (Y/N) ";QUESTION$
1320 V=0
1330 CLS
1340 IF QUESTION$="Y" THEN GOTO 30 ELSE GOTO 220
1345 ENDPROC
1350 REM ~~~~~~~~~~~~~~~~~~~~~~~~~~~~~~~~~~~~~~~~~~~~~~~~~~~~~~~~~~~~~~~~
1360 DEF PROCvolt
1370 Y%=Y
1380 A%=&93
1390 X%=&FC
1400 CALL &FFF4
1410 ENDPROC
1420 REM ~~~~~~~~~~~~~~~~~~~~~~~~~~~~~~~~~~~~~~~~~~~~~~~~~~~~~~~~~~~~~~~~
1430 DEF PROCtrigger
```

```
1440 TIME=0
1450 A%=&96
1460 X%=&6C
1470 Y%=0
1480 CALL &FFF4
1490 REPEAT
1500 A%=&96
1510 X%=&6D
1520 N%=USR(&FFF4)
1530 UNTIL (N% AND &20000)=&20000
1540 IF TIME>=80 THEN GOTO 1610
1550 TIME=0
1560 A%=&97
1570 X%=&61
1580 Y%=0
1590 CALL &FFF4
1600 GOTO 1490
1610 ENDPROC
```

Appendix III

Digital-to-analogue Converter and Amplifier

The BASIC program initiates the sending of an 8-bit number from the 1 MHz interface of the BBC Microcomputer to the digital-to-analogue converter. The digital-to-analogue converter then produces a corresponding analogue signal, which needs amplification to conform to the requirements of the Metrohm potentiostat.

The circuit diagrams of the amplifier and power supply are given.

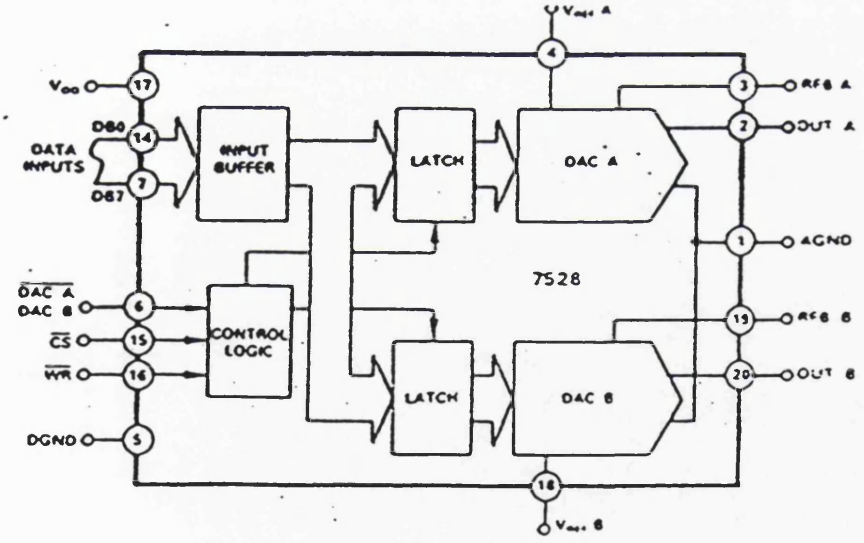

Block diagram of digital-to-analogue converter

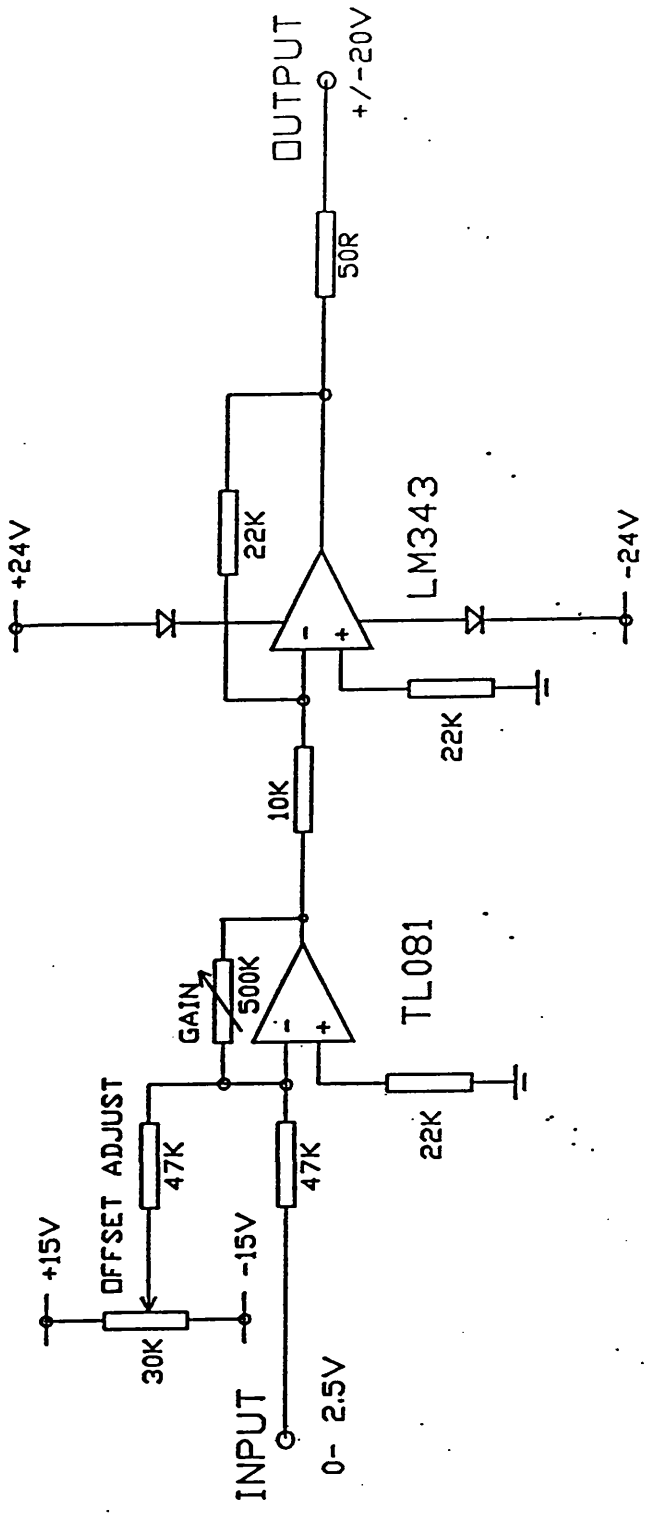

Amplifier for digital-to-analogue converter

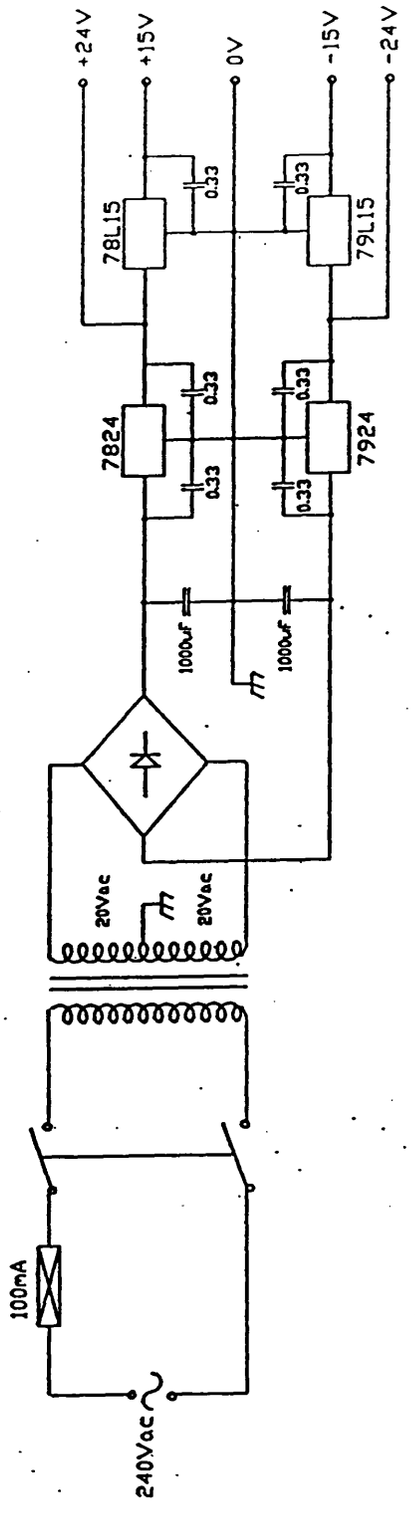

Power supply

Appendix 4

Peak-fitting Program

The form in which the spectrum is held on the Bruker FTIR spectrometer is not compatible with the BBC microcomputer software. It is, therefore, initially transformed into an ASCII file for transfer to the BBC microcomputer, which is carried out using the "KERMIT" program. The ASCII file, now on the microcomputer, is converted into a form more easily accepted by the BASIC peak-fitting program. Both the conversion and the peak-fitting program are listed here.

Conversion Program

```
10 DIM IR%(4000)
20 VMIN=0:VMAX=0:ZFF%=0:RES=0:CMIN%=0:CMAX%=0:N%=0
30 INPUT "ENTER THE FILENAME";A$
40 A%=OPENUP A$
50 REPEAT
60 A$=" "
70 REPEAT A=BGET#A%
80 A$=A$+CHR$(A)
90 UNTIL A=13
100 IF MID$(A$,2,5)="FIRST" THEN VMIN=VAL(MID$(A$,12,20)):PRINT A$
110 IF MID$(A$,2,4)="LAST" THEN VMAX=VAL(MID$(A$,10,20)):PRINT A$
120 IF MID$(A$,2,5)="#POI" THEN N%=VAL(MID$(A$,11,20))-1:PRINT A$
130 IF MID$(A$,2,5)="ZEROF" THEN ZFF%=VAL(MID$(A$,11,20)):PRINT A$
140 IF MID$(A$,2,5)="RESOL" THEN RES=VAL(MID$(A$,13,20)):PRINT A$
150 UNTIL MID$(A$,2,4)="DATA"
160 FOR I%=0 TO N%
170 IF VMIN>VMAX THEN P%=N%-I% ELSE P%=I%
180 A$=" "
190 REPEAT A=BGET#A%
200 A$=A$+CHR$(A)
210 UNTIL (A=32) OR (A=13) OR (A=10)
220 IF LEN(A$)=1 THEN GOTO 180
230 IR%(P%)=VAL(A$)*1E6
240 NEXT I%
250 IF VMIN>VMAX THEN DUM=VMIN:VMIN=VMAX:VMAX=DUM
260 A$=" "
```

```
270 REPEAT A=BGET#A%
280 A$=A$+CHR$(A)
290 UNTIL (A=32) OR (A=13) OR (A=10)
300 IF LEN(A$)=1 THEN GOTO 260
310 PRINT A$
320 CLOSE#A%
330 CMIN%=IR%(0):CMAX%=CMIN%
340 FOR I%=0 TO N%
350 IF CMIN%>IR%(I%) THEN CMIN%=IR%(I%)
360 IF CMAX%<IR%(I%) THEN CMAX%=IR%(I%)
370 NEXT I%
380 FOR I%=0 TO N%
390 IR%(I%)=1E6*(IR%(I%)-CMIN%)/(CMAX%-CMIN%)
400 NEXT %
410 INPUT "ENTER THE NEW FILENAME",A$
420 A%=OPENOUT A$
430 PRINT#A%,N%
440 PRINT#A%,VMIN
450 PRINT#A%,VMAX
460 PRINT#A%,CMIN%
470 PRINT#A%,CMAX%
480 PRINT#A%,ZFF%
490 PRINT#A%,RES
500 FOR I%=0 TO N%
510 PRINT#A%,IR%(I%)
520 NEXT I%
530 CLOSE#A%
540 PRINT N%,VMIN,VMAX,CMIN%,CMAX%,ZFF%,RES
550 END
```

Peak-fitting Program

```
10 REM ------------------------------------------------------------------------------------------------------------
20 REM PROGRAM TO FIT FTIR/MCP DATA AND A GAUSSIAN/LORENTZIAN BANDSHAPE
30 REM S.P.BEST/SAC  AUGUST,1989
40 REM ------------------------------------------------------------------------------------------------------------
50 *FX225,140
60 DIM IR%(4000),Pos(9),FWHH(9),Ht(9),GL(9),P(9),W(9)
70 VMIN=0:VMAX=0:CMIN%=0:CMAX%=0
80 N%=0:ZFF%=0:RES=0
90 B%=0:O%=50:S%=0
100 REM ------------------------------------------------------------------------------------------------------------
110 MODE 1
120 GCOL0,2
130 PROCbox
140 COLOUR 2
150 PRINT TAB(4,11);"f1";TAB(6);"READ THE SPECTRUM FILE"
160 PRINT TAB(4,13);"f2";TAB(6);"SAVE THE PEAK FILE"
170 PRINT TAB(4,15);"f3";TAB(6);"READ A PEAK FILE"
180 PRINT TAB(4,17);"f4";TAB(6);"SET UP BANDSHAPES"
190 PRINT TAB(4,19);"f5";TAB(6);"PLOT FITTED SPECTRUM"
```

```
200 PRINT TAB(4,21);"f6";TAB(6);"HARDCOPY OF PARAMETERS"
210 PRINT TAB(4,24);"f0";TAB(6);"EXIT FROM THE PROGRAM"
220 COLOUR 1
230 PRINT TAB(3,6);"KEY";TAB(10);"COMMAND"
240 PRINT TAB(10,27);"INPUT KEY......";
250 COLOUR 3
260 REPEAT G%=GET:UNTIL (G%>139) AND (G%<147)
270 IF G%=140 THEN MODE 0:END
280 IF G%=141 THEN PROCpread
290 IF G%=142 THEN PROCpwrite
300 IF G%=143 THEN PROCpfile
310 IF G%=144 THE PROCsetup
320 IF G%=145 THEN PROChaplot
330 IF G%=146 THEN PROCprint
340 GOTO 110
350 REM ~~~~~~~~~~~~~~~~~~~~~~~~~~~~~~~~~~~~~~~~~~~~~~~~~~~~~~~~~~~~~~~~~~~~~~~~~~~~~~~~~~
360 DEF PROCpread
370 REM ~~~~~~~~~~~~~~~~~~~~~~~~~~~~~~~~~~~~~~~~~~~~~~~~~~~~~~~~~~~~~~~~~~~~~~~~~~~~~~~~~~
380 PROCbox
390 PRINT TAB(3,8);"PLACE DATA DISC IN DRIVE 0"
400 PRINT TAB(10,14);"FILENAME....."
410 PRINT TAB(3,16);"max of 10 chaaracter"
420 INPUT TAB(25,14);A$
430 ON ERROR GOTO 3140
440 Z%=OPENUP(A$)
450 INPUT #Z%,N%,VMIN,VMAX,CMIN%,CMAX%,ZFF%,RES
460 FOR I%=0 TO N%
470 INPUT #Z%, IR%(I%)
480 NEXT I%
490 CLOSE #Z%
500 PRINT TAB(3,20);"VMIN=";VMIN;TAB(3,22);"VMAX=";VMAX
510 PRINT TAB(18,20);"CMIN=";CMIN%;TAB(18,22);"CMAX="; CMAX%
520 PRINT TAB(30,20);"ZFF=";ZFF%;TAB(30,22);"RES=";RES
530 PRINT TAB(3,24);"No. DATA POINTS=";N%
540 PRINT TAB(3,27);"Press <RETURN> to continue"
550 REPEAT G%=GET:UNTIL G%=13
560 ON ERROR OFF
570 *MOUNT0
580 ENDPROC
590 REM ~~~~~~~~~~~~~~~~~~~~~~~~~~~~~~~~~~~~~~~~~~~~~~~~~~~~~~~~~~~~~~~~~~~~~~~~~~~~~~~~~~
600 DEF PROCpwrite
610 REM ~~~~~~~~~~~~~~~~~~~~~~~~~~~~~~~~~~~~~~~~~~~~~~~~~~~~~~~~~~~~~~~~~~~~~~~~~~~~~~~~~~
620 PROCbox
630 PRINT TAB(3,27);"PLACE DATA DISC IN DRIVE 1"
640 PRINT TAB(10,12);"FILENAME......"
650 PRINT TAB(3,14);"max of 10 characters"
660 INPUT TAB(12,16);A$
670 IF LEN(A$)>10 THEN GOTO 620
680 ON ERROR GOTO 3140
690 Z%=OPENOUT(A$)
700 PRINT #Z%,N%,VMIN,VMAX,CMIN%,CMAX%,ZFF%,RES
710 FOR I%=0 TO N%
720 PRINT #Z%, IR%(I%)
730 NEXT I%
740 PRINT #Z%,B%,O%,S%
750 FOR I%=0 TO B%
760 PRINT #Z%,GL(I%),Pos(I%),FWHH(I%),Ht(I%)
770 NEXT I%
```

```
780 CLOSE #Z%
790 ON ERROR OFF
800 *MOUNT0
810 ENDPROC
820 REM ~~~~~~~~~~~~~~~~~~~~~~~~~~~~~~~~~~~~~~~~~~~~~~~~~~~~~~~~~~~~~~~~~~~~
830 DEF PROCpfile
840 REM ~~~~~~~~~~~~~~~~~~~~~~~~~~~~~~~~~~~~~~~~~~~~~~~~~~~~~~~~~~~~~~~~~~~~
850 PROCbox
860 PRINT TAB(3,7);"PLACE DATA DISC IN DRIVE 1"
870 PRINT TAB(10,12);"FILENAME......"
880 PRINT TAB(3,14);"max of 10 characters"
890 INPUT TAB(12,16);A$
900 IF LEN(A$)>10 THEN GOTO 850
910 ON ERROR GOTO 3140
920 Z%=OPENIN (A$)
930 INPUT #Z%,N%,VMIN,VMAX,CMIN%,CMAX%,ZFF%,RES
940 FOR I%=0 TO N%
950 INPUT #Z%,IR%(I%)
960 NEXT I%
970 INPUT #Z%,B%,O%,S%
980 FOR I%=0 TO B%
990 INPUT #Z%,GL(I%),Pos(I%),Ht(I%)
1000 NEXT I%
101 CLOSE #Z%
1020 ON ERROR OFF
1030 *MOUNT0
1040 ENDPROC
1050REM~~~~~~~~~~~~~~~~~~~~~~~~~~~~~~~~~~~~~~~~~~~~~~~~~~~~~~~~~~~~~~~~~~~~~
1060 DEF PROCsetup
1070 REM ~~~~~~~~~~~~~~~~~~~~~~~~~~~~~~~~~~~~~~~~~~~~~~~~~~~~~~~~~~~~~~~~~~~
1080 MODE 0;VDU 19,1,2,0,0,0
1090 P%=0:E%=5*N%:CS%=N%*2.5:C%=CS%:OC%=-10
1100 *FX4,1
1110 PRINT TAB(6,0);"EXIT";TAB(14,0);"REDRAW";TAB(43,0);"ADD ANOTHER BAND"
1120 PRINT TAB(26,0);"CHANGE BAND";TAB(63,0);"DELETE BAND"
1130 PRINT TAB(3,1);"BAND #";TAB(14,1);"GAUS/LOR MIX";TAB(30,1);"POSITION"
1140 PRINT TAB(43,1);"FWHH";TAB(52,1);"HEIGHT";TAB(63,1);"OFFSET";TAB(74,1);"SLOPE"
1150 COLOUR 0:COLOUR 129
1160 PRINT TAB(1,0);"<RET>";TAB(12,0);"f0";TAB(24,0);"f1";TAB(41,0);"f2"
1170 PRINT TAB(61,0);"f3";TAB(12,1);"f4";TAB(28,1);"f5";TAB(41,1);"f6"
1180 PRINT TAB(50,1);"f7";TAB(61,1);"f8";TAB(72,1);"f9"
1190 COLOUR 1:COLOUR 128
1200 VDU 28,2,2,78,2
1210 PROCsplot
1220 CLS
1230 PRINT TAB(3,0);P%;TAB(15,0);GL(P%);TAB(27,0);Pos(P%);TAB(40,0);FWHH(P%)
1240 PRINT TAB(50,0);Ht(P%);TAB(61,0);O%;TAB(71,0);S%;
1250 L$=CHR$(136)+" , "+CHR$(137)+" TO MOVE CURSOR"
1260 X%=500:Y%=40:PROClabel
1270 REPEAT G%=GET
1280 UNTIL (G%=13) OR (G%=136) OR (G%=137) OR (G%>139) AND (G%<150)
1290 CLS
1300 IF G%=140 THEN PROCsplot
1310 IF G%=141 THEN P%=(P%+1) MOD (B%+1)
1320 IF (G%=142) AND (B%<9) THEN B%=B%+1:P%=B%
1330 IF (G%<>143) OR (B%=0) THEN GOTO 1390
1340 FOR I%=P% TO B%
1350 Pos(I%)=Pos(I%+1):FWHH(I%)=FWHH(I%+1)
```

```
1360 Ht(I%)=Ht(I%+1):GL(I%)=GL(I%+1)
1370 NEXT I%
1380 B%=B%-1:P%=B%
1390 IF G%=144 THEN INPUT "ENTER % LORENTZIAN CHARACTER (0-100)...;GL(P%)
1400 IF G%=145 THEN INPUT "ENTER THE POSITION...";Pos(P%)
1410 IF G%=136 THEN OC%=CS%:CS%=CS%-1:C%=CS%:PROCcursor
1420 IF G%=137 THEN OC%=CS%:CS%=CS%+1:C%=CS%:PROCcursor
1430 IF G%=146 THEN INPUT "ENTER THE FWHH...";FWHH(P%)
1440 IF G%=147 THEN INPUT "ENTER THE HEIGHT...";Ht(P%)
1450 IF G%=148 THEN INPUT "ENTER THE OFFSET...";O%
1460 IF G%=149 THEN INPUT "ENTER THE SLPOE...";S%
1470 IF G%<>13 THEN GOTO 1220
1480 *FX4,0
1490 ENDPROC
1500 REM ~~~~~~~~~~~~~~~~~~~~~~~~~~~~~~~~~~~~~~~~~~~~~~~~~~~~~~~~~~~~~~~~~~~~~~~~
1510 DEF PROChaplot
1520 REM ~~~~~~~~~~~~~~~~~~~~~~~~~~~~~~~~~~~~~~~~~~~~~~~~~~~~~~~~~~~~~~~~~~~~~~~~
1530 ON ERROR GOTO 3140
1540 IF N%>1 THEN GOTO 1570
1550 PRINT "YOU MUST HAVE SOME DATA READY TO PLOT, PRESS 'RETURN' TO
CONTINUE"
1560 REPEAT UNTIL 13=GET:ENDPROC
1570*IEEE
1580 C%=OPENIN("COMMAND")
1590 Z%=OPENIN("DATA")
1600 PRINT #C%,"BBC DEVICE NO",0
1610 PRINT #C%,"CLEAR"
1620 P%=OPENOUT("5")
1630 PRINT #C%,"LISTEN",P%,"EXECUTE"
1640 PRINT #Z%,"IN;IP 500,600,10500,7300;IW"
1650 PRINT #Z%,"VS 5;TL 0.5;SR .7,1.7;CS1"
1660 A$="SC"+STR$(N%)+",0,0102;"
1670 PRINT #Z%,A$
1680 A$="SR.7,1.7;SP 1;PA 0,OPD;"
1690 PRINT #Z%,A$
1700 IF (VMAX-VMIN)>=400 THEN T%=100:E%=((VMIN+90)DIV100)*100:GOTO 1740
1710 IF (VMAX-VMIN)>=200 THEN T%=50:E%=((VMIN+25)DIV50)*50:GOTO 1740
1720 IF (VMAX-VMIN)>=100 THEN T%=25:E%=((VMIN+24)DIV25)*25:GOTO 1740
1730 T%=10:E%=((VMIN+9)DIV10)*10
1740 FOR J%=E% TO VMAX STEP T%
1750 I%=(J%-VMIN)*N%/(VMAX-VMIN)
1760 A$="PA"+STR$(I%)+",0;XT;"
1770 PRINT #Z%,A$
1780 NEXT J%
1790 A$="PA"+STR$(N%)+",0,"+STR$(N%)+",102,0,102,0,0PU;"
1800 PRINT #Z%,A$
1810 FOR J%=E% TO VMAX STEP T%
1820 I%=(J%-VMIN)*N%/(VMAX-VMIN)
1830 T1=-LEN(STR$(J%))/2
1840 A$="PA"+STR$(I%)+",0;CP"+STR$(T1)+",-1;LB"+STR$(J%)+CHR$(3)
1850 PRINT #Z%,A$
1860 NEXT J%
1870 A$="SR1,2.2;PA"+STR$(N%/2)+",0;CP-8,-2;LBWavenumber/cm-1"+CHR$(3)
1880 PRINT #Z%,A$
1890 A$="PA"+STR$(N5/2)+",0;CP5,-1.7;LB-1"+CHR$(3)
1900 PRINT #Z%,A$
1910 A$="DI0,1;PA"+STR$(N5)+",51;CP-5,.5;LBIntensity"+CHR$(3)
1920 PRINT #Z%,A$
```

```
1930 A$="DI1,0;CP-.75,0;LB^"+CHR$(3)
1940 PRINT #Z%,A$
1950 REM ----------
1960 @%=&0102050A
1970 A$="SP2;IW500,600,10500,7300"
1980 PRINT #Z%,A$
1990 FOR I%=0 TO N%
2000 T1=IR%(I%)/1E4
2010 A$="PA"+STR$(I%)+","+STR$(1+T1)+"PDPU;"
2020 PRINT #Z%,A$
2030 NEXT I%
2040 FOR I%=0 TO B%
2050 P(I%)=(Pos(I%)-VMIN)*N%/(VMAX-VMIN)
2060 W(I%)=FWHH(I%)*N%/(VMAX-VMIN)
2070 NEXT I%
2080 A$="PA 0,"+STR$(O%)+"PD;"
2090 PRINT #Z%,A$
2100 FOR X=0.2 TO N% STEP 0.2
2110 TY=O%*100+100*S%*X/N%
2120 FOR J%=0 TO B%
2130 IF FWHH(J%)=0 THEN GOTO 2160
2140 TY=TY+GL(J%)/(1+4*((P(J%)-X)/W(J%)*((P(J%)-X)/W(J%)))
2150 TY=TY+(100-GL(J%))*Ht(J%)*EXP(-2.772589*(P(J%)-X*(P(J5)-X)/W(J%)*W(J%)))
2160 NEXT J%
2170 A$="PA"+STR$(X)+","+STR$(1+TY/100)+";"
2180 PRINT #Z%,A$
2190 NEXT X
2200 FOR J%=0 TO B%
2210 IF FWHH(J%)=0 THEN GOTO 2310
2220 PRINT #Z%,"LT 5,4;PU"
2230 FOR X=P(J%)-3*W(J%) TO P(J%)+3*W(J%) STEP 0.2
2240 IF (X<0) OR (X>N%) GOTO 2300
2250 IF Ht(J%)<0 THE TY=9800 ELSE TY=100
2260 TY=TY+GL(J%)*Ht(J%)/(1+4*((P(J%)-X)/W(J%))*((P(J%)-X)/W(J%)))
2270 TY=TY+(100-GL(J%))*Ht(J%)*EXP(-2.772589*(P(J%)-X)*(P(J%)-X)/(W(J%)*W(J%)))
2280 A$="PA"+STR$(X)+","+STR$(1+TY/100)+"PD;"
2290 PRINT #Z%,A$
2300 NEXT X
2310 NEXT J%
2320 PRINT #Z%,"PU;SP0;IW;LT;"
2330 @%=10:CLOSE# 0:*ADFS
2340 ON ERROR OFF
2350 ENDPROC
2360 REM ~~~~~~~~~~
2370 DEF PROCprint
2380 REM ~~~~~~~~~~
2390 MODE 0:VDU 2
2395 PRINT TAB(10);"PARAMETR SET    FILE-";A$
2400 PRINT TAB(10);"BAND #   LORENTZ/GAUSS MIX   POSITION/cm-1   HEIGHT   FWHH/cm-1"
2410 FOR I%=0 TO B%
2420 PRINT TAB(12);I%;TAB(25);GL(I%);TAB(43);Pos(I%)
2430 PRINT TAB(58);Ht(I%);TAB(68);FWHH(I%)
2440 NEXT I%
2450 PRINT:PRINT
2460 PRINT TAB(10);"Offset=";O%,"Slope=";S%
2465 PRINT TAB(10);"CMAX=";CMAX%,"CMIN=";CMIN%,N%;"DATA POINTS"
2466 PRINT:PRINT:PRINT:PRINT
2470 VDU 3:ENDPROC
```

```
2480 REM ~~~~~~~~~~~~~~~~~~~~~~~~~~~~~~~~~~~~~~~~~~~~~~~~~~~~~~~~~~~~~~~~~~~
1490 DEF PROCbox
2500 REM ~~~~~~~~~~~~~~~~~~~~~~~~~~~~~~~~~~~~~~~~~~~~~~~~~~~~~~~~~~~~~~~~~~~
2510 CLS
2520 MOVE 50,50:DRAW 1200,50:DRAW 1200,900:DRAW 50,900:DRAW 50,50
2530 ENDPROC
2540 REM ~~~~~~~~~~~~~~~~~~~~~~~~~~~~~~~~~~~~~~~~~~~~~~~~~~~~~~~~~~~~~~~~~~~
2550 DEF PROCsplot
2560 REM ~~~~~~~~~~~~~~~~~~~~~~~~~~~~~~~~~~~~~~~~~~~~~~~~~~~~~~~~~~~~~~~~~~~
2565 @%=%0100040A
2570 VDU 24,0;0;1279;920;:CLG
2580 MOVE 40,76:DRAW 40,912:DRAW 1240,912:DRAW 1240,76:DRAW 40,76
2590 VDU 24,40;76;1240;912;
2600 MOVE 40,106+IR%(0)/1288.66
2610 FOR I%=1 TO N%
2620 PLOT 69,40+I%*1200/N%,106+IR%(I%)/1288.66
2630 NEXT I%
2640 VDU 24,0;0;1279;912;
2650 X%=1240:Y%=50:L$=STR$(VMAX):PROClabel
2660 X%=40:Y%=50"L$=STR$(VMIN):PROClabel
2670 FOR I%=0 TO B%
2680 P(I%)=(Pos(I%)-VMIN)*N%/(VMAX-VMIN)
2690 W(I%)=FWHH(I%)*N%/(VMAX-VMIN)
2700 NEXT I%
2710 IF (B%=0) AND (FWHH(0)=0) THEN GOTO 2830
2720 MOVE 40,76+O%*8.36
2730 FOR I%=0 TO 600
2740 X=N%*I%/600
2750 TY=100*O%+100*S%*X/N%
2760 FOR J%=0 TO B%
2770 IF FWHH(J%)=0 THEN GOTO 2800
2780 TY=TY+GL(J%)*Ht(J%)/(1+4*((P(J%)-X)/W(J%)*((P(J%)-X)/W(J%)))
2790 TY=TY+(100-GL(J%))*Ht(J%)*EXP(-2.772589*(P(J%)-X)*(P(J%)-X)/(W(J%)*W(J%)))
2800 NEXT J%
2810 DRAW I%*2+40,TY*0.0776+106
2820 NEXT I%
2825 @%=&0002020A
2830 ENDPROC
2840 REM ~~~~~~~~~~~~~~~~~~~~~~~~~~~~~~~~~~~~~~~~~~~~~~~~~~~~~~~~~~~~~~~~~~~
2850 DEF PROClabel
2860 REM ~~~~~~~~~~~~~~~~~~~~~~~~~~~~~~~~~~~~~~~~~~~~~~~~~~~~~~~~~~~~~~~~~~~
2870 VDU 5
2880 MOVE X%+8-LEN(L$)*8,Y%
2890 PRINT L$
2900 VDU 4
2910 ENDPROC
2920 REM ~~~~~~~~~~~~~~~~~~~~~~~~~~~~~~~~~~~~~~~~~~~~~~~~~~~~~~~~~~~~~~~~~~~
2930 DEF PROCcursor
2940 REM ~~~~~~~~~~~~~~~~~~~~~~~~~~~~~~~~~~~~~~~~~~~~~~~~~~~~~~~~~~~~~~~~~~~
2950 VDU 18,4,1
2960 C%=40+(C%-2)*1200/(E%-2):OC%=40+(OC%-2)*1200/(E%-2)
2970 MOVE OC%,952:DRAW OC%,76
2980 MOVE C%,952:DRAW C%,76
2990 VDU 18,0,1
3000 VDU 24,740;5;940;70;:CLG
3010 D%=VMIN+(VMAX-VMIN)*(C%-40)/1200
3020 X%=800:Y%=40:L$=STR$(D%):PROClabel
3030 VDU 24,40;76;1240;912;
```

```
3040 ENDPROC
3050 REM ~~~~~~~~~~~~~~~~~~~~~~~~~~~~~~~~~~~~~~~~~~~~~~~~~~~~~~~~~~~~~~~~
3060 CLOSE #0
3070 PRINT TAB(6,20);:REPORT
3080 PRINT TAB(6,24);"PROBLEMS WITH DISC READ OR WRITE"
3090 PRINT TAB(3,26);"PRESS <RETURN> TO CONTINUE";
3100 REPEAT UNTIL 13=GET
3110 ON ERROR OFF
3120 GOTO 110
3130 REM ----------------------------------------------------------------
3140 @%=10:CLOSE #0
3150 *ADFS
3160 ON ERROR OFF
3170 GOTO 110
```